Characterisation of the Conserved Protein IMPACT from Yeast (Yih1)

A thesis presented in partial fulfilment of the requirements for the degree of

Master of Science

in

Biochemistry

at Massey University, Manawatu,

New Zealand.

Natalie Sarah Burr

2012

Abstract

Regulation of translation under conditions of amino acid starvation is an important survival mechanism to ensure the continued viability of an organism. The accumulation of uncharged tRNA under amino acid starvation conditions triggers the activation of Gcn2, a kinase that phosphorylates the translation initiation factor eIF2α, inhibiting translation initiation. The protein IMPACT has been shown to inhibit Gcn2 by sequestering Gcn1, a protein that binds Gcn2 and is required for its function *in vivo*. IMPACT is a highly conserved protein, but despite its conservation, little is known about the role(s) it plays in the cell.

The initial aim of this study was to investigate the three dimensional structure of Yeast IMPACT Homologue 1 (Yih1) using X-ray diffraction, in the hope that knowledge of the structure would inform further understanding of its many and varied complex biological functions. Because of the difficulties in obtaining diffraction quality crystals, a number of different techniques were employed that resulted in the production of a number of different plasmids for protein expression. These included surface entropy engineering, the use of folding and stability tags, and co-crystallisation with known binding partners.

Further investigation into why the protein refused to crystallise revealed an innate heterogeneity that included a propensity to bind nucleic acids. Efforts were made to determine if this was related to function without success.

Acknowledgements

Science is never a one-person endeavour. There are too many people to thank but I especially wish to say thank you to the following:

Most of all, my supervisor Gill Norris. Thank you for the opportunities, support, and confidence you have given me. It is your belief in me that has allowed me cope when things just wouldn't work.

My co-supervisor Mark Patchett for great help, advice and ideas, and also for assistance with proof-reading this thesis.

My other co-supervisor Evelyn Sattlegger for the original constructs and her assistance from afar.

The members of X-lab past and present, especially the all-knowing Trevor Loo. Thank you for the discussions, the clarifications, your patience and general conversations. I couldn't have asked for a better group of people to work with.

The Massey structural biology group for the weekly junk food fix, and listening to me prattle on about trying to figure out what Yih1 was up to.

Alexander Goroncy for his help and interest in the science of Yih1 alone. I wish you all the luck in your work now and in the future.

Mum and Dad for being the best parents ever, allowing me to find my own way in life and supporting me no matter what direction I went in. Thank you for all the discussions we had about my work and the effort to understand what the hell it was that I was doing.

Last but not least I want to thank my partner Ben. Your love and support gave me the drive to follow my passion.

Abbreviations

× g	Multiples of gravitational force
°C	Degrees Celsius
µL	Microlitre
µm	Micrometre
3D	Three-dimensional
Å	Angstrom (10^{-10}m)
A_{260}	Absorbance at 260 nm
A_{280}	Absorbance at 280 nm
AEX	Anion Exchange Chromatography
ATF4	Activating transcription factor 4
ATP	Adenosine-5'-triphosphate
CD	Circular Dichroism
CV	Column Volumes
Da	Dalton
DEPC	Diethylpyrocarbonate
DNA	Deoxyribonucleic acid
dNTP	Deoxyribonucleotide Triphosphate
dsDNA	Double-stranded Deoxyribonucleic acid
DTT	Dithiothreitol
EDTA	Ethylenediaminetetraacetic acid
eIF	Eukaryotic Initiation Factor
EtBr	Ethidium Bromide
g	Gram
Gcn	General Control Non-derepressible
$Gcn1_{frag}$	Gcn1 fragment consisting of residues 2050-2428
GDP	Guanosine-5'-diphosphate
GST	Glutathione S-transferase
GTP	Guanosine-5'-triphosphate
H	Hydrogen
His_6	Hexa-histidine tag

His_6-$Yih1_{cys-}$	His_6-Yih1 C67A, C99A
HTS	High-throughput Screening
IDD	Intrinsically disordered domain
IDO	Indoleamine 2,3-dioxygenase
IMPACT	Imprinted and Ancient
IPTG	Isopropyl-β-D-thio-galactoside
IUP	Intrinsically unfolded protein
kB	Kilobases
kBp	Kilobase-pair
kDa	Kilodalton
kPa	Kilopascal
L	Litre
LB	Luria Bertani media
LB-AB	Luria Bertani media with antibiotics
M	Mole
mAU	Milli absorbance units
mg	Milligram
Min	Minute
mJ	Millijoule
mL	Millilitre
mM	Millimole
mRNA	Messenger ribonucleic acid
MW	Molecular Weight
NAD	Nicotinamide adenine dinucleotide
NADP	Nicotinamide adenine dinucleotide phosphate
NMR	Nuclear magnetic resonance
NZ	New Zealand
OD_{600}	Optical density at 600 nm
Pa	Pascal
PAGE	Polyacrylamide gel electrophoresis
PBS	Phosphate buffered saline
PCR	Polymerase chain reaction

pH	Negative decadal logarithm of proton concentration
pKa	Negative decadal logarithm of acid dissociation constant
RBS	Ribosome binding site
RNA	Ribonucleic acid
RPM	Revolutions per minute
SAXS	Small-angle X-ray scattering
SD	Selective dropout media
SDM	Site-directed Mutagenesis
SDS	Sodium dodecyl sulfate
SEC	Size exclusion chromatography
SER	Surface entropy reduction
TAE	Tris-acetate-EDTA buffer
TCEP	Tris(2-carboxyethyl)phosphine
TE	Tris-EDTA buffer
TEMED	Tetramethylethylenediamine
tRNA	Transfer ribonucleic acid
USA	United States of America
UV	Ultra violet
V	Volt
Yih1	Yeast IMPACT homologue 1
Yih1-56	Yih1 E56A, E57A
Yih1-116	Yih1 E116A, E117A, E118A

Amino Acid Abbreviations

Name	3-letter code	1-letter code	Structure
Alanine	Ala	A	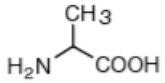
Arginine	Arg	R	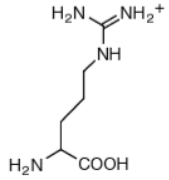
Asparagine	Asn	N	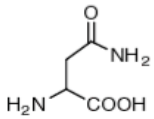
Aspartic Acid	Asp	D	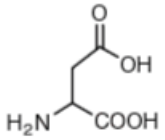
Cysteine	Cys	C	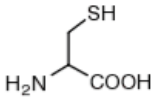
Glutamine	Gln	Q	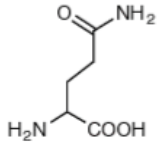
Glutamic Acid	Glu	E	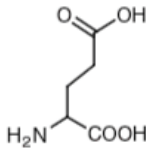
Glycine	Gly	G	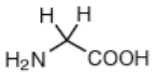
Histidine	His	H	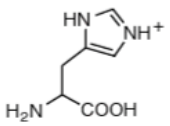
Isoleucine	Ile	I	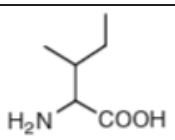

Leucine	Leu	L	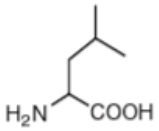
Lysine	Lys	K	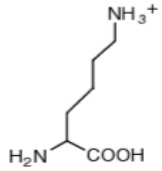
Methionine	Met	M	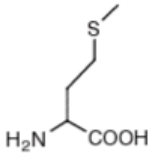
Phenylalanine	Phe	F	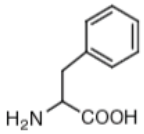
Proline	Pro	P	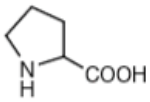
Serine	Ser	S	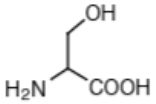
Threonine	Thr	T	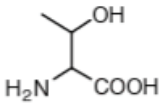
Tryptophan	Trp	W	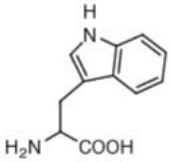
Tyrosine	Tyr	Y	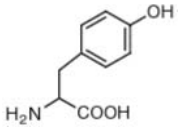
Valine	Val	V	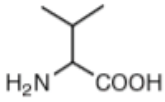

Nucleic Acid Abbreviations

Base	One-letter Code
Adenosine	A
Thymidine	T
Guanine	G
Cytosine	C
Uracil	U

TABLE OF CONTENTS

List of Tables

List of Figures

1. INTRODUCTION AND LITERATURE REVIEW

1.1 The structure of Yeast IMPACT Homologue 1

The yeast IMPACT Homologue (Yih1) in *Saccharomyces cerevisiae* has been the most extensively studied member of the IMPACT family due to the relative simplicity of the yeast system. Yih1 consists of 258 amino acid residues with a hypothetical average molecular weight of 29017.47 Da. As the calculated pI of Yih1 is 4.52, it is an acidic protein at physiological pH.

Yih1 consists of two domains; an N-terminal RWD domain, that is similar to domains found in Ring finger proteins, WD-repeat proteins and DEXDc-helicase proteins; and a C-terminal Ancient domain that is present in various proteins from all domains of life. The high conservation of this domain throughout evolution, and of IMPACT in eukarya, indicates that IMPACT must play a key role in the cell, although its function has not yet been completely elucidated.

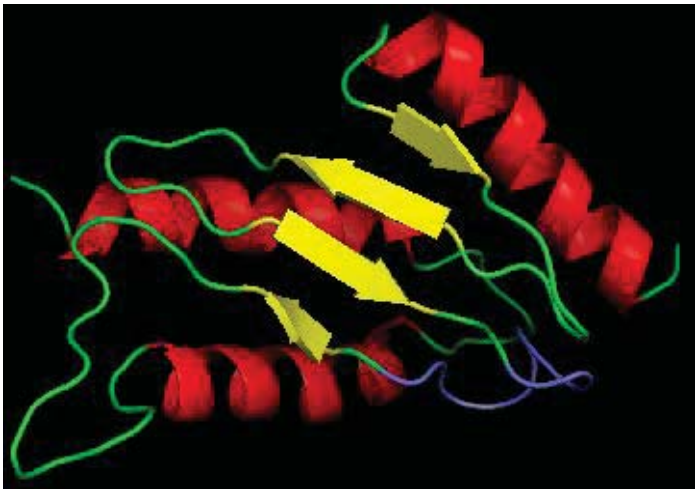

Figure 1.1 Model of Yih1 RWD Domain

Proposed structure of the RWD domain of Yih1 modelled on the RWD domain of Gcn2 (PDB 1UKX) Modified from Sattlegger *et al*. (2011). α-Helices are coloured in red, β-sheet in yellow, and the conserved triple turn is highlighted in blue.

The RWD domain of IMPACT shows little sequence similarity to the RWD domain of Gcn2. Despite this, there are sequence motifs conserved between the two proteins that may be important in the structure/function and which are characteristic of the RWD domain. Sequence analysis shows that in Yih1 there is a conserved $YPX_{3-4}P$ motif (where x denotes any amino acid) that is present in a triple turn, a structural motif only present in RWD and UEV domains which reside within the ubiquitin-conjugating enzyme-like superfamily. Although there is no three-dimensional structure of Yih1, the Yih1 RWD domain has been modelled using on the structure of the RWD domain of GCN2 (Sattlegger *et al.*, 2011), and is predicted to adopt a two-layered α-β sandwich fold with an αββββαα topology.

The Ancient domain is more highly conserved in the IMPACT family than is the RWD domain, with a DDGE motif being absolutely conserved in all species so far investigated (Sattlegger *et al.*, 2011). The N-terminal domain of the *E. coli* protein YigZ shares only 26% sequence identity with the Ancient domain of Yih1. Figure 1.2 shows the Yih1 Ancient domain modelled on the structure of the N-terminal domain

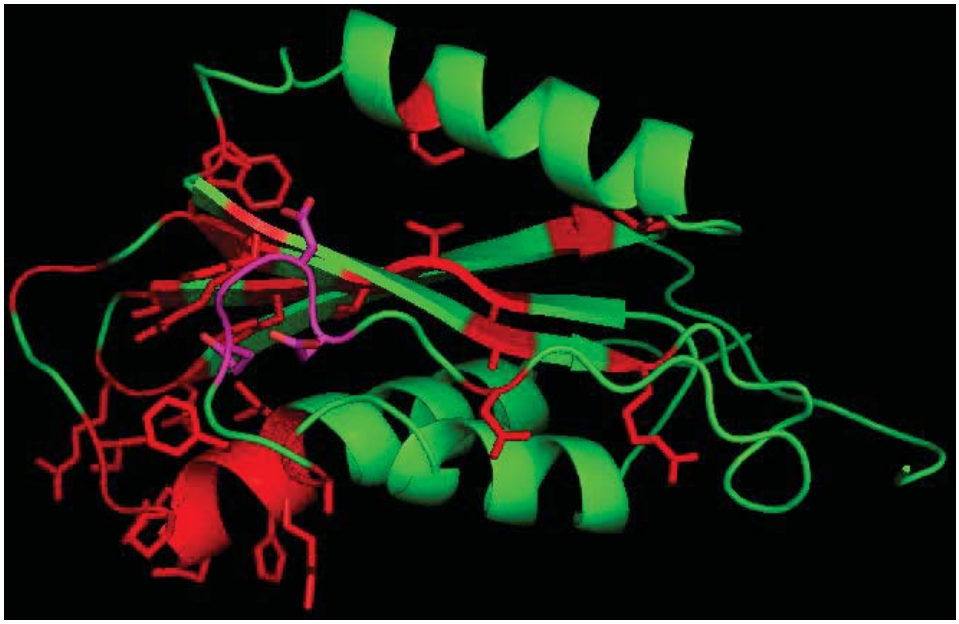

Figure 1.2 Model of Yih1 Ancient Domain

Proposed Structure of the Ancient domain of Yih1 modelled on the N-terminal domain of YigZ (PDB 1VI7). Modified from Sattlegger *et al*. (2011). Highly conserved residues are shown as sticks and highlighted in red. The absolutely conserved DDGE motif is highlighted in magenta.

of YigZ (PDB 1VI7) (Sattlegger *et al.*, 2011). It displays a three-layered αβα sandwich with a ββαβαβα topology (Sattlegger *et al.*, 2011), that is characteristic of the ribosomal protein S5 domain 2-like superfamily. This type of fold is found in proteins such as DNA modifying enzymes, translation machinery, ribonucleases and kinases. The evolutionarily conserved residues are shown as red sticks in Figure 1.2. They cluster on one side of the domain to form a putative binding surface for an as yet unknown molecule. Identification of the physiological binding partners of Yih1 could help to unravel the function of IMPACT in the cell.

1.1 The Function of Yih1

1.1.1 Translation in Yeast

Translation is a complex process that requires a large number of factors to achieve the reliable synthesis of protein encoded by an mRNA transcript. Translation proceeds in three phases: initiation, elongation and termination. Initiation consists of the formation of an eIF2 ternary complex consisting of three subunits (α, β and γ) bound to GTP and the initiator methionyl-tRNA ($tRNA_i^{met}$) (See Figure 1.3). This complex associates with the 40S ribosomal subunit (Kimball, 1999) along with the initiation factors eIF1 (stabilises the interaction between the eIF2 ternary complex and the 40S ribosome), eIF3 (assists in positioning the eIF4 complex on the ribosome), eIF5A (assists in hydrolysis of eIF2α-bound GTP) and eIF1A (required for later association of the 60S ribosomal subunit to the 40S subunit) (Acker and Lorsch, 2008), resulting in the formation of the 43S preinitiation complex. mRNA is recruited to the preinitiation complex by the eIF4 complex, where it is bound to the 5´ cap and 3´ poly-A tail of the mRNA by the subunits eIF4E and eIF4G respectively. The mRNA is scanned for the AUG start codon, and upon its recognition by $tRNA_i^{met}$ bound in the ribosomal P-site, the eIF2α-bound GTP is hydrolysed to GDP releasing P_i and eIF1, eIF3, eIF5A and eIF2-GDP are displaced from the 60S ribosomal subunit. The binding of the 60S subunit to the ribosomal complex is mediated by the interaction of eIF5B with eIF1A and the hydrolysis of the eIF5B-bound GTP to form the 80S initiation complex (Pestova *et al.*, 2001) which is now competent for translation elongation.

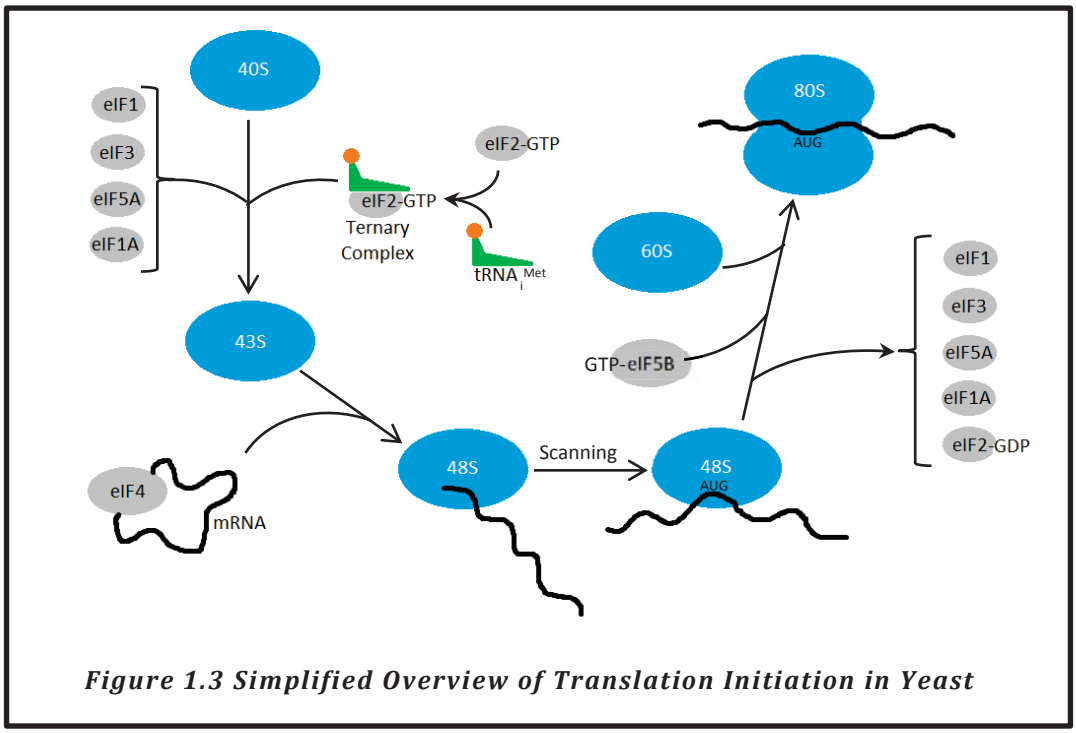

Figure 1.3 Simplified Overview of Translation Initiation in Yeast

Translation elongation is a cyclic reaction in which an aminoacylated tRNA complexed to the elongation factor eEF1A-GTP enters the A-site of the ribosome and forms base pairs with the complementary mRNA codon, facilitated by the hydrolysis of the eEF1A-bound GTP. The polypeptide chain is cleaved from the tRNA in the P-site and ligated to the amino group of the amino acid covalently attached to the tRNA in the A-site. This reaction is catalysed by the ribosomal peptidyl transferase centre which consists of both protein and RNA within the ribosome. The A-site tRNA carrying the growing peptide chain is transferred into the P-site by the action of eEF2 with the concomitant hydrolysis of GTP. Concurrently, the uncharged tRNA that was in the P-site is transferred to the E-site, and released from the ribosome through the action of eEF3 a factor unique to higher fungi. The action of eEF3 also causes a conformational change in the ribosome readying the A-site for the entry of the next eEF1A/GTP/aminoacyl-tRNA complex (Triana-Alonso *et al.*, 1995).

Translation termination involves the recognition of a stop codon and the subsequent hydrolysis of the peptide chain from the P-site tRNA. The stop codon is recognised not by tRNA but by the release factor protein complex. This complex consists of

eRF1 and eRF2 which enters the ribosomal A-site, recognises the stop codon and acts to cleave the peptide chain from the P-site tRNA in a GTP dependent manner.

1.1.2 Regulation of Translation Initiation

Regulation of protein synthesis is an important survival technique necessary for organisms to overcome various forms of stress. Amino acid starvation is one such stress that organisms have evolved to endure *via* regulation of the initiation of translation.

For initiation to occur, the alpha subunit of eIF2 (eIF2α) must be in its GTP-bound state (Walton and Gill, 1975). The non-functional eIF2α:GDP released after translation initiation is recycled back to its functional state by the activity of the guanine nucleotide exchange factor eIF2B (Webb and Proud, 1997). Under amino acid starvation conditions, serine-51 of eIF2α is phosphorylated by Gcn2, an eIF2α kinase. Phosphorylated eIF2α has an increased affinity for eIF2B, converting eIF2α from a substrate to an inhibitor, sequestering the limited levels of eIF2B in the cell (Pavitt *et al.*, 1998). As a result, eIF2α cannot be recycled to its active GTP bound form, causing a drop in the pool of active eIF2α. Global protein translation is therefore decreased because GDP-bound eIF2α is unable to participate in translation initiation.

Although general protein synthesis decreases under these conditions, there is an increase in the translational flux of specific transcriptional activators such as Gcn4 in yeast, and Activating Transcription Factor 4 (ATF4) and C/EBP Homologous Protein (CHOP) in mammals, *via* a mechanism involving sequences upstream from the coding region of their respective mRNA's (Mueller and Hinnebusch, 1986). These transcriptional activators increase expression of amino acid biosynthetic genes to maintain amino acid homeostasis (Hope and Struhl, 1985). This is termed the general amino acid control, as starvation for one amino acid signals for an increase in the synthesis of all 20 amino acids (Hinnebusch, 1988).

1.1.3 The General Control Nonderepressable Complex

eIF2α kinases act to phosphorylate eIF2α under a myriad of different environmental cues. Although there are four known eIF2α kinases in mammalian cells, Gcn2 is the sole eIF2α kinase in yeast. Gcn2 is a homodimeric protein with a monomeric molecular weight of 191.2 kDa. It is proposed to reside on the ribosome in a complex with Gcn1 and Gcn20 (Marton *et al.*, 1997). Gcn2 consists of 5 domains (Figure 1.4): an RWD domain required for interaction with Gcn1 (Sattlegger and Hinnebusch, 2000); a pseudo-kinase domain (ψPK) of unknown function; a protein kinase domain (PK) that acts to phosphorylate serine-51 of eIF2α (Dever *et al.*, 1992); a histidyl-tRNA synthetase-like (HisRS) domain that together with the C-terminal domain (CD) binds uncharged tRNA (Wek *et al.*, 1995); the C-terminal domain also facilitates dimerization of Gcn2 and interacts with the ribosome (Qiu *et al.*, 1998, Zhu and Wek, 1998).

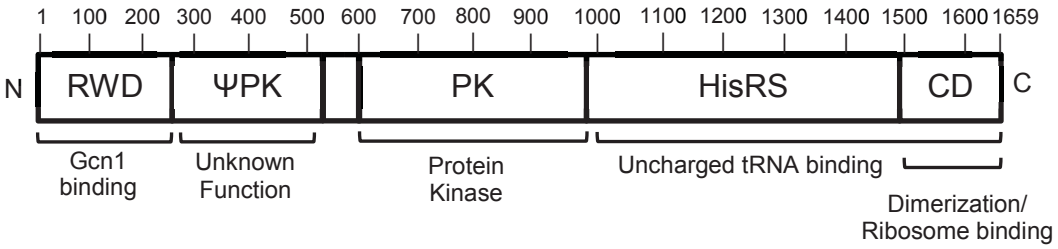

Figure 1.4 Gcn2 Domain Structure

The 1659-residue Gcn2 sequence is depicted as a rectangular box showing the experimentally identified function(s) for each regions of the protein. The residues are numbered above from N- to C-terminus.

Gcn2 is activated under multiple stress stimuli including amino acid starvation (Hinnebusch, 1984), purine starvation (Goossens *et al.*, 2001), UV light (Deng *et al.*, 2002), $NO^{\bullet}$ (Wang *et al.*, 2010), and sodium toxicity (Goossens *et al.*, 2001). The most well studied mechanism of Gcn2 activation is by amino acid starvation. Low amino acid levels in the cell result in an increase in the cellular concentration of uncharged tRNA that bind to Gcn2 *via* its HisRS domain (Wek *et al.*, 1995). The kinase domain of Gcn2 is intrinsically inert due to an occluded ATP-binding pocket (Qiu *et al.*, 2002) and activation of the kinase domain requires an interaction of uncharged tRNA with the N-terminus of the HisRS domain to reveal the ATP-binding

pocket which only occurs upon the binding of a molecule of uncharged tRNA to the HisRS domain (Qiu *et al.*, 2001, Wek *et al.*, 1989). Activation of the kinase domain of Gcn2 results in autophosphorylation of the Gcn2 homodimer on residues threonine-882 and threonine-887 (Romano *et al.*, 1998), which then phosphorylates eIF2α at serine-51 (Dong *et al.*, 2000, Qiu *et al.*, 2001).

Amino acid starvation is not the only activation signal for Gcn2. Activation of Gcn2 by glucose limitation, rapamycin and purine limitation are also dependent on the presence of a functional tRNA-binding domain (Yang *et al.*, 2000, Cherkasova and Hinnebusch, 2003, Rolfes and Hinnebusch, 1993) and are therefore likely to be mediated by binding of tRNA to Gcn2. Gcn2 undergoes post-translational modification by a variety of proteins to modulate its binding affinity for tRNA. This has been shown *in vivo* by treatment of cells with rapamycin. Under normal conditions, the protein kinase TOR (Target of Rapamycin) promotes the inhibition of the protein-phosphatase Sit4 by its inhibitor Tap42 (Di Como and Arndt, 1996). Treatment with rapamycin inactivates TOR (Brown *et al.*, 1994) resulting in the activation of Sit4. Sit4-mediated dephosphorylation of Gcn2 at serine-577 (which is constitutively phosphorylated by an as yet unknown kinase), increases the binding affinity of uncharged tRNA to Gcn2, allowing it to be activated by basal levels of uncharged tRNA (Cherkasova and Hinnebusch, 2003).

The ability of Gcn2 to become activated by amino acid starvation is dependent on its interaction with Gcn1 (Sattlegger and Hinnebusch, 2000). Gcn1 is a large protein of ~297 kDa containing a ribosomal binding domain, a RWD-binding domain and a Gcn20 binding domain (Marton *et al.*, 1993, Marton *et al.*, 1997). Because of its sequence similarities to Elongation Factor 3 (eEF3) (which functions in translation elongation to facilitate removal of the deacetylated (uncharged) tRNA from the E-site of the ribosome (Triana-Alonso *et al.*, 1995)), it has been proposed that Gcn1 acts to facilitate the transfer of uncharged tRNA from the ribosomal A-site to the HisRS domain of Gcn2, activating the kinase domain of Gcn2 (Marton *et al.*, 1993, Marton *et al.*, 1997).

The RWD-binding domain of Gcn1 forms an interaction with the RWD domain of Gcn2 (Kubota *et al.*, 2000, Sattlegger and Hinnebusch, 2000, Garcia-Barrio *et al.*,

2000), an interaction dependent on the presence of arginine-2259 in Gcn1, as mutation of this residue abolishes Gcn2 binding (Sattlegger and Hinnebusch, 2000). Without the interaction with Gcn1, Gcn2 is unable to respond to increased levels of uncharged tRNA (Sattlegger and Hinnebusch, 2000). Reports differ on the dependence of Gcn2 on Gcn1 binding under alternative activation signals. While one paper shows that Gcn2 is not activated in rapamycin-treated *gcn1*Δ cells (Kubota *et al.*, 2003), more recent work shows that it is (Nomura *et al.*, 2010). Assuming the latter is correct, it suggests that the interaction between Gcn2 and Gcn1 is only required when Gcn2 is phosphorylated at serine-557 and thus has a lower affinity for uncharged tRNA, supporting the theory that Gcn1 plays a role in facilitating the binding of uncharged tRNA to Gcn2.

Although Gcn1 is found associated with the ribosome, cytosolic pools of Gcn1 have also been observed (Marton *et al.*, 1997, Sattlegger and Hinnebusch, 2000). The cellular function of this non-ribosomal Gcn1 is as yet unknown.

Gcn1 forms a specific interaction with Gcn20, a protein of ~85 kDa that has two ATP binding domains. The sequences of these domains are highly homologous to the ATP binding cassette (ABC) family; and like Gcn1, Gcn20 displays sequence similarity to eEF3 (a member of the ABC family) (Vazquez de Aldana *et al.*, 1995). The Gcn2/1/20 complex is associated with ribosomes undergoing elongation *via* ribosomal-binding domains within both Gcn1 and Gcn2 (Marton *et al.*, 1997, Ramirez *et al.*, 1991, Sattlegger and Hinnebusch, 2000). Deletion of the *gcn20* gene reduces eIF2α phosphorylation by Gcn2 under amino acid starvation conditions *in vivo* (Vazquez de Aldana *et al.*, 1995), indicating that its presence somehow assists the efficiency of Gcn2 activation. The presence of putative ATP-binding domains, make it possible that Gcn20 may act to hydrolyse ATP to assist in the putative uncharged tRNA shuttling activity of Gcn1 (Marton *et al.*, 1997).

1.1.4 *Impact* gene

Gene imprinting is a phenomenon whereby only one parental allele is expressed and the other is inactive. The mechanism of inactivation is due to epigenetic modifications such as DNA methylation that are formed in either the maternal or paternal gamete and persist throughout the life of the resulting cell to silence that parental allele. The

impact gene (IMPrinted and AnCienT) was originally identified during a search for imprinted genes in mice which revealed that the maternal copy of mouse *impact* is silenced (Hagiwara *et al.*, 1997). Although there is a high level of conservation between mouse and human *impact*, the latter is not subject to imprinting, most likely due to lack of the intronic CpG islands in the human *impact* gene that are responsible for the epigenetic imprinting of *impact* in mice (Okamura *et al.*, 2000). It has been shown that *impact* expression is higher in organisms that display imprinting of *impact* compared to those that show biallelic expression of the gene (Okamura *et al.*, 2004). On this basis it was proposed that the imprinting of *impact* had evolved as a dosage-compensation mechanism to negate increased expression resulting from changes to the *impact* promoter (Yamada *et al.*, 1999, Okamura *et al.*, 2004, Okamura *et al.*, 2005), suggesting that it is important to tightly regulate IMPACT protein levels. Some support for this comes from the observation that over-expression of the IMPACT homologue in *Xenopus* oocytes results in abnormal embryonic development (Yamada *et al.*, 1999).

1.1.5 Yih1 is a Negative Regulator of Gcn2

Although Gcn2 and Yih1 do not share a high overall sequence homology, the regions in Gcn2 known to be important for interaction with Gcn1 are similar to those in Yih1 (Kubota *et al.*, 2000) . Yih1 has been shown to bind to the same region of Gcn1 as Gcn2 and on this basis it was proposed that Yih1 may function as a negative regulator of Gcn2 by competing with Gcn2 to interact with Gcn1 (Kubota *et al.*, 2000). When overexpressed in *S. cerevisiae*, Yih1 acted to down-regulate the general amino acid control response in an RWD domain dependent manner (Kubota *et al.*, 2000). Interestingly the response was stronger when the RWD domain was expressed on its own rather than in the context of the whole protein (Kubota *et al.*, 2000, Sattlegger *et al.*, 2011). This suggests that the Ancient domain may have a regulatory role in modulating the Yih1-Gcn1 interaction, which would in turn modulate the activation state of Gcn2. Conditions where this happens are, however, as yet unknown.

Interestingly, Yih1 knockout mutants show no phenotype under any conditions tested thus far (Sattlegger *et al.*, 2004), which appears strange given the high degree of

evolutionary conservation in the IMPACT family of proteins. However, deletion of Yih1 results in a 1.4 fold increase in glutathione levels relative to wild type yeast (Suzuki *et al.*, 2011). Given the role of glutathione as a cellular reducing agent, an increase in its levels may be a response to increased oxidative stress. How deletion of Yih1 would increase oxidative stress has not been explored and was not commented on by Suzuki *et al*.

1.1.6 Protein-Yih1 Interactions and Their Proposed Functionality

It has been shown using various methods that Yih1 is able to interact with a variety of proteins within the cell, although the specificity and hence functionality of many of the interactions has not as yet been demonstrated. Many hypotheses have been proposed to account for these interactions, few of which have actually been experimentally verified.

As outlined earlier, Yih1 has been shown to specifically interact with Gcn1. The regions of Yih1 involved in this interaction have been mapped to residues 68-132 (see Figure 1.5), found in the C terminal portion of the RWD domain, by the use of Yih1 deletion mutants in pull-down assays (Sattlegger *et al.*, 2011).

Interestingly, the ability of Yih1 to interact with Gcn1 is not sufficient to prevent activation of Gcn2. Although a fragment of Yih1 comprising residues 68-258 ($Yih1_{[68-258]}$) had a greater affinity for Gcn1 compared to wild-type, it had a reduced ability to prevent Gcn2 activation (Sattlegger *et al.*, 2011). It is therefore possible that although residues 68-132 are sufficient for Gcn1 interaction, residues 2-67 are involved in masking the binding site of Gcn2. If that is the case then it is possible that Gcn2 and $Yih1_{[68-258]}$ may be able to simultaneously bind to the same Gcn1 molecule.

It is worth noting that no *in vivo* interaction between Yih1 and Gcn1 has so far been observed when Yih1 is not overexpressed (Sattlegger *et al.*, 2004). The authors suggest Yih1 may be sequestered from interacting with Gcn1 at normal cellular concentrations. When overexpressed, this sequestering mechanism is swamped, and excess non-complexed Yih1 is free to interact with Gcn1. An alternative explanation is that the binding affinity between Yih1 and Gcn1 is such that significant

binding does not occur until a particular concentration of Yih1 is reached, signalling that inactivation of Gcn2 is necessary.

It was demonstrated by Sattlegger and colleagues (2004) that Yih1 expressed at normal cellular concentrations co-purified with monomeric actin (G-actin) in a 1:1 ratio. This interaction was further confirmed by *in vivo* and *in vitro* pull-down assays (Sattlegger *et al.*, 2004, Sattlegger *et al.*, 2011). Actin is a major component of the cellular cytoskeleton and an interaction between Yih1 and actin may implicate Yih1 in cross-talk between cytoskeletal rearrangement and translation control. The region of

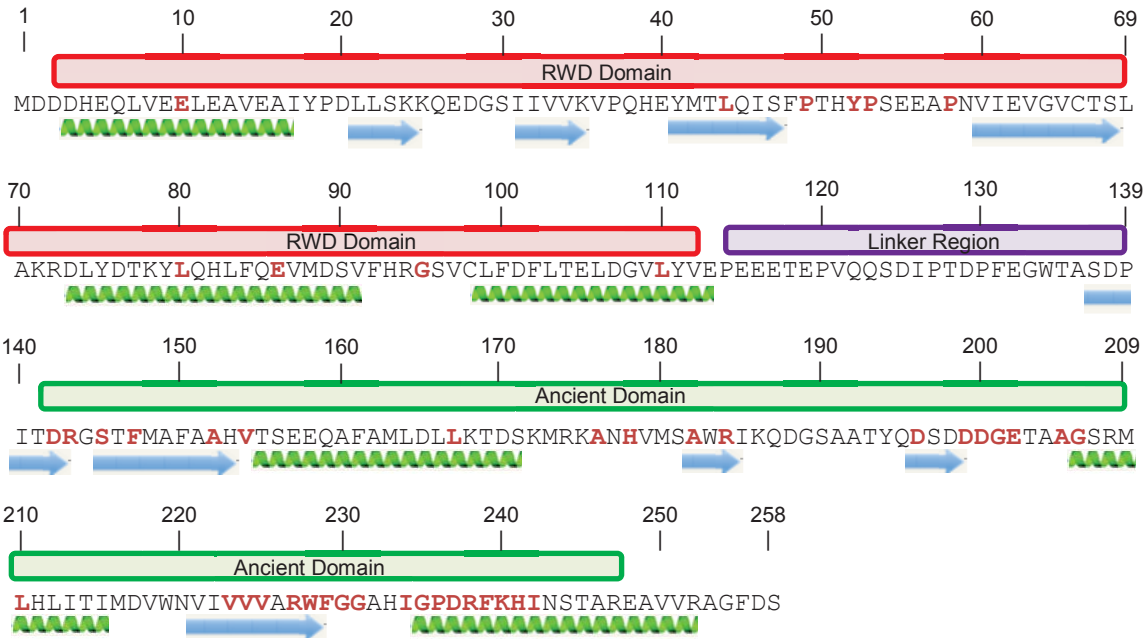

Figure 1.5 Prediction of the Domain and Secondary Structure of Yih1

The sequence of Yih1 is shown above with highly conserved residues in red. Domains are indicated above the sequence and predicted secondary structure elements are indicated below the sequence (α-helices as green helices and β-strands as blue arrows). Modified from Sattlegger *et al.* (2011).

Yih1 required for interaction with G-actin has been mapped by the use of Yih1 partial deletion mutants to residues 68-258 encompassing the same C-terminal region of the RWD domain required for interaction with Gcn1 and some or all of the Ancient domain. The overlap of the actin and Gcn1 binding sites indicate that Yih1 is likely to bind either actin or Gcn1, not both simultaneously (Sattlegger *et al.*, 2011). As alluded to above, it has been proposed that under normal conditions, Yih1 remains in

an “inactive” state. It is possible that G-actin sequesters Yih1, immobilising it until localised actin polymerisation (due to processes such as cell budding) results in the release of Yih1 which is then able to bind Gcn1, resulting in the inhibition of Gcn2 ensuring high levels of protein synthesis for the growing bud (Sattlegger *et al.*, 2004).The authors were able to provide more evidence supporting this as a heterozygous actin mutant (act1/ACT1-) with reduced actin levels was unable to elicit a general amino acid control response in the presence of Yih1. As deletion or overexpression of Yih1 does not detectably alter the actin cytoskeleton morphology (Sattlegger *et al.*, 2004), it is likely that the role of the actin:Yih1 interaction is to allow Yih1 to sense actin cytoskeletal rearrangements and relay that information to the translation machinery. The proposed sequestering of Yih1 by actin may provide an explanation as to why expression of its RWD domain alone appears to elicit a greater inactivation of Gcn2 compared to full-length Yih1 (Kubota *et al.*, 2000). Removal of the Ancient domain would prevent actin from sequestering Yih1 and thus allowing its interaction with Gcn1.

High-throughput screening (HTS) is an effective way of gaining large amounts of interaction data. The two most common methods used for HTS of protein-protein physical interactions are affinity capture followed by mass spectrometric analysis (affinity capture-MS) and yeast-2-hybrid screens. Affinity capture-MS involves the immobilisation of the target protein from a protein suspension by either immunoprecipitation or affinity tag methods followed by gel-based identification of the associated protein binding partner(s) by mass spectrometry. A yeast-2-hybrid assay involves the co-expression of two putative binding partners, one fused to the Gal4 DNA binding domain and the other fused to the Gal4 activation domain. If a physical interaction occurs between the two proteins being tested, the Gal4 activation domain will activate transcription of a lacZ reporter gene. Various proteins (other than Gcn1 and actin) that physically interact with Yih1 have been identified using HTS and these are outlined in Table 1.1. Although HTS is useful in identifying possible leads, the occurrence of false positives or false negatives can be substantial depending on the method used and therefore the data should be confirmed using other methods.

Table 1.1 Yih1 Physical Binding Partners Identified by High-Throughput Screening

Protein	Function	Experiment
URH1	Cleaves N-glycosidic bonds in nucleotides, involved in pyrimidine and NAD^+/H salvage pathways	Yeast two-hybrid (Uetz *et al.*, 2000)
UBI4	Ubiquitin, targets proteins for degradation *via* proteasomal pathway	Affinity Capture-MS (Peng *et al.*, 2003, Starita *et al.*, 2012)
PCI8	Shared subunit of COP9 signalosome and eIF3, has possible dual functions in transcriptional and translational control	Affinity Capture-MS (Krogan *et al.*, 2006)
HRB1	Poly A^+ binding protein, involved in export of mRNA from nucleus to cytoplasm	Affinity Capture-MS (Krogan *et al.*, 2006)
TEF1	Translation Elongation factor EF-1α, facilitates binding reaction of aminoacyl-tRNA and ribosomes, possible role in tRNA re-export form the nucleus	Affinity Capture-MS (Krogan *et al.*, 2006)
YJL160C	Putative protein of unknown function, non-essential gene required for sporulation	Two Hybrid (Uetz *et al.*, 2000)

Modified from Biological General Repository for Interaction Datasets (www.thebiogrid.org)

Many proteins are known to self-associate and form multimers. Gcn2 is a good example of a protein that self-associates as it is only functional as a homo-dimer (Qiu *et al.*, 1998). The evidence regarding the self-association of Yih1 is not consistent. His_6-Yih1 (31.8 kDa) elutes from a size exclusion column at the retention time expected for a 48 kDa protein, indicating that Yih1 is either an elongated monomer or is present as a compact dimer. As treatment with the chaotropic salt KI was not able to modulate the retention time of Yih1 as would be expected when dissociating a dimer, it appears that Yih1 is most probably an elongated monomer. Yeast-2-hybrid experiments also give evidence that Yih1 does not self-associate (Sattlegger *et al.*, 2011) and this is supported by preliminary NMR studies in which Yih1 appears to be monomeric under the conditions tested (A. Goroncy, personal communication).

However, the same paper by the Sattlegger group showed that both GST-Yih1$_{[2-171]}$ and GST-Yih1$_{[68-171]}$ pulled down actin in cells with endogenous Yih1 present but not in a Yih1 knockout strain suggesting that under as yet unknown conditions, the function of Yih1 may depend on oligomerisation.

1.1.7 Localisation of Mammalian IMPACT and Relationship to Memory

The tissue specific expression of the *impact* gene appears to be differentially regulated in different species. Pereira and coworkers (2005) found that mouse IMPACT protein is most abundant in the brain, with moderate levels found in the lung, kidney, spleen and testicles but no detectable levels in the heart, liver and pancreas. This is supported by the earlier findings that mouse IMPACT mRNA levels are highest in the brain (Hagiwara *et al.*, 1997). In contrast to this, human IMPACT mRNA is present in all cell types tested (Okamura *et al.*, 2000), however human IMPACT protein levels appear to be highest in the brain with moderate levels detected in the kidney, liver and spleen (Pereira *et al.*, 2005). Given that mouse *impact* is subject to imprinting but human *impact* is not, it is probable that IMPACT mRNA is also subjected to different post-transcriptional regulation between the two species and this may explain the apparent contradictions seen in tissue specific levels of IMPACT mRNA between mouse and human. In fact two species of human IMPACT mRNA have been observed (3.9 kb and 2.1 kb) and it was suggested that these two species differ in their polyadenylation post-transcriptional modifications (Okamura *et al.*, 2000) and therefore are likely to represent differentially regulated populations of IMPACT mRNA within the same tissues/cells. Tissue specific levels of phosphorylated eIF2α were shown to be inversely correlated with levels of IMPACT protein (Pereira *et al.*, 2005). The authors concluded that tissues with high levels of IMPACT must require a high level of non-phosphorylated eIF2α and therefore are likely to have a higher translational flux.

Although the brain exhibits the highest levels of IMPACT mRNA and protein, IMPACT levels are not homogenously expressed in all regions or cell types of the brain. The hypothalamus has been shown to contain the highest levels of IMPACT protein, most notably the arcuate and suprachiasmatic nuclei (Bittencourt *et al.*, 2008). These are involved in the secretion of various compounds such as dopamine, growth hormone

releasing hormone, melatonin and molecules involved in the regulation of the circadian cycle. IMPACT may function in these areas of the brain to ensure continued protein synthesis for these important regulatory processes. Within these neurons, it appears that IMPACT is present mainly in the cytoplasm and proximal portions of the dendrites and axons, but is absent from the nucleus (Bittencourt *et al.*, 2008). This is consistent with the proposed functions of IMPACT in translation and actin cytoskeletal regulation and sensing.

Although no direct experiments have been carried out to show whether IMPACT is involved in long-term memory (LTM), it has been shown that the activation state of Gcn2, and thus the levels of phosphorylated eIF2α, affect late-long-term potentiation (late-LTP) (Costa-Mattioli *et al.*, 2005). Late-LTP is the substantial, long-lasting increase in signalling between two neurons that is proposed to lead to the formation of LTM. This process is dependent on the synthesis of new proteins both to induce and maintain LTP and memory. Deletion of *gcn2* in mice results in a reduction of the threshold required to induce late-LTP and LTM (Costa-Mattioli *et al.*, 2005), which is most likely due to the increased levels of general protein synthesis that occurs when levels of phosphorylated eIF2α are low. The same group also showed that eIF2α S51A mutants that are unable to be phosphorylated by Gcn2 had a reduced threshold for inducing late-LTP and LTM (Costa-Mattioli *et al.*, 2007), supporting the involvement of Gcn2 in memory processes. The authors went on to note that it appears that “Gcn2 regulates the switch from short-term to long-term memory”. As the presence of Gcn2 inhibits protein synthesis which is required for LTM formation, inactivation of Gcn2 by the high levels of IMPACT in the brain may allow higher rates of protein synthesis and thus an increased ability to form LTM (Sattlegger *et al.*, 2011).

1.1.8 The Link Between Indoleamine 2,3 Dioxygenase and IMPACT

Indoleamine 2,3 dioxygenase (IDO) is the first enzyme in the tryptophan catabolic pathway which is involved in the *de novo* biosynthesis of the redox pairs $NAD(P)^+$/NAD(P)H. IDO acts to breakdown tryptophan to form N-formylkynurenine which is subsequently converted to kynurenine (Mehler and Knox, 1950), a toxic product that has been shown to non-enzymatically modify protein residues by

forming covalent adducts (Garner *et al.*, 2000). IDO is activated by interferon gamma which is produced during infection, and it is thought that part of the role of IDO may be to deplete levels of tryptophan upon infection as a protective mechanism to limit pathogen growth (Pfefferkorn, 1984). In T-cells, high activity of IDO depletes the cellular levels of tryptophan, activating Gcn2 and resulting in cell death. However, Gcn2 is not activated under these same conditions in fibroblasts or pancreatic tissues (Jalili *et al.*, 2009, Habibi *et al.*, 2010). IMPACT displays high levels in the same tissues as IDO apart from the notable exception of T-cells where it is present at very low levels (Habibi *et al.*, 2010). Habibi and co-workers (2010) showed that the high levels of IMPACT in fibroblasts act to protect the cells from IDO-induced cell death by repressing Gcn2 activation. However, it was not able to completely rescue the cells from the toxic effects of a high kynurenine concentration.

1.1.9 Gaps in the Structural Biology of Yih1

The structure of a protein is intrinsically linked to its function and thus the elucidation of the structure of a given protein can provide clues to its function. The structure of Yih1 is yet to be solved; the closest available are models based on protein structures sharing moderate sequence similarity to Yih1 (See Figure 1.1 and Figure 1.2). Although such models agree with data from circular dichroism experiments that suggest YIH1 contains ~29% α-helices, 24% β-strand, 20% turns, and 28% random structure (Sattlegger *et al.*, 2011); the lack of finer differences mean that the overall shape of the molecule is not known, including the relative orientation of the two domains to each other along with the identity of putative ligand binding domains. This lack of structural knowledge impedes the understanding of the functionality of Yih1. As described in Section 1.1.6, Yih1 appears to exist as an elongated monomer, suggesting there are little if any interactions occurring between the two domains. Given the predicted disorder and thus flexibility of the linker region joining the two domains as shown in Figure 1.6, it is possible that the two domains of Yih1 may interact with one another under as yet unknown conditions such as upon interaction with another molecule. A structure of Yih1 bound to either Gcn1 or G-actin would provide the evidence for or against this theory.

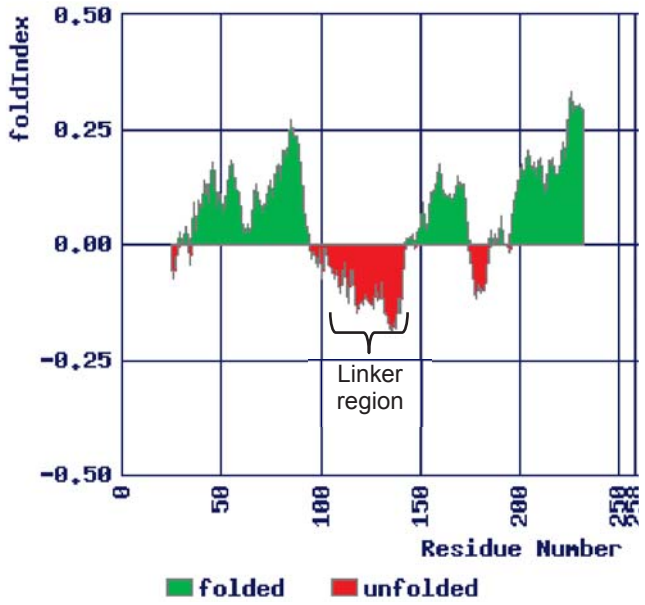

Figure 1.6 Foldindex Disorder Prediction of Yih1

The sequence of Yih1 was submitted to the FoldIndex© server (http://bip.weizmann.ac.il/fldbin/findex) using default values.

1.2 AIMS OF THIS INVESTIGATION

The primary aim of this investigation was to solve the structure of Yih1 by the expression, purification, crystallisation and X-ray diffraction of Yih1. Given difficulties in crystallising Yih1, additional effort was put into further characterising the protein by investigating and attempting to control the formation of homooligomers of Yih1, and optimise interactions with other molecules to both increase the chances of crystallisation and also to enhance our knowledge of the protein to attempt to further understand the roles it may play *in vivo*.

2. MATERIALS AND METHODS

2.1 Equipment

2.1.1 Polymerase Chain Reaction

Polymerase chain reaction (PCR) thermal cycling was performed by a T gradient PCR cycler (Biometra; Goettingen, Germany).

2.1.2 Fast Protein Liquid Chromatography

Unless stated otherwise, Fast Protein Liquid Chromatography was performed on an ÄKTA explorer system (GE Healthcare; USA) at 4°C.

2.1.3 Purified Water

Purified water was obtained from a Sybron/Barnstead NANOpure II filtration system (Maryland, USA) comprised of two ion exchange and two organic filter cartridges. This water is referred to as H_2O throughout this thesis.

2.1.4 Filter Equipment

Where indicated, sterile Minisart syringe filters of 0.22 µm and 0.80 µm (Sartorius Stedim Biotech; France) were used to filter samples/buffers less than 60 mL. Buffers larger than 60 mL were filtered using a 0.22 µm filter (Millipore; MA, USA).

2.2 Materials and Methods

2.2.1 Media

2.2.1.1 Sterilisation

Media was sterilised by autoclaving at 121°C and 2 x 10^5 Pa for 20 minutes. Solutions that have undergone autoclaving are referred to as “sterile” in this thesis.

2.2.1.2 Luria-Bertani (LB) media

25 g of LB media (Invitrogen; Scotland) was made up to 1 L with H_2O and autoclaved. LB containing appropriate antibiotics is referred to as LB-AB in this thesis. Solid media was made by the addition of agar (Bacto; Mt Pritchard, NSW, Australia) to a final concentration of 1% (w/v) in LB before being autoclaved.

2.2.1.3 SD media

1.9 g Yeast Nitrogen base (Formedium; Hunstanton, England) and 5 g Ammonium Sulfate (Ajax UNIVAR; VIC, Australia) was made up to 950 mL with H_2O and autoclaved. 50 mL of filter-sterilised 40% glucose, 20 mL of filter-sterilised ILV (3.28 g/L isoleucine, 13.1g/L leucine, 2.95g valine) and 10 mL of filter-sterilised tryptophan (8 g/L) was added aseptically. This is referred to as SD-glucose-Trp in this thesis. Solid media was made by the addition of Agar (Bacto; Mt Pritchard, NSW, Australia) to a final concentration of 2% (w/v) in LB before being autoclaved.

2.2.1.4 Minimal Media Components

Minimal Media Base:

Na_2HPO_4	3.39 g
KH_2PO_4	1.5 g
NaCl	0.25 g
1M $MgSO_4$	1 mL
1M CaCl	50 µL
H_2O	To 500 mL

Sterilised by autoclave

Metal and Labelling Mix:

Glucose (unlabelled or 13C labelled)	1.75 g
$^{15}NH_4Cl$	0.25 g
Thiamine	5 mg
$Fe_{(III)}Cl_3$	6.75 mg
H_2O	10 mL

Filter sterilised

2.2.2 Bacterial Strains Used

Table 2.1 Bacterial Strains used in this project

Strain Name	Genotype	Source
BL21 (DE3)	T7 polymerase expressed from IPTG-induced LacUV5 promoter to allow high expression of plasmid-encoded protein driven by T7 promoter	Stratagene; CA, USA.
XL-1 Blue	Endonuclease deficient to allow higher quality plasmid extraction	Stratagene; CA, USA.
C41	Derived from BL21, more tolerant of toxic protein expression due to uncharacterised mutation(s)	Lucigen; WI, USA.

2.2.3 Plasmid Constructs Used

Initial constructs were kindly provided by either Dr Evelyn Sattlegger (INS, Massey University, Auckland, New Zealand) or Dr Beatriz Castilho (Departamento de Microbiologia, Universidade Federal de São Paulo, São Paulo, Brazil).

Table 2.2 Plasmids used in this project

Plasmid Name	Encoding	Size	Vector	Source
pES317-15b	Yih1	6.4 kb	pET28a[a]	E. Sattlegger
pES318-110-16b	Yih1-His_6	6.4 kb	pET28a[a]	E. Sattlegger
pES319-110-17c	His_6-Yih1	6.4 kb	pET28a[a]	E. Sattlegger
pBE499	His_6-thrombin-T7 tag-Yih1C67A,C99A	6.5 kb	pET28a[a]	B. Castilho
pES123-B1	GST-gcn1 [2052-2428]	6.0 kb	pGEX-6p-3[b]	E. Sattlegger
pETDUET-actinA4	*S. cerevisiae* actin	6.5 kb	pETDUET-1[c]	E. Sattlegger
pNAT56	Yih1 EE56-57AA	6.4 kb	pET28a[a]	This study
pNAT116	Yih1 EEE116-118AAA	6.4 kb	pET28a[a]	This study
pNAT56.116	Yih1 EE56-57AA,EEE116-118AAA	6.4 kb	pET28a[a]	This study
pNAT04	His_6-Yih1[137-253](Ancient Domain)	5.7 kb	pET32a(*Bam*HI)[d]	This study

[a] See appendix 4 , [b] See appendix 5 , [c] See appendix 6, [d] See appendix 7.

2.2.4 Storage of Cultures

2.2.4.1 Bacterial

E. coli strains were stored in the form of glycerol stocks at -80°C. Cells were streaked onto a sterile LB-AB-agar plate and grown overnight at 37°C. A colony was picked and inoculated into 5 mL of sterile LB-AB and grown at 37°C with shaking until reaching an OD_{600} of ≈0.5. 700 µL of this log phase culture was added to 300 µL of sterile 50% w/v glycerol and flash frozen in liquid nitrogen before being transferred to a -80°C freezer for long term storage.

2.2.4.2 Yeast

S. cerevisiae strains were stored in the form of glycerol stocks at -80°C. Cells were streaked onto sterile SD-glucose-Trp agar and grown at 30°C for 2 days. Single colonies were picked and inoculated into 5 mL of sterile SD-glucose-Trp then grown at 30°C with shaking overnight to an OD of ≈ 1. 700 µL of this culture was added to

300 µL of sterile 50% w/v glycerol and transferred to a -80°C freezer for long term storage.

2.2.5 Antibiotics

Antibiotic 1000x stock solutions were prepared as outlined in Table 2.3, filter sterilised with a 0.22 µm minisart filter and stored as 1 mL aliquots in sterile Eppendorf tubes at -20°C. Antibiotics were diluted 1/1000 into cooled (<50°C) sterile media.

Table 2.3 Antibiotics Used in this Study

Antibiotic	Stock concentration	Solvent	Sourced from
Ampicillin Na-salt (Amp)	100 µg/mL	H_2O	Sigma
Kanamycin sulfate (Kan)	30 µg/mL	H_2O	Sigma
Chloramphenicol (Cam)	34 µg/mL	20% ethanol	Applichem

2.2.6 Agarose Gel Electrophoresis

2.2.6.1 Gel Preparation

Agarose (Sigma, Auckland, NZ) was dissolved in 30 mL of TAE buffer by heating in a microwave then subsequently made up to 30 mL with H_2O to compensate for evaporation. The solution was allowed to cool slightly before being poured into the gel casting apparatus (Minisubcell GT, Biorad; Milan, Italy) and left to set.

2.2.6.2 Gel Electrophoresis

Sample preparation consisted of the addition of 6x DNA loading Buffer (2% Bromophenol blue, 50% glycerol) to the sample to yield 1x concentration. After loading, gels were run at 70 V till the dye had migrated over halfway through the gel.

2.2.6.3 Ethidium Bromide Staining of Gels

Agarose gels were placed into a 2 µg/mL ethidium bromide (USB, Ohio, USA) solution for 30 minutes before being transferred to H_2O for 15 minutes to remove

excess ethidium bromide. Gels were scanned using a "Biorad Gel Doc XR^{+}" equipped with Image Lab™ software.

2.2.7 Transformation of *E. coli* Cells

2.2.7.1 Production of Chemically Competent Cells

To make cells amenable to transformation, 50 mL of LB was inoculated with 50 µL of an overnight LB culture of the *E. coli* strain and grown to an OD of ~0.3. The culture was chilled on ice for 15 minutes then centrifuged at 3000 x g for 15 minutes at 4°C. The supernatant was removed and the cell pellet was resuspended in 16 mL of filter-sterilized transformation buffer 1 and incubated on ice for 15 minutes. The cells were spun down as before, resuspended in 4 mL filter-sterilized transformation buffer 2, then stored in 50 µL aliquots at -80°C until required.

Transformation Buffer 1:

RbCl	12 g/L
$MnCl_2 \cdot 4H_2O$	10 g/L
1M potassium acetate pH 7.5	30 mL/L
$CaCl_2 \cdot 2H_2O$	1.5 g/L
glycerol	15%

Transformation Buffer 2:

0.5M MOPS pH 6.8	20 mL/L
RbCl	1.2 g/L
$CaCl_2 \cdot 2H_2O$	11 g/L
glycerol	15%

2.2.7.2 Transformation of Chemically Competent Cells

To transform bacterial strains with a plasmid, 50 ng of plasmid DNA was added to 50 µL of thawed competent *E. coli* cells and incubated on ice for 30 minutes. The cells were then heat shocked at 42°C for 45 seconds in a TS1 Thermoshaker heating block (Biometra; Goettingen, Germany) and placed back on ice for 5 minutes. After addition of 900µL of sterile LB, the cells were incubated at 37°C with shaking for 30

minutes (1 hour if ligating). 200 µL of culture was then plated onto sterile LB-AB-agar and incubated at 37°C overnight. A 'no DNA control' was also prepared by adding a volume of sterile H_2O equal to that of the plasmid DNA to 50 µL of competent cells.

2.2.8 Plasmid Isolation

5 mL of LB-AB was inoculated with a single colony from an overnight LB-AB-agar plate and grown overnight at 37°C with shaking. 3 mL of this culture was harvested by centrifugation at 10,000 x g for 1 minute and plasmid isolation was performed using a "High Pure Plasmid Isolation Kit" (Roche; Auckland, NZ) according to the manufacturer's instructions. Plasmid was eluted from the kit column with 100 µL of TE buffer.

TE Buffer :

Tris 10 mM

Na_2EDTA 1 mM

pH 8.0

2.2.9 Measurement of Optical Density of Cultures

Cell culture optical density was measured at 600 nm on a Smart Spec TM Plus spectrophotometer (BioRad; Milan, Italy). If required, dilution was performed with sterile culture media. Sterile culture media was used as the blank.

2.2.10 Measurement of Protein Concentration

Protein concentration was determined by UV absorbance at 280 nm. Measurements were done on a Smart Spec TM Plus (BioRad; Milan, Italy) using a trUView cuvette (BioRad; Milan, Italy). Appropriate buffers were used to zero the instrument. Protein concentrations were calculated using Beers Law and the appropriate extinction coefficient as calculated by ProtParam (ExPASy- http://web.expasy.org/protparam/).

2.2.11 Measurement of Nucleic Acid Concentration

The concentration of nucleic acid samples was measured using a Nanodrop ND-1000 spectrophotometer (Thermo Scientific; Wilmington, DE, USA).

2.2.12 Polyacrylamide Gel Electrophoresis

2.2.12.1 SDS-PAGE

Proteins were separated on the basis of size by discontinuous SDS-PAGE according to Lammeli et al. (1970). Gel solutions were prepared as outlined in Tables 2.4 and 2.5. Solutions were degassed for a minimum of 10 minutes before the addition of TEMED and ammonium persulfate and gels were cast and run using a Biorad Mini-Protean II system. One part 10X SDS-PAGE sample buffer was added to 9 parts sample and boiled for 5 minutes before loading. Electrophoresis was performed at room temperature at 200 V until the dye front reached the bottom of the gel (approximately 45 minutes).

Table 2.4 Preparation of Separating Gel for SDS-PAGE

Component	10%	12.5%	15%
1.5M Tris-HCl, pH8.8	2.5 mL	2.5 mL	2.5 mL
40% Acrylamide:Bis 29.1:0.9	2.5 mL	3.125 mL	3.75 mL
10% (w/v) SDS	100 µL	100 µL	100 µL
H_2O	4.79 mL	4.165 mL	3.54 mL
TEMED	10 µL	10 µL	10 µL
10% ammonium persulfate	100 µL	100 µL	100 µL
Total Volume	10 mL	10 mL	10 mL

Table 2.5 Preparation of Stacking Gel for SDS-PAGE

Component	4%
0.5M Tris-HCl, pH 6.8	1.25 mL
40% Acrylamide:Bis 29.1:0.9	0.5 mL
10% (w/v) SDS	50 µL
H_2O	3.17 mL
TEMED	5 µL
10% ammonium persulfate	25 µL
Total Volume	5 mL

10X SDS-PAGE sample buffer:

0.5 M Tris-HCl pH 6.8	2 mL
Glycerol	2 mL
10% (w/v) SDS	3.2 mL
DTT	0.77 g
0.1% (w/v) Bromophenol blue	0.8 mL

5x Running Buffer:

Tris	15 g
Glycine	72 g
SDS	5 g
H_2O	Up to 1L

2.2.12.2 Native PAGE

Proteins were separated on the basis of their mass to charge ratio by discontinuous native PAGE, a modification of SDS-PAGE. The same solutions were used as with SDS-PAGE (2.2.12.1) except that SDS and DTT were excluded and their volumes replaced with H_2O. 9 µL of sample was mixed with 1 µL of 10x native PAGE sample buffer, loaded directly onto the gel (not boiled) and electrophoresed at 150 V at 4°C until the dye front reached the bottom of the gel (unless noted otherwise).

2.2.12.3 Urea PAGE

Nucleic acids were separated on the basis of mass by urea-PAGE where the urea and high temperatures reached during electrophoresis act to denature any nucleic acid secondary structure.

12% urea polyacrylamide gels were prepared by combining 1.25 mL of 10x TBE, 5.25 g of urea, 3.75 mL of 40% acrylamide and 3.7 mL of H_2O and heating the mixture gently in a microwave for 15 seconds to dissolve the urea. The solution was syringe filtered with a 0.22 µm filter into a sidearm flask and degased for 5-10 minutes. After the addition of 12.5 µL of TEMED and 75 µL of 10% APS, the gel was cast, set and loaded then run using a Mini-Protean II system (Biorad; Hercules, CA,

USA). 1x TBE was used as the running buffer and the gel was pre-electrophoresed at 240 V for 15 minutes to warm up silverthe apparatus. Samples were prepared by adding an equal volume of sample buffer (100 µL formamide, 1 µL 0.5M EDTA (pH 8) and 1 µL bromophenol blue) to the RNA sample, heated at ~95°C for 1 minute to denature the RNA, then placed on ice until loaded. The samples were run at 180 V for approximately 2 hours before undergoing silver staining (2.2.12.6).

10x TBE Buffer:

Tris	890 mM
Boric acid	890 mM
Na_2EDTA	20 mM
H_2O	Up to 1L

2.2.12.4 Coomassie Blue Staining of Gels

Gels were stained with 0.1% Coomassie Brilliant Blue R-250 in 40% methanol/10% acetic acid for 30 minutes (or overnight) at room temperature with gentle agitation. Destaining was performed by replacing the staining solution with destaining solution (40% methanol/10% acetic acid) and incubating until background staining was removed. Gels were then placed into H_2O to be photographed and stored.

2.2.12.5 Stains-all Staining of Polyacrylamide Gels

Gels were fixed in 25% isopropanol for 15 minutes before incubation overnight in the Stains-all working solution (5 mL formamide, 7 mL isopropanol, 7.25 mL H_2O and 25 mg of Stains-all (Sigma; Auckland, NZ)) on a shaker and protected from light with aluminium foil. Gels were destained in H_2O with light until discrete bands were visible.

2.2.12.6 Silver Staining of Polyacrylamide Gels

Silver staining can detect both protein and nucleic acids. All steps were performed with gentle agitation. The gel was fixed with a 50% ethanol/10% acetic acid solution overnight, rinsed with H_2O for 5 minutes three times, washed in a 0.2 g/L $Na_2S_2O_3.5H_2O$ solution for 2 minutes, rinsed with H_2O for 5 minutes, incubated in a 2

g/L $AgNO_3$ solution for 20 minutes, rinsed with H_2O for 20 seconds twice before being developed in a solution containing 6 g Na_2CO_3, 50 µL of 37% formaldehyde, and 2 mL of a 0.2 g/L $Na_2S_2O_3.5H_2O$ solution in a final volume of 100 mL. To stop the reaction, the gel was incubated in cold 5% acetic acid for 5 minutes before being rinsed in H_2O. It was stored in a solution of 30% methanol and 3% glycerol.

2.2.13 Protein Expression Trials

To assess expression and solubility of recombinant protein, cells were grown to an OD_{600} of ~0.5 at 37°C. The culture was moved to 25°C and protein expression was induced by the addition of IPTG to a final concentration of 0.1 mM. Cultures were left to grow with shaking overnight before being harvested. The volume (µL) of culture to harvest by centrifugation was calculated to be $500/OD_{600}$. The resulting cell pellet was resuspended in 50 µL 1x SDS-PAGE sample buffer, boiled for 10 minutes and subjected to SDS-PAGE. An uninduced control sample was also analysed for comparison.

2.2.14 Protein Solubility Trials

Cells were grown and protein expression was induced as described in Section 2.2.13. After harvesting a volume of culture (µL) (determined by the calculation 1000/OD) by centrifugation, the cells were resuspended in 300 µL PBS buffer and subjected to sonication to achieve lysis. The whole cell extract was spun at 16,000 x g in a microcentrifuge for one minute to pellet unlysed cells, cellular debris and insoluble protein. The pellet was resuspended in 300 µL PBS by vortexing. The supernatant and resuspended pellet were analysed by SDS-PAGE. An uninduced control sample was also analysed for comparison.

PBS buffer:

NaH_2PO_4	10.0 mM
NaCl	150 mM

Adjusted to pH 7.4 with 10mM Na_2HPO_4

2.2.15 DNA Sequencing

Sequencing was performed by the Massey Genome Service using a capillary ABI3730 Genetic Analyzer (Applied Biosystems Inc.) on samples prepared according to their instructions. Primers used are listed in Appendix 8.

2.2.16 Site-Directed Mutagenesis by PCR

Quikchange site-directed Mutagenesis works on the principle that amplification of a circularised double-stranded plasmid using complementary primers carrying the required mutation flanked by sequences matching those flanking the site desired for mutation will result in the introduction of that mutation. Removal of non-mutant plasmid is achieved by digestion with the methylation-dependent restriction enzyme *Dpn*I. *Dpn*I specifically degrades the wild-type Dam-methylated parental DNA template, leaving the unmethlated synthetic DNA carrying the mutation.

Site-directed mutagenesis was performed using a Quikchange XL Site-Directed Mutagenesis Kit (Stratagene; CA, USA). 50 µL PCR reactions were setup (as outlined in Table 2.6) in sterile thin-walled PCR tubes on ice, then subjected to temperature cycling (according to Table 2.7) in a PCR cycler T grade (Biometra; Goettingen, Germany). Primer sequences are given in Appendix 8.

Table 2.6 Components of Site-Directed Mutagenesis Reaction

Solution	Volume	Final Concentration
10x Reaction Buffer	5 µL	1x
10 mM dNTP mix	0.5 µL	0.1 mM
1 pmol/µL Forward Primer	12.5 µL	0.25 pmol/µL
1 pmol/µL Reverse Primer	12.5 µL	0.25 pmol/µL
5 ng/µL pES137-15b	2 µL	0.2 ng/µL
H_2O	16.5 µL	-
2 U/µL TURBO Polymerase	1 µL	0.05 units/µL
Total Volume	50 µL	

Table 2.7 Thermal Cycling Protocol for Site-Directed Mutagenesis Reaction

Process	Temperature	Time	Repeat
Denaturation	95°C	5 minutes	-
Denaturation	95°C	50 seconds	18 Cycles
Annealing	60°C	50 seconds	
Extension	70°C	7 minutes	
Extension	70°C	7 minutes	-

To the completed PCR reaction, 1 µL of the restriction enzyme *Dpn*I (Stratagene; CA, USA) was added and the reaction was incubated at 37°C for 1 hour. 4 µL of the digested reaction mix was transformed into 50 µL of *E. coli* XL-1 Blue competent cells (2.2.7)

2.2.17 PCR for Cloning

Solutions were mixed in sterile thin walled PCR tubes on ice as indicated in Table 2.8 before being subjected to temperature cycling according to the parameters outlined in Table 2.9. DNA was purified after the reaction using a "DNA Clean and Concentrate kit" (Zymo; CA, USA) according to manufacturer's instructions, and the DNA was eluted in 10 µL of elution buffer.

Table 2.8 Components of Ancient Domain PCR

Solution	Volume	Final Concentration
5x iProof HF Buffer (Biorad)	10 µL	1x
10 mM dNTP mix (Biorad)	1 µL	0.2 mM
100 mM Forward Primer	0.25 µL	0.5 mM
100 mM Reverse Primer	0.25 µL	0.5 mM
2 mg/ml pES137-15b	2 µL	0.08 mg/mL
H_2O	36 µL	-
2 U/µL iProof Polymerase (Biorad)	0.5 µL	0.02 U/µL
Total Volume	50 µL	

Table 2.9 Thermal Cycling Protocol for Ancient Domain PCR

Process	Temperature	Time	Repeat
Denaturation	98°C	30 seconds	-
Denaturation	98°C	10 seconds	30 Cycles
Annealing	63°C	30 seconds	
Extension	72°C	30 seconds	
Extension	72°C	10 minutes	-

2.2.18 Restriction Enzyme Digest

Restriction enzyme digests were set up according to manufacturer's instructions before incubation at 37°C for 2 hours.

2.2.19 Ligation

Restriction enzymes and other impurities such as buffer salts were removed by using a DNA Clean & Concentrate Kit (Zymo; CA, USA) according to manufacturer's instructions and eluted in 10 µL of EB buffer. The purified product was quantified using UV absorbance (2.2.11). Digested insert and vector were ligated in a 10 µL reaction volume containing ligation buffer (1x) and 0.5 µL of T4 Ligase (Roche; Auckland, NZ) using a 3:1 molar ratio of insert to vector. The reaction was incubated for 1 hour at 37°C after which the T4 ligase was inactivated by heating at 65°C for 20 min. The reaction was dialysed against H_2O to remove the ligation buffer components by placing a drop on a Type VS 0.022 µm filter membrane (Millipore; MA, USA) which was then floated on water.

2.2.20 Large Scale Protein Expression

1 L of sterile LB-AB was inoculated with 10 mL of a 20 mL overnight *E. coli* culture in LB-AB and incubated at 37°C with shaking to an OD_{600} of 0.5. Cultures were induced by the addition of filter-sterilised IPTG to a final concentration of 1 mM and the culture was incubated at 25°C overnight with shaking.

2.2.21 Large Scale Cell Harvesting and Lysis

Cells were harvested by centrifugation in a GS3 rotor (Piramoon Technologies Inc.; Santa Clara, USA) at 6000 rpm (6090 x g) for 15 minutes at 4°C in a Sorvall Evolution RC centrifuge before resuspension in 20 mL of the appropriate buffer including Complete™ EDTA-free protease inhibitor (Roche; Auckland, NZ) at 1x concentration. Cells were lysed by liquid homogenization using two passages through a French pressure cell (Aminco Instruments Co.;USA) at 4 kPa with a Wabash hydraulic press (Wabash, USA). DNase I (Sigma; Auckland, NZ) was added to a final concentration of 50 µg/mL and the mixture was incubated on ice for 30 minutes. To remove cellular debris and unlysed cells, the cell lysate was centrifuged at 16000 rpm (30600 x g) for 30 minutes at 4°C in an SS34 rotor (Piramoon Technologies Inc.; Santa Clara, USA).

2.2.22 Anion Exchange Chromatography

Clarified cell lysate (~20 mL) was dialysed against 20 volumes of AEX buffer overnight at 4° with two changes of buffer. When the conductivity was roughly equal to that of the buffer, the sample was syringe-filtered through a 0.8µm filter to remove particulates before being loaded at 1 mL/min onto a Hiload 26/10 Q sepharose HP column (GE Pharmica, USA) pre-equilibrated with AEX buffer. Protein was eluted using a gradient between 0 and 1M NaCl at 1 mL/min and collected in 10 mL fractions which were subsequently analysed by 12.5% SDS-PAGE. The purest fractions were pooled and concentrated in 10000 MW cutoff concentrators (GE Healthcare, USA).

<u>AEX buffer:</u>

MES 20.0 mM

TCEP 2.0 mM

EDTA 2.0 mM

Made to pH 5.8 with NaOH

2.2.23 Immobilized Metal Affinity Chromatography

Clarified cell lysate (~20 mL) was syringe-filtered through a 0.8 µm filter and loaded onto a 5 mL HisTRAP column (GE Healthcare, USA) pre-equilibrated with IMAC buffer at room temperature. A Microtube pump MP-3 peristaltic pump (EYELA; Tokyo, Japan) was used to control the mobile phase. Protein was eluted stepwise with increasing concentrations of imidazole: 30 mM, 40 mM, 50 mM, 100 mM, 250 mM and 500 mM imidazole. Fractions were collected on ice and analysed by 12.5% SDS-PAGE. The purest fractions were pooled and concentrated in 10000 MW cutoff concentrators (GE Healthcare, USA) Complete™ EDTA-free protease inhibitor (Roche; Auckland, NZ) was added to 1x concentration.

IMAC buffer:

Tris	20.0 mM
NaCl	500.0 mM
TCEP	2.0 mM
Imidazole	20.0 mM

Made to pH 8.0 with HCl

2.2.24 Size Exclusion Chromatography

The sample (~5 mL) was syringe-filtered through a 0.22µm filter and loaded (250 µL per run) onto a pre-equilibrated Superdex 75 10/300 GL (GE Healthcare, USA) at 4°C and eluted isocratically at 0.5 mL/min with 1.2CV of SEC buffer. 300 µL fractions were collected and analysed by 12.5% SDS-PAGE. The purest fractions were pooled and concentrated in 10000MW cutoff concentrators (GE Healthcare, USA), snap frozen in liquid nitrogen and stored at -80°C until required.

SEC buffer:

NaH_2PO_4	10.0 mM

Adjusted to pH 7.0 with 10 mM Na_2HPO_4

TCEP	2.0 mM
EDTA	2.0 mM

Readjusted to pH 7.0 with HCl

2.2.25 Large Scale Expression of Labelled Protein for NMR

An overnight *E. coli* culture in LB-AB was used to inoculate 1 L of LB-AB (1% inoculum) and grown overnight at 37°C. Cells were harvested by centrifugation in sterile bottles in a GS3 rotor (Piramoon Technologies Inc.; Santa Clara, USA) at 6000 rpm (6090 x g) for 15 minutes at 4°C in a Sorvall Evolution RC. Cells were washed in 200 mL minimal media base (2.2.1.4) to remove LB media components, and re-centrifuged. Cells were resuspended in 250 mL minimal media base and 10 mL of metal and labelling mix (2.2.1.4) in a 1 L flask and incubated with shaking at 37°C for 1 hour to recover. Recombinant protein expression was then induced by the addition of 260 µL of 1M IPTG and the culture was incubated overnight at 25°C.

2.2.26 Far UV Circular Dichroism

Protein (2 mg/mL in SEC buffer, pH 7) was diluted to a final concentration of 0.01 mg/mL with H_2O in a final volume of 3 mL, degassed and introduced to a clean 10mm pathlength quartz cell (Hellma; Germany). Buffer was diluted in the same way to act as a control. Circular Dichroism spectra were measured at 25°C on a Chirascan spectrophotometer (Applied Photo Physics; Surrey; UK). A wavelength range of 190nm-250nm was measured using a wavelength interval of 0.5 nm, time to point of 0.5 seconds, and a bandwidth of 1nm. Ten replicates were performed per run.

2.2.27 HPLC

Yih1 samples were loaded onto a Jupiter C18 column, 4.6mm x 250mm with a 5 µM particle size (Phenomenex; CA, USA) pre-equilibrated in 0.1% trifluoroacetic acid using a Dionex Summit HPLC system (CA, USA). A gradient up to 100% Acetonitrile was performed and peak fractions were collected manually into Protein Lobind microcentrifuge tubes (Eppendorf; Germany)

2.2.28 Mass Spectrometry

Peak fractions collected from HPLC were subjected to Mass spectrophotometric analysis on an Agilent 6220 Q-TOF spectrometer. Data was acquired and processed using Mass Hunter Workstation Software, Qualitative Analysis, Version B.03.01 and Rev B.02.01 SP1.

2.2.29 Gcn1 Expression, Harvesting and Lysis

Production of recombinant Gcn1, harvesting and lysis of cells were carried out as outlined in Sections 2.2.20 and 2.2.21, the exception being that a 2.5 L culture was grown in a Minifo fermenter (Infors HT; Bottmingen, Switzerland).

2.2.30 Gcn1 Purification by Glutathione-agarose

The clarified cell extract (~25 mL) was made to 1% Triton X-100 and filtered through a 0.80 µm syringe filter before overnight incubation with glutathione-agarose prepared according to manufacturer's instructions and pre-equilibrated with equilibration buffer (GEQ buffer) at 4°C. Triton X-100 was included to minimise non-specific binding to the resin. The flow-through was collected and the resin was washed with 5 CV of GEQ buffer containing 1% Triton X-100. The protein-bound resin was re-equilibrated in 5 CV of PreScission cleavage buffer (PC buffer) before the addition of 10 units/mL of PreScission Protease (GE Healthcare, USA) diluted in 1 CV of PC buffer and incubated with rotation overnight at 4°C. The resin was packed into a column and the flow-through was collected. The resin was then washed with 4 CV of PC buffer before elution of the protein with 4 CV of glutathione elution buffer (GEL buffer). Fractions were analysed by SDS-PAGE (2.2.12.1).

<u>GEQ buffer:</u>

NaH_2PO_4	10.0 mM
Adjusted to pH 7.4 with 10 mM Na_2HPO_4	
NaCl	150 mM
DTT	1 mM
Readjusted to pH 7.4 with HCl	

PC buffer:

Tris	50 mM
NaCl	150 mM
DTT	1 mM
EDTA	1 mM

pH 7.0

GEL buffer:

Tris	50 mM
Reduced Glutathione	25 mM

pH 9.0

2.2.31 Actin Expression and Preparation of Cellular Extract

BL21 (DE3) *E .coli* transformed by heat shock (2.2.7.2) with actin-pETduet-A4 were grown and harvested as outlined in sections 2.2.20 and 2.2.21. Cells were resuspended in depolymerisation buffer and lysed two passages through a French pressure cell (Aminco Instruments Co.; USA) at 4 kPa using a Wabash hydraulic press (Wabash, USA.) Insoluble cellular debris was removed by centrifugation at 16000 rpm (30600 x g) for 30 minutes in an SS34 rotor (Piramoon Technologies Inc.; Santa Clara, USA) at 4°C.

Depolymerisation buffer:

Tris	10.0 mM
Na_2ATP	0.2 mM
DTT	1.0 mM
$CaCl_2$	0.2 mM

Made to pH 8.0 with HCl

2.2.32 Actin and Yih1 Size Exclusion Chromatography

Lyophilized actin (95%, Sigma; Auckland, NZ) was reconstituted in depolymerisation buffer to a concentration of 7.5 mg/ml. Samples containing 750 µg actin and 522 µg Yih1 (equimolar amounts) were made up to 200 µL with depolymerisation buffer and left to interact for two hours before being loaded on a Superdex 200 10/300 column (GE Healthcare; USA) pre-equilibrated with depolymerisation buffer. The column was isocratically eluted with depolymerisation buffer using a flow rate of 0.4 mL/min and 300 µL fractions were collected then analysed by SDS PAGE (2.2.12.1) and Native PAGE (2.2.12.2) (200V at room temperature).

2.2.33 Analytical Source Q Anion Exchange Chromatography

200 µL of 20 mg/ml Yih1 was filtered with a 0.80 µm syringe filter and loaded onto a home-packed Source 15Q column pre-equilibrated with Q buffer at 4°C, washed with 2 CV buffer then eluted by applying a linear gradient of NaCl between 0 and 1M over 10 CV. Fractions of 5 mL were collected, analysed by SDS-PAGE (2.2.12.1), and those fractions containing the Yih1 band were pooled, diluted 10 fold in Q buffer then reapplied to a re-equilibrated Source Q column.

Q buffer:

Tris	20.0 mM
TCEP	1.0 mM
DTT	1.0 mM

Made to pH 8.0 with HCl

2.2.34 Glutaraldehyde Crosslinking

5 µL of 2.3% glutaraldehyde was incubated with 100 µg of Yih1 (3:1 molar ratio of Yih1:glutaraldehyde) in 100 µL of 10 mM phosphate buffer, pH 7 for 5 minutes at 37°C. The reaction was terminated by the addition of 10 µL of 1M Tris-HCl, pH 8.5 and the sample was subjected to SDS-PAGE separation (2.2.12.1) and staining with Coomassie blue (2.2.12.4).

2.2.35 tRNA EMSA

tRNA (Sigma; Auckland, NZ) was made to 10mg/ml in RNase-free H_2O then stored at -80°C until required. Final concentrations for the reactions were 1 mg/ml tRNA and 0-2 mg/ml His_6-Yih1 made to 10 µL in Q buffer. Reactions were incubated at 21°C for 4.5 hours before they were analysed using a 2% agarose gel (2.2.6). The gel was initially stained with ethidium bromide (2.2.6.3), photographed, washed with water for 20 minutes with agitation and subsequently stained with Coomassie Blue (2.2.12.4)

2.2.36 Production of Yeast Total RNA

A glycerol stock of *S. cerevisiae* strain 1079 (gifted by E. Sattlegger) was streaked onto a sterile SD-Glu-Trp Agar plate and incubated for two days at 30°C. A colony was chosen to inoculate 10mL SD-Glu-Trp and grown at 30°C with shaking for 2 days. Total yeast RNA was extracted from the culture using an Illustria RNAspin mini RNA isolation kit (GE Healthcare, USA). The cells were spun down at 5000 x g for 10 minutes at room temperature before being resuspended in 700 µL of RA1 buffer and 5µL of β-mercaptoethanol. The resuspended cells were added to 0.5 mL of DEPC-treated glass beads before being subjected to lysis in a Ribolyser (Hybaid; Teddington, England) for 40 seconds at a frequency of 4. RNA was eluted in 40 µL of RNase-free H_2O and quantified by nanodrop (2.2.11) before being stored at -80°C until required.

2.2.37 *In vitro* UV crosslinking with Yeast Total RNA

UV crosslinking reaction mixtures were set up in RNase-free eppendorfs containing 0.1 µL Protector RNase Inhibitor (Roche; Auckland, NZ), 1 µL of 10x NEBuffer 3 (New England BioLabs inc; MA, USA), total RNA to a final concentration of 150 ng/µL, Yih1 to a final concentration of 0.5 mg/mL and RNase-free H_2O was added to make a total volume of 10 µL. Controls lacking RNA or Yih1 were also produced. UV crosslinking was performed by placing 2 µL drops of the reaction mix on parafilm then subjecting them to 120,000 mJ of energy 7 times in a Stratalinker 2400 (Stratagene; Santa Clara, CS, USA). Samples were recovered and (where appropriate) treated with 0.5µL of 10 mg/ml RNase A or 1 µL of 0.5 mg/mL Proteinase K (Roche; Auckland, NZ) in PBS then incubated at 37°C for 15 minutes.

Samples were run on SDS-PAGE (2.2.12.1) and Native PAGE (2.2.12.2) and were stained with Coomassie (2.2.12.4) before being stained with ethidium bromide (2.2.6.3).

2.2.38 Acidic Phenol/Chloroform Extraction

0.1 volume of 2M Sodium Acetate (pH 4.0) and 1 volume of water-saturated phenol, (pH 4.0), was added to the purified Yih1 sample and mixed vigorously. 0.2 volumes of chloroform was added and the sample was incubated on ice for 15 minutes before centrifugation at 10000 x g for 30 minutes at 4°C. The upper aqueous layer was transferred to a new tube containing 0.5 volumes of chloroform and 0.5 volumes of water-saturated phenol and centrifuged as before. The upper layer was again transferred to a new tube and 1 volume of cold isopropanol was added and incubated overnight at -20°C to precipitate the RNA. The sample was centrifuged at 10000 x g for 15 minutes and the pellet dried before resuspension in 10 µL of RNase-free H_2O.

2.2.39 The Effects of Salt on the Heterogeneity of Yih1

Reactions containing 1 mg/mL Yih1 and the indicated concentrations of salt in a final volume of 9 µL were incubated at 37°C for 30 minutes before being analysed by Native PAGE (2.2.12.2) and staining with Coomassie (2.2.12.4).

2.2.40 Binding Studies

Reactions containing 1 mg/mL Yih1 and potential ligands at various concentrations ranging from 0 to 3 mM in a final volume of 9µL were incubated at 37°C for 30 minutes before being analysed by Native PAGE (2.2.12.2) and stained with Coomassie (2.2.12.4).

2.2.41 Sample Preparation for Crystallisation Trials

Samples in a low concentration of buffer were either filtered through a 0.22µm Ultrafree-MC spin filter (Millipore) to remove particulates; or spun at 16000 x g in a microcentrifuge for 5 minutes to sediment particulates prior to setup of crystallisation experiments.

2.2.42 96-Well Sitting Drop Crystallisation

Initial screens were done in Greinger 96 well Intelli-plates (Hampton; Aliso Viejo, USA) with 200 nL drops of both protein and mother liquor being dispensed using a Mosquito robot (TTP Labtech; Melbourn, England) and mixed in tip. Crystal trays were sealed with Thermal seal RTS (Excel Scientific; Victorville, CA, USA) and left for a specific time (usually 1 week) before they were inspected using a binocular dissecting microscope (Olympus).

2.2.43 24-Well Hanging Drop Optimisation

Conditions which looked promising, i.e. those that produced microcrystals or phase separation were optimised in 24 well VDX plates (Hampton Research; Aliso Viejo, USA). Each well contained 500 µL of mother liquor sealed with snow white petroleum jelly (Shell; England). 1 µL protein drops were placed on a siliconised glass circle coverslip (Hampton Research; Aliso Viejo, USA), then 1 µL of mother liquor was added to the protein drop before the coverslip was inverted over the top of the well and sealed.

2.2.44 *In situ* Proteolysis

96-well crystal screens were prepared according to section 2.2.42 with the exception that protease was added to the protein solution immediately before set-up in a ratio of 1:1000 w/w protease:Yih1. Chymotrypsin and trypsin were sourced from Sigma (Auckland, NZ).

2.2.45 *In vitro* Proteolysis

Pure Yih1 (8 mg/mL) was subjected to proteolysis by proteases for 30 minutes at room temperature in a volume of 6 µL. The reactions were separated by SDS PAGE (2.2.12.1) and stained with Coomassie blue (2.2.12.4)

2.2.46 Microbatch Crystallisation

Terazaki plates (NUNC, Roskilde, Denmark) were flooded with 3mL of either 1:1 Silicon oil:Paraffin oil (Al's oil) or Paraffin oil (Hampton Research; Aliso Viejo, USA)

and 1 µL protein drops were added to each well. 1 µL of mother liquor were added to the protein drops under the oil.

2.2.47 Matrix Seeding Crystallisation

A seed stock was prepared by crushing a crystal in 1 µL of mother liquor. This was transferred to an eppendorf containing 10 µL of mother liquor and vortexed briefly. A 96 well screen was prepared according to Section 2.2.42 with the exception that 100 nL of seed stock as also added to each drop by the mosquito robot (TTP Labtech; Melbourn, England).

2.2.48 Diffraction Trials of Crystals

Crystals were transferred to a cryoprotectant solution (generally the mother liquor made to 10-20% glycerol) and fished into a microloop (Mitegen; Ithaca, NY, USA) before being flash frozen in a Cryostream (Oxford Cryosystems; Long Hanborough, England). Oscillation data was collected using exposures ranging from 5-15 minutes, and an oscillation range of 0.5° using a data collection system comprising of a Rigaku rotating anode MM007 X-ray generator, an AXCO PX50 capillary optic and a Rigaku R-axis IV^{++} detector.

3. CRYSTALLISATION OF YIH1

3.1 Introduction

3.1.1 Crystallography

A protein's function *in vivo* is dependent on the formation of its correct three-dimensional (3D) structure. Often proteins that share similar folds or structural motifs perform similar functions. The elucidation of the structure of a protein, and its comparison to similar structures can provide clues about its function for further biochemical investigations.

There are two main methods used to solve the 3D structure of protein's; solution NMR and X-ray crystallography. Solution NMR provides not only structural data, but also protein dynamic data that gives information on the proteins movements allowing monitoring of protein 'breathing'. NMR requires large amounts of isotopically labelled protein, the main disadvantages of NMR are the size constraints that current technology imposes and the large amounts of time required to assign peaks. At 29 kDa, Yih1 is on the upper limit of protein size to be analysed by NMR.

X-ray crystallography captures the protein in a static state and although no direct protein dynamic data is collected, some inferences may be drawn about flexible regions as they often give poor diffraction data. Protein crystallisation requires a highly pure (preferably >99%), homogeneous protein solution and the correct conditions to drive the organisation of those protein molecules into an ordered crystalline lattice. The protein crystal is analysed by X-ray diffraction and the resulting data is processed by various methods to produce an electron density map into which each amino acid in the primary sequence can be modelled.

The main bottleneck in X-ray crystallography is the formation of diffraction quality crystals. The conditions required to form crystals varies from protein to protein and there is no way to predict what conditions are likely to work for any given protein. Proteins which are inherently flexible will generally not form crystals due to conformational heterogeneity.

3.1.2 Expression and Purification of Yih1

In the study of proteins by crystallography, pure protein is required. Pure Yih1 was obtained by expression in the heterologous host *Escherichia coli* and purification from the resulting cellular extract by standard biochemical chromatographic techniques.

Various Yih1 constructs were expressed and purified in the attempt to crystallise Yih1. The rationale behind this is that the addition of tags at either the N-terminus or C-terminus of a protein can affect the formation of crystal contacts. Yih1 was expressed without a tag (Yih1), with an N-terminal His_6-tag (His_6-Yih1), a C-terminal His_6-tag (Yih1-His_6), or as an N-Terminal His_6 tagged mutant where the cysteines of Yih1 had been mutated to alanines (His_6-$Yih1_{cys-}$). His_6-$Yih1_{cys-}$ was used to prevent the possible formation of inter- or intra-molecular disulfide bonds involving the two cysteines present in the RWD of Yih1. As Yih1 is a cytosolic protein, it would not be expected to form disulphide bonds. The formation of both intra- and inter-molecular disulphide bonds during extraction and purification therefore has the potential to add to the heterogeneity of the sample, reducing the likelihood of forming an ordered crystalline lattice.

Two purification steps were carried out to separate the tagged and untagged Yih1 from endogenous *E. coli* proteins. Untagged Yih1 was purified by anion exchange chromatography followed by size exclusion chromatography whereas His_6-tagged variants were purified by immobilised metal affinity chromatography again followed by size exclusion chromatography. The rationale behind the different purification methods are outlined below.

Anion exchange chromatography (AEX) utilises the charge differences between various proteins to separate them. The more negatively charged a protein is at the experimental pH, the higher the concentration of Cl^- ions are required to displace it from the more positively charged matrix.

Immobilised Metal Affinity Chromatography (IMAC) exploits the properties of divalent metal ions (most commonly Ni^{2+}) that interact with indole-containing compounds. Proteins containing a His-tag (six or more Histidine residues in a row at the N- or C-

terminus of the protein) bind to the nickel-charged matrix and can be eluted with increasing concentrations of imidazole which competes with the protein for interaction with the matrix.

Size Exclusion chromatography (SEC) separates proteins based on their hydrodynamic/Stokes radius with larger proteins eluting before smaller proteins due to the smaller proteins being able to enter the pores in the resin, more fully retarding their progression through the column.

3.1.3 Biochemical Analysis of Yih1 and Variants

A protein's expression and solubility are two important factors on the path to forming diffraction quality crystals, but neither guarantees that the protein of interest is folded correctly or reveals if it has any modifications made to it. To tackle these questions, Yih1 and some variants of Yih1 were subjected to analysis by circular dichroism and mass spectrometry.

Far UV Circular Dichroism (CD) is a method that utilises the ability of protein secondary structure to differentially absorb left and right circularly polarised light to

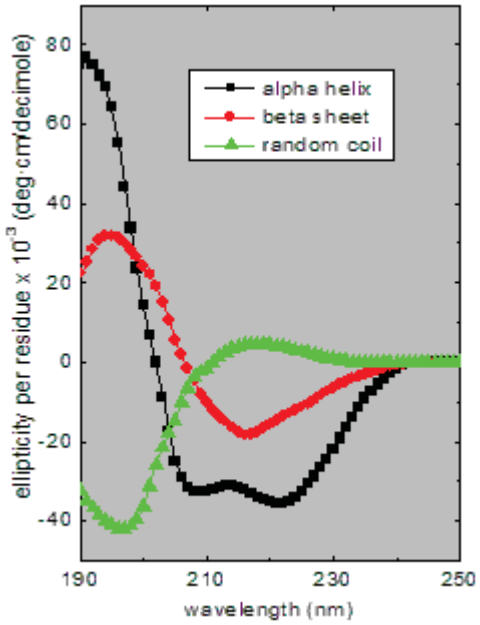

Figure 3.1 Circular Dichroism Standards

Figure reproduced from http://www.ap-lab.com/circular_dichroism.htm.

determine structural elements present within a protein. The three main forms of secondary structure, α-helix, β-sheet and random coil, all have CD spectra characterised by specific maxima and minima, and hence specific shapes (see Figure 3.1). Analysis of CD spectra and comparison with a database of measurements from a number of proteins whose structure have been solved by X-ray diffraction allow predictions to be made on the ratios of the different secondary structural elements that are likely to be present. There are various algorithms used to deduce the proportions of secondary structural elements from far UV CD spectra, none of which are 100% accurate. Although Yih1 has been previously analysed by far UV CD and predicted to be composed of 29% helices, 24% β-sheets, 20% turns, and 28% random structure (Sattlegger *et al.*, 2011), the analysis of purified Yih1 by CD is one way to check that the protein being used in crystallisation experiments is folded.

Mass Spectrometry accurately measures the mass-to-charge ratio of components within a sample. It allows the identification of post-translational modifications such as phosphorylation and oxidation that can affect the propensity of a protein sample to crystallise.

3.2 Results and Discussion

3.2.1 Expression and Purification of Untagged Yih1

3.2.1.1 Untagged Yih1 Expression and Solubility

Untagged Yih1 and variants were successfully expressed in a soluble form. Figure 3.2 shows a typical result of expression and solubility trials for Yih1 and its variants. The dark band indicated by an arrow is present in the induced whole cell extract (Lane 1), but is not present in the uninduced whole cell extract (Lane 2) indicating that recombinant Yih1 is produced at high levels with only minimal 'leaky' expression in the uninduced sample (Lane 2). A large proportion of Yih1 appears to be soluble (Lane 3), although some was present in the pellet (Lane 4). As the pellet contains many of the same bands present in the supernatant fraction, it appears to be contaminated with soluble protein, possibly due to incomplete cell lysis or insufficient washing of the pellet, which may have contributed to the apparent presence of Yih1 in the insoluble fraction.

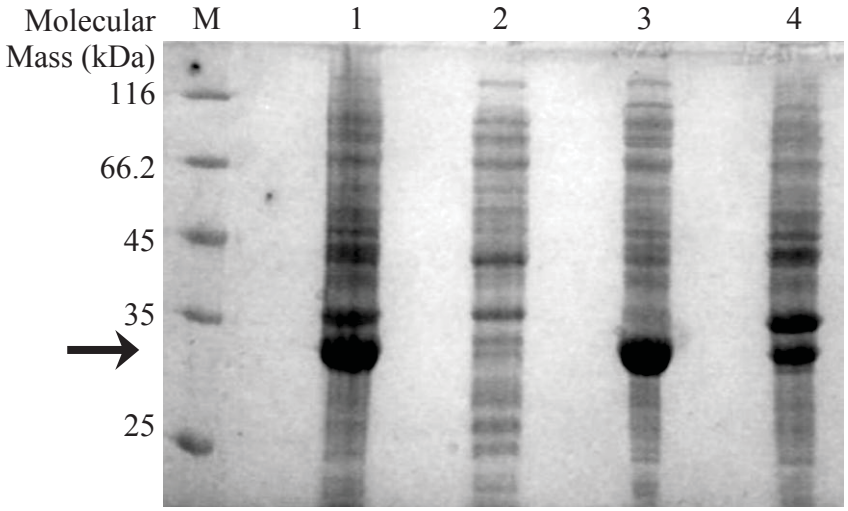

Figure 3.2 SDS PAGE of Yih1 Expression and Solubility

Yih1 expression and solubility was analysed by 12.5% SDS PAGE. Lane M: Fermentas Protein Molecular Weight Marker ; Lane 1: Whole cell lysate of cells induced with 0.1mM IPTG; Lane 2: Uninduced Whole cell lysate control; Lane 3: Soluble fraction of induced cells; Lane 4: Insoluble fraction of induced cells.

3.2.1.2 Anion Exchange Chromatography

To isolate the untagged Yih1 from the host *E. coli* proteins, its low pI (4.52 for WT Yih1) was exploited through anion exchange chromatography. The A_{280} and A_{260} trace of a typical Yih1 anion exchange procedure is shown in Figure 3.3. Yih1 eluted in two peaks at approximately 0.25-0.35mM NaCl as shown by SDS PAGE analysis of the recovered fractions (Figure 3.4). The two peaks contain similar protein bands, and thus can only be explained by either differences in the association of Yih1 with itself, a native *E. coli* protein, or a non-proteinacious molecule affecting the surface charge of the protein. Alternatively the two peaks could represent two populations of Yih1 molecules differing in surface charge because of conformational differences or post translational modifications such as phosphorylation. As there is a well conserved homologue of the Ancient domain in *E. coli* (YigZ), it is possible that any modification machinery present in the host cell that may act on YigZ may be able to act upon the recombinant Yih1 Ancient domain. However, very little is known about the *in vivo* role of YigZ, including whether or not it undergoes any form of post-translational modification.

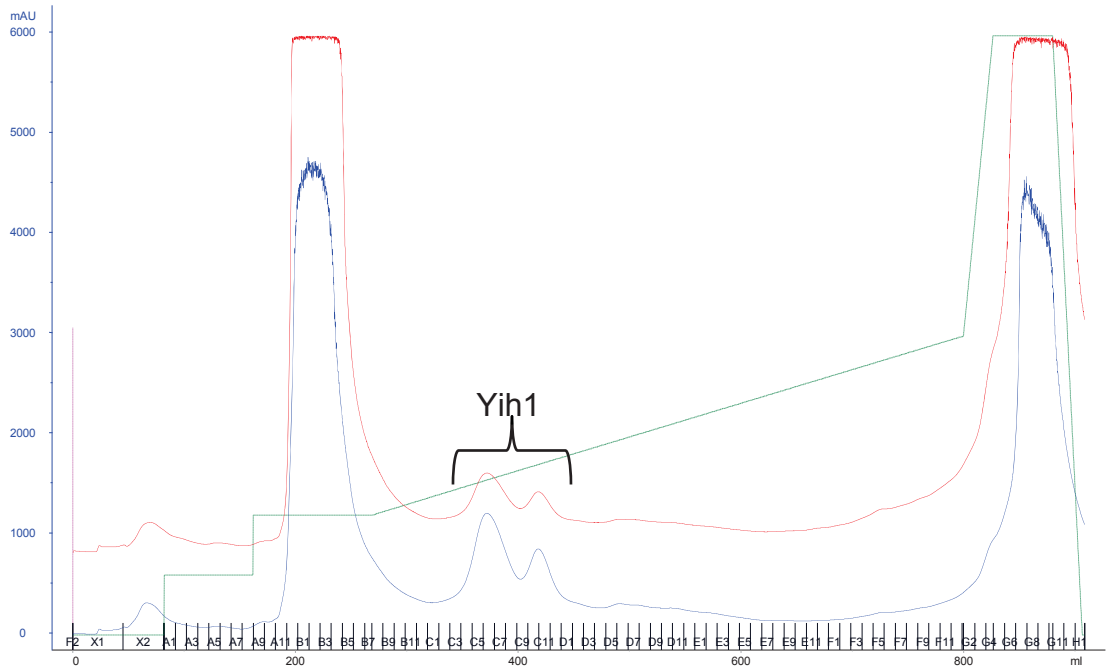

Figure 3.3 Chromatogram of Anion Exchange Chromatography of Yih1

Blue line: A_{280}; Red Line: A_{260}; Green dotted line: NaCl gradient.

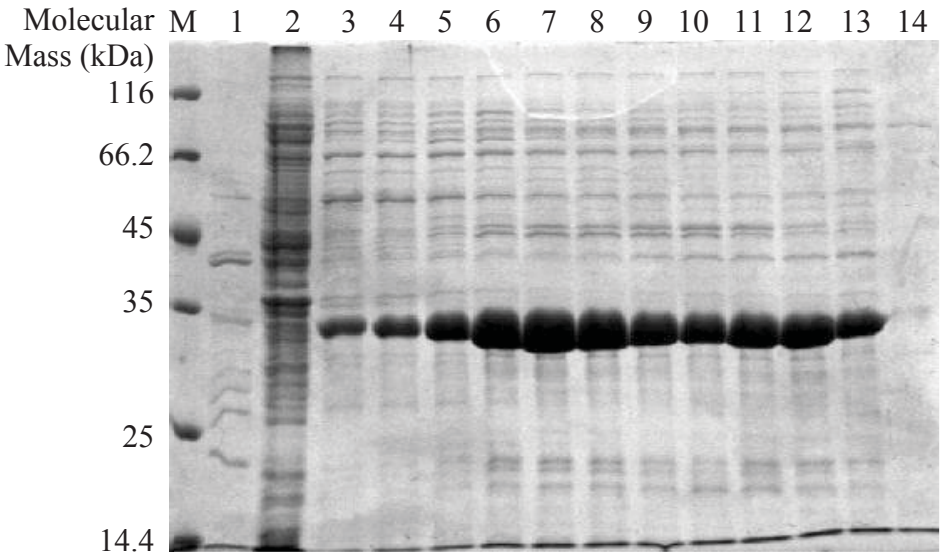

Figure 3.4 SDS PAGE of Anion Exchange Chromatography of Yih1

12.5% SDS PAGE analysis of fractions collected from anion exchange purification step. Lane M: Molecular Weight Marker; Lane 1: Fraction X2; Lane 2: Fraction B2; Lanes 3-13: Fractions C2-C12; Lane 14: Fraction G7.

3.2.1.3 Untagged Yih1 Size Exclusion Chromatography

Yih1 generally eluted as a single peak when subjected to size exclusion chromatography (see Figure 3.5).This peak contained mostly pure Yih1 as shown in Figure 3.6 although some proteolysis of Yih1 appeared to occur despite the addition of Complete™ protease inhibitor. Representative yields are outlined in Table 3.1.

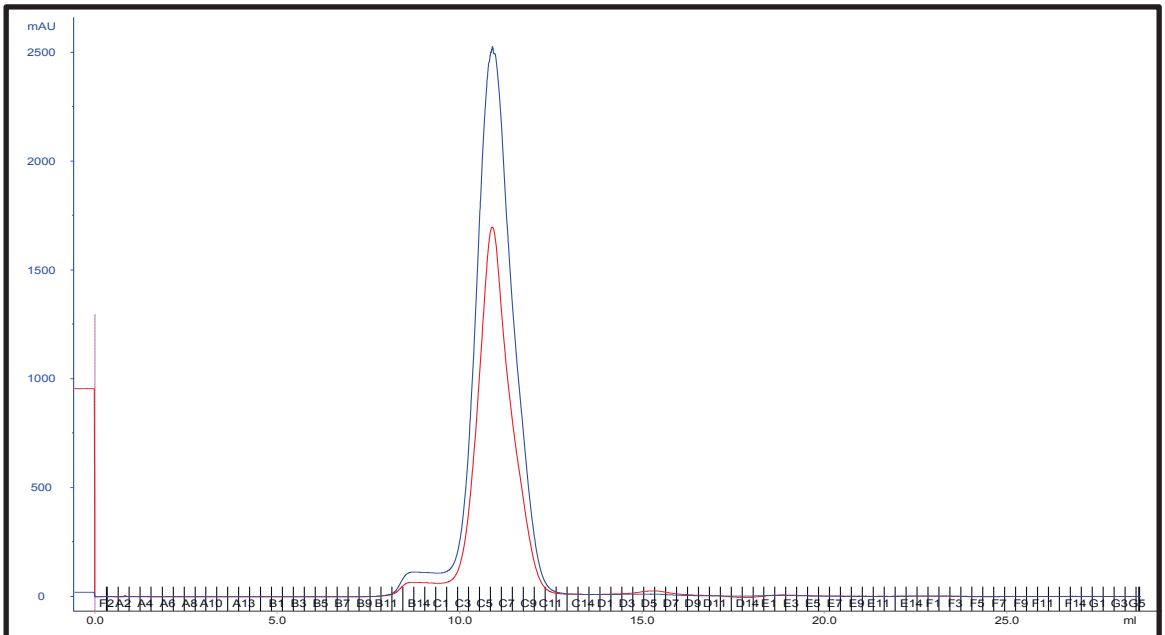

Figure 3.5 Chromatogram of Yih1 Size Exclusion Chromatography

Blue line: A_{280}; Red Line: A_{260}.

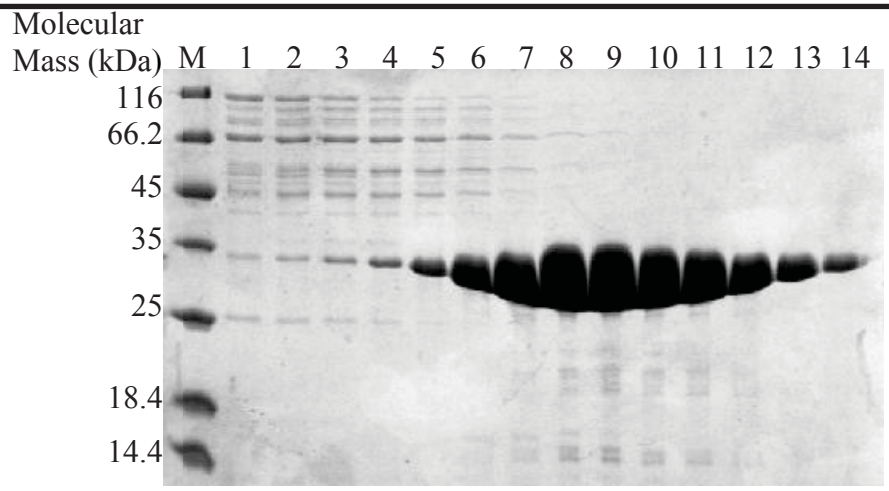

Figure 3.6 SDS PAGE of Yih1 Size Exclusion Chromatography Fractions

12.5% SDS PAGE analysis of fractions collected from size exclusion purification step. Lane M: Molecular weight marker; Lanes 1-14: Fractions B14-C12.

Table 3.1 Purification of Untagged Yih1 from E. coli

Fraction	Volume (mL)	Protein Concentration (mg/mL)	Total Protein (mg)
Clarified Cell Lysate	25.0	53.0	1325.0
Anion Exchange Chromatography	100.0	0.87	87
Size Exclusion Chromatography	25	0.6	15

Yih1 that had been single-labelled (^{15}N) or double-labelled (^{15}N and ^{13}C) was also successfully produced for NMR studies. This was achieved by culturing cells in minimal media containing $^{15}NH_4Cl$ and ^{13}C-glucose allowing the incorporation of these isotopes into the protein (2.2.1.4). However, the protein expression levels and therefore yield of Yih1 was reduced compared to that of cells grown in LB, likely due to the lower levels of nutrients present in the minimal media. NMR analysis of these samples is currently underway.

3.2.2 Expression and Purification of His_6-Tagged Yih1

3.2.2.1 Expression and Solubility of His_6-tagged Yih1

All His_6-tagged Yih1 variants displayed high expression and were soluble indicating that the addition of the histidine residues at either the N- or C-terminus of Yih1 had no detrimental effect on the stability of the protein *in vivo*.

3.2.2.2 Immobilised Metal Affinity Chromatography

Cell lysate was subjected to immobilised metal affinity chromatography using Ni^{2+} as the immobilised divalent ion. As there is no prominent band at the expected mobility of Yih1 in the flow-through fraction (Lane 1, Figure 3.7), it appeared that Yih1 had successfully bound to the column indicating that the His-tag was not masked within the protein but was accessible and available for interaction. The majority of other proteins present in the cell lysate had passed through the column and were mostly eliminated by the two washes (Lanes 2 and 3). The wash buffer used to wash out the unbound protein was the same as that used to resuspend the cells for lysis. Despite

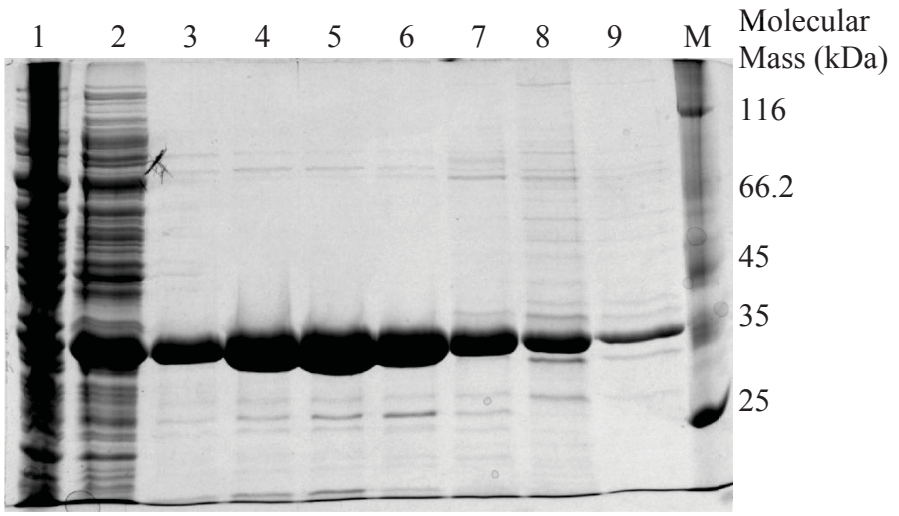

Figure 3.7 SDS PAGE of IMAC fractions

Fractions collected for IMAC were analysed by 12.5% SDS PAGE. Lane 1: Column Flow-through; Lane 2: Wash 1; Lane 3: Wash 2; Lane 4: 30mM imidazole elution; Lane 5: 40mM imidazole elution; Lane 6: 50mM imidazole elution; Lane 7: 100mM imidazole elution; Lane 8: 250mM imidazole elution; Lane 9: 500mM imidazole elution; Lane M; Molecular Weight Marker.

this, a small proportion of Yih1 appears to have been eluted in these wash steps. This could be due to overloading of the column. However, as Yih1 eluted during all the step-wise increases in imidazole, it is possible that there may be different populations of Yih1 differing in fold, protein-protein association or protein-resin association.

3.2.2.3 Size Exclusion Chromatography of His_6-tagged Yih1

Results for size exclusion chromatography of His_6-tagged variants of Yih1 were similar to that of wild type (Figure 3.8) but the increased purity rendered by IMAC compared to AEX resulted in an increase in the overall purity of Yih1 obtained by SEC. Despite this, there still appears to be some proteolysis of Yih1 occurring (Figure 3.9) contributing to the heterogeneity of the Yih1 sample. Representative yields are outlined in Table 3.2.

Table 3.2 Purification of Yih1-His_6 from E. coli

Fraction	Volume (mL)	Protein Concentration (mg/mL)	Total Protein (mg)
Clarified Cell Lysate	25.0	56.5	1412.5
Immobilised Metal Affinity Chromatography	50	1.2	60.0
Size Exclusion Chromatography	30	0.6	18

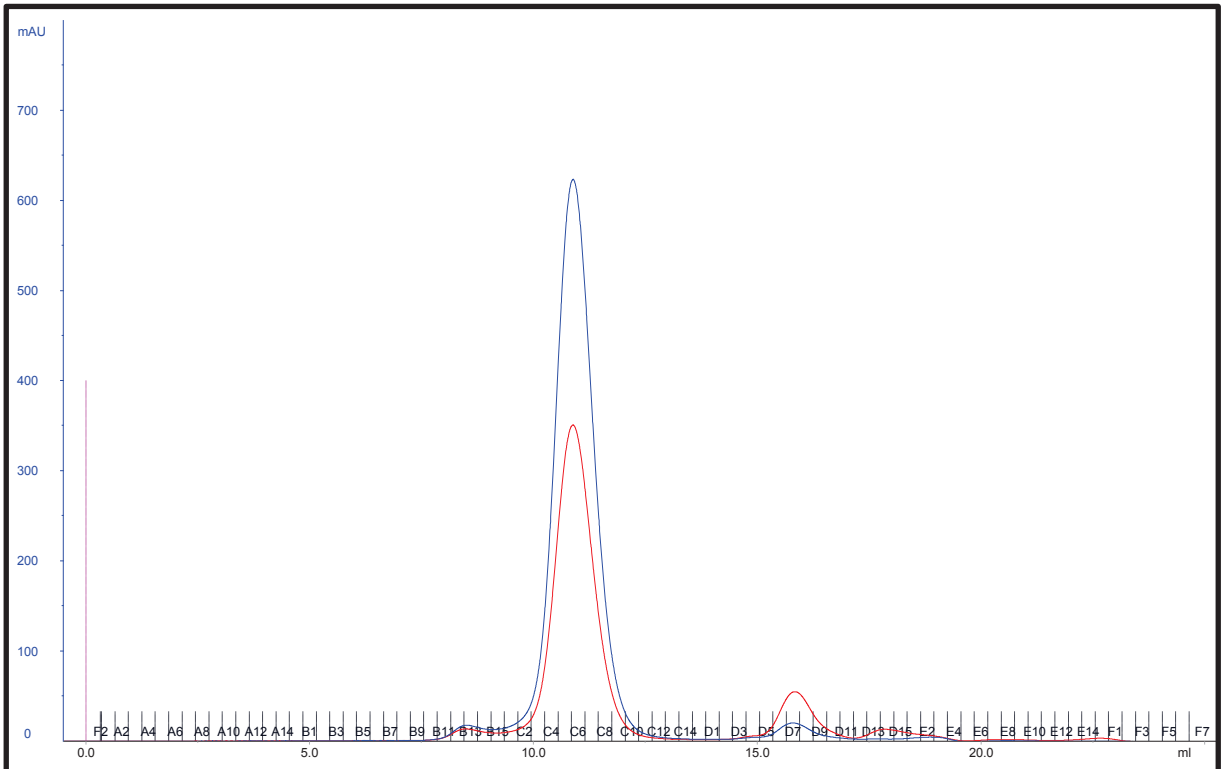

Figure 3.8 Chromatogram of Size Exclusion of His tagged Yih1 Variants

Blue line: A_{280}; Red Line: A_{260}.

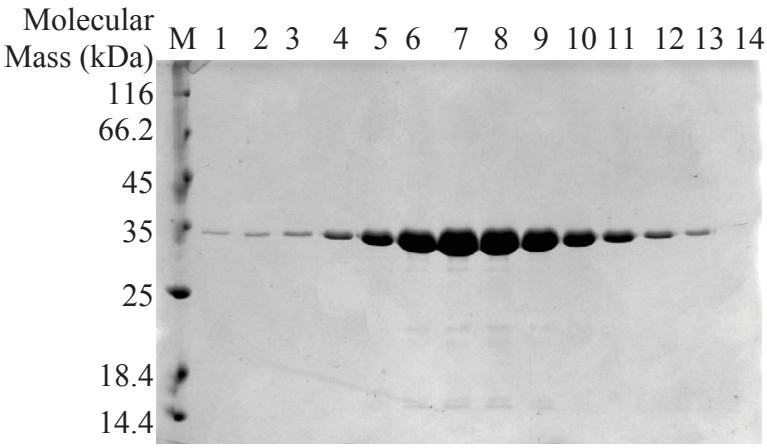

Figure 3.9 SDS PAGE of His-tagged Size Exclusion Chromatography Fractions

12.5% SDS PAGE analysis of fractions collected during size exclusion chromatography. Lane M: Molecular Weight marker; Lanes 1-13: fractions B15-C12; lane 14: fraction D7.

3.2.3 Interaction with other Biomolecules

Occasionally Yih1 would behave oddly, eluting as multiple peaks during size exclusion chromatography despite there being no detectable contamination by other proteins observed on Coomassie-stained 12.5% SDS gels. The most anomalous behaviour was observed during the purification of a His_6-Yih1 cysteine to alanine double mutant (His_6-$Yih1_{cys-}$) (Figure 3.10). Possible explanations for these different peaks included: the formation of multimeric species; the association of Yih1 with other small peptides or smaller than can be resolved on the 12.5% SDS PAGE gel; or an interaction with a non-proteinaceous molecule or molecules. Yih1 has only two cysteines at positions 67 and 99 in the RWD domain, which are not evolutionarily conserved. His_6-$Yih1_{cys-}$ is unable to form disulphide bonds, so any multimerisation is likely to be specifically linked to the structure of Yih1 and may be related to the *in vivo* function of Yih1. It is possible that Yih1 may form an interaction with a non-protein molecule that may allow two Yih1 molecules to interact either directly if for

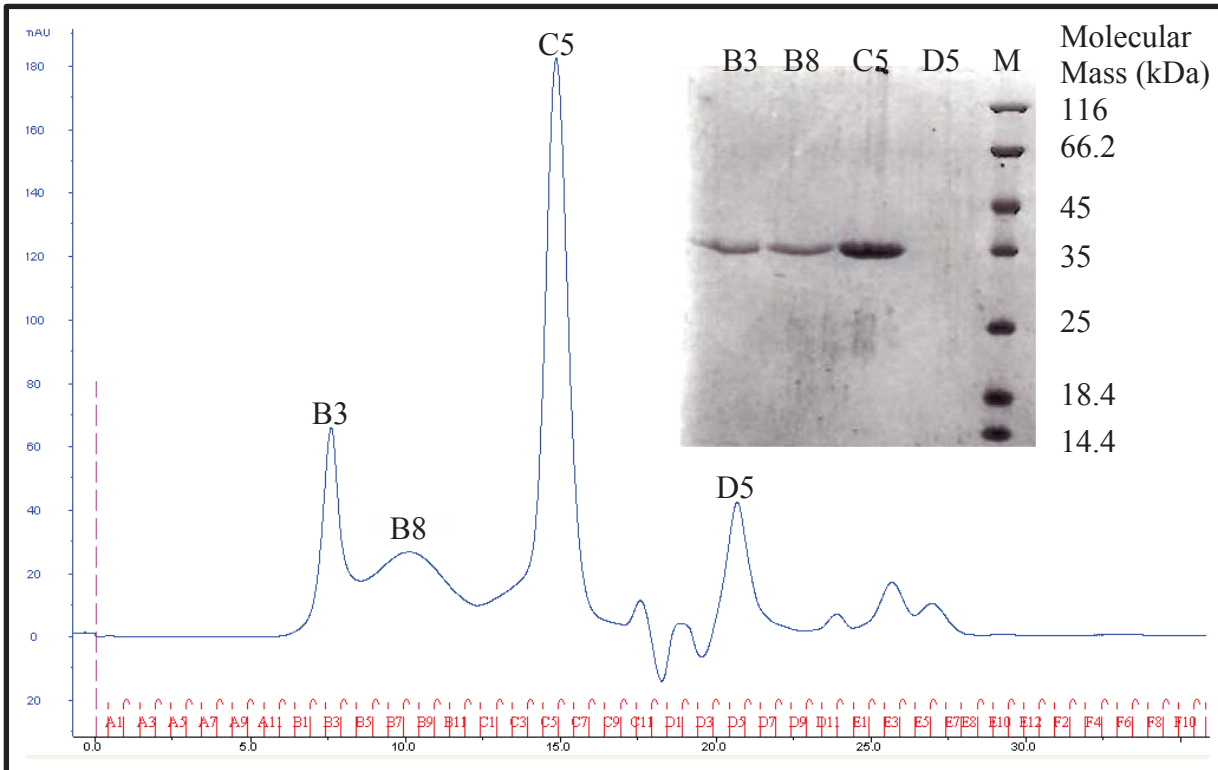

Figure 3.10 His_6-$Yih1_{cys-}$ Size Exclusion Chromatography

Chromatogram of SEC of His_6-$Yih1_{cys-}$. Inset is the SDS polyacrylamide gel of peak fractions B3, B8, C5 and D5. M: Molecular Weight Marker.

example the binding of a metabolite caused a conformational change in Yih1 that allowed dimerization; or indirectly if for example multiple Yih1 monomers could bind to a single non-protein molecule.

3.2.4 Biochemical analysis of Yih1 and variants

3.2.4.1 Circular Dichroism

The results for circular dichroism experiments of Yih1 were variable. Generally all the Yih1 variants displayed similar spectra that indicated a mix of alpha-helical and beta-sheet structures (Figure 3.11). Proportions of secondary structure of untagged Yih1 are ~ 37% α-helix, 16% β-strand, 16% β-turn and 30% random coil when deconvoluted using CDNN 2.1 software (Applied Photophysics). This result agrees with the homology-based structural model proposed by Sattlegger and co-workers (2011). However, it appears that Yih1 may be unstable in the conditions under which the spectra were measured. Figure 3.12 shows temporal measurements of Yih1 in which the alpha-helical character trough at ~210nm reduces over the time course, indicating that the protein may be losing α-helical structure. However, this was not always the case as a second sample from the same batch that yielded identical repeats in one experiment, showed instability when measured on a different occasion even though it had been stored at -80°C as had the previous sample. As the buffered

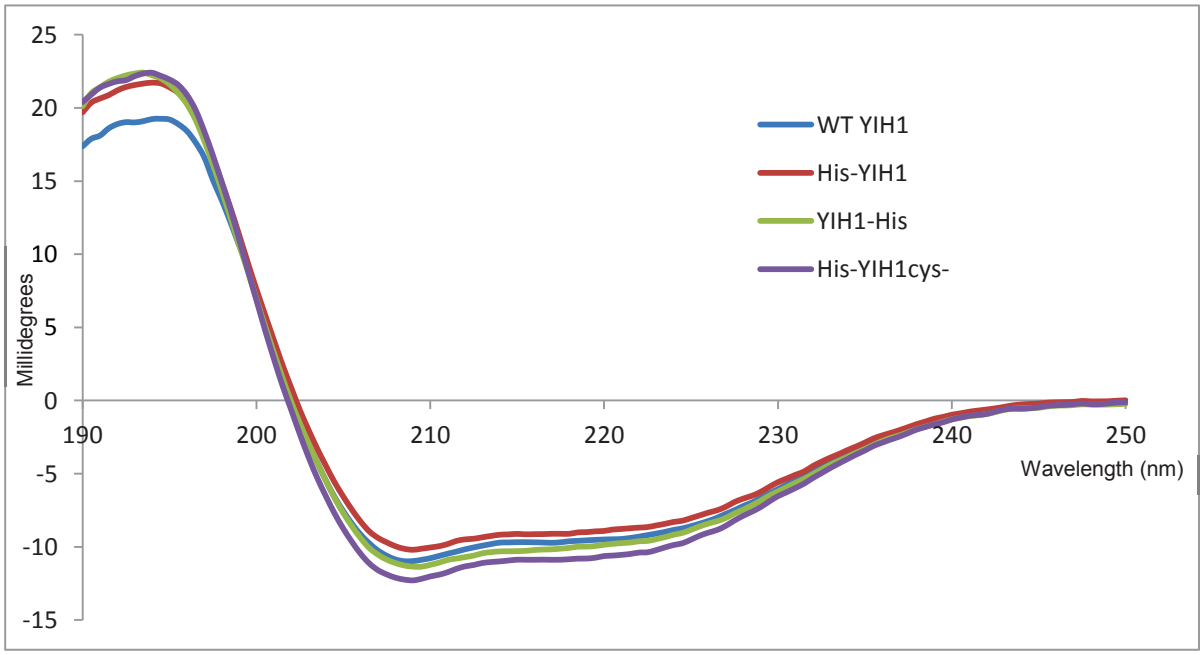

Figure 3.11 CD spectra of Yih1 variants

protein solution had been considerably diluted in H_2O, it may simply reflect the instability of Yih1 in very dilute solutions. This is not unusual for proteins; especially those that are flexible. The changes in CD over time may also reflect changes in secondary structure due to increased oligomerisation with time.

As the different variants of Yih1 have similar CD spectra, it appears that the modifications made (addition of tags or mutations) have not resulted in a large change in the secondary structural elements that make up the protein. Therefore all the constructs appear suitable for structural studies and any conclusions drawn are likely to be applicable to the wild-type protein.

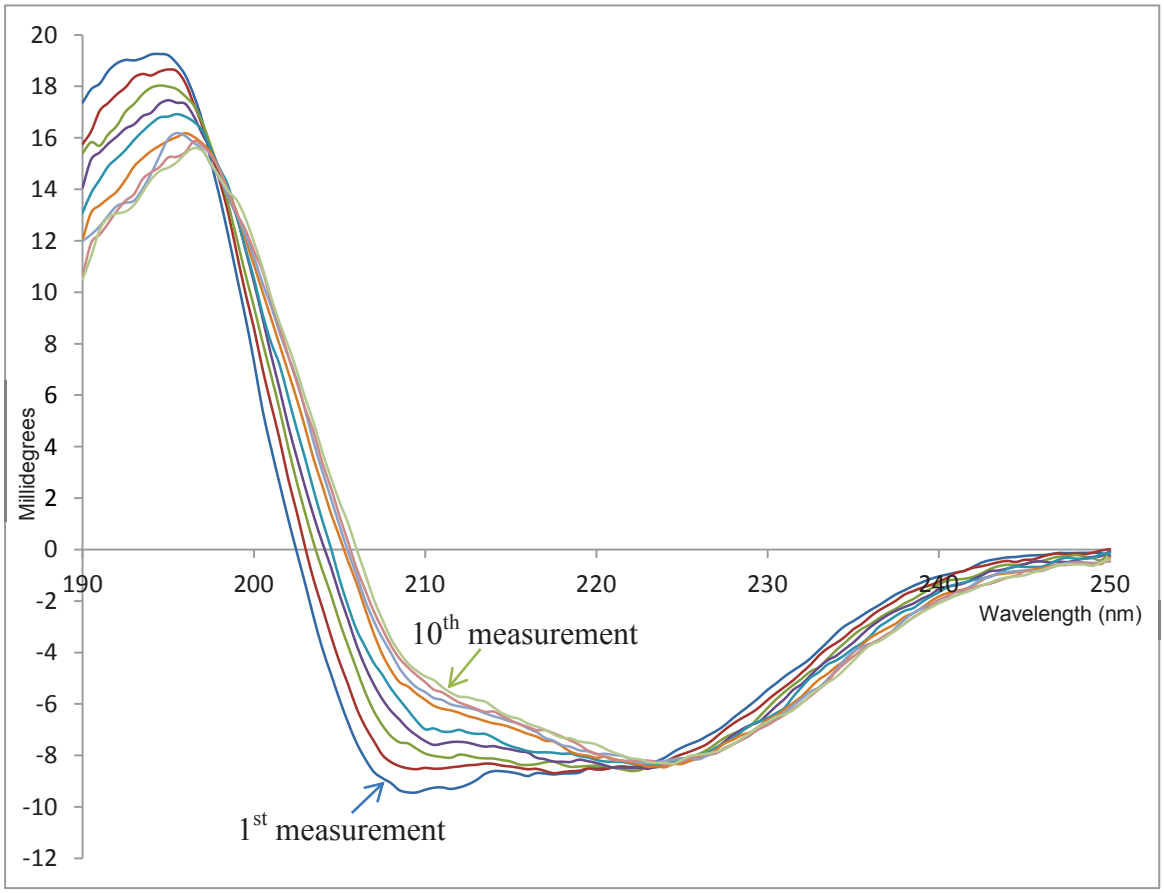

Figure 3.12 Circular Dichroism Spectra of Unstable Yih1

3.2.4.2 High Performance Liquid Chromatography

High resolution separation of Yih1 from contaminants and buffer constituents was performed by Reverse Phase-High Performance Liquid Chromatography (RP-HPLC) (2.2.27) in preparation for mass spectrometry analysis.

Yih1 elutes as a single peak after approximately 26 minutes. There also appears to be a few smaller peaks with lower retention times. These small peaks are likely to be buffer components, contaminants such as degradation products or possibly even molecules that interact with Yih1 but are released under the denaturing conditions of RP-HPLC. This experiment confirmed observations from SDS-PAGE that within the resolution of the column, a single chemical species of Yih1 is present in the purified samples.

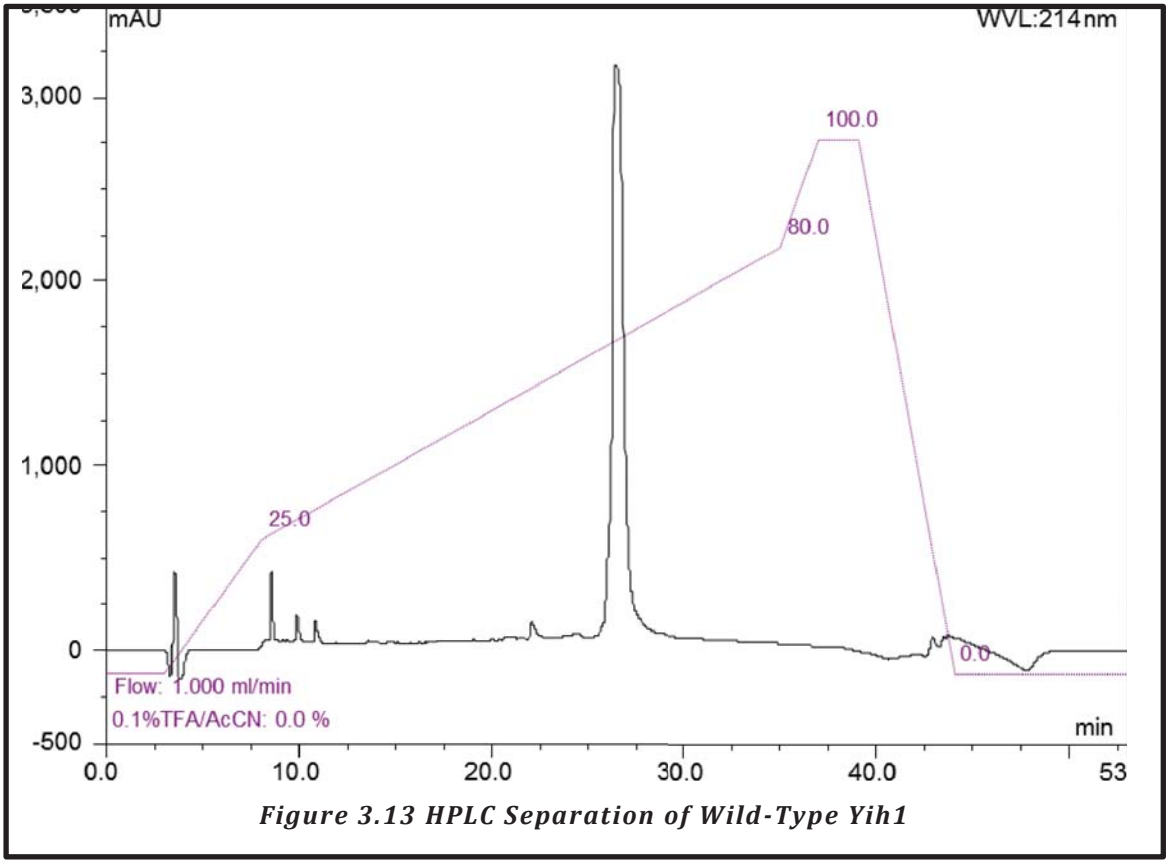

Figure 3.13 HPLC Separation of Wild-Type Yih1

3.2.4.3 Mass Spectrometry

The peak fractions obtained by RP-HPLC were analysed by mass spectrometry (2.2.28) to confirm the identity of the purified protein as Yih1 and to investigate the presence of other molecules that it may be bound to. Keeping in mind that Yih1 was expressed in *E. coli*; an expression system that lacks the machinery to create many eukaryotic modifications, any lack of modification in this analysis does not exclude the possibility that Yih1 may undergo post-translational modification in its native *S. cerevisiae* cell.

The measured molecular weight for Yih1 is 29,018.96 Da. As there was one main peak in the deconvoluted spectra, this is further evidence that the purified Yih1 consists of one chemical species. The expected average mass of untagged Yih1 (expressed from pES317-15b) is 29,017.47Da ($(M+H)^+$ of 29,018.47) which agrees with the measured mass $(M+H)^+$ of 29018.86, confirming the identity of Yih1. This measured molecular weight also confirms that in this sample, Yih1 is not carrying post-translational modifications. Analysis of the other HPLC peaks did not reveal the presence of any identifiable molecule other than buffer constituents that had been present in the Yih1 sample.

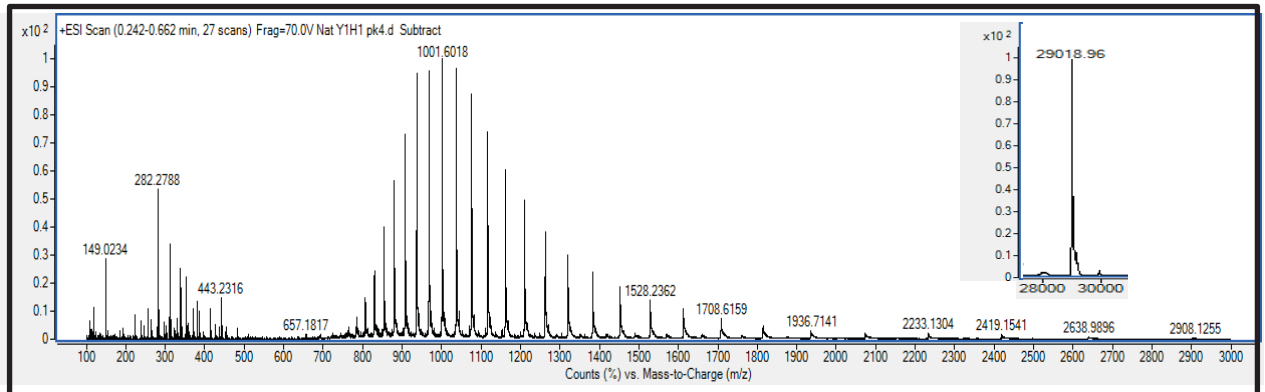

Figure 3.14 Mass Spectrometric analysis of Yih1

The data output from mass spectrometry of Yih1 is shown with the deconvoluted peak inset on the right.

3.2.5 Crystallisation of Yih1, His_6-Yih1, Yih1-His_6 and His_6-$Yih1_{cys-}$

Yih1 and tagged variants were subjected to many crystallisation trials (Table 3.3). Both sparse matrix- and grid-type screens were utilised to test different areas of crystallisation space.

No diffracting protein crystals were obtained in any of the conditions tested for tagged or untagged Yih1. Crystals that grew were tested by X-ray diffraction and were shown to be salt or did not diffract. Figure 3.15 shows a typical diffraction pattern obtained from the salt crystals. The diffraction spots are set far apart due to a small unit cell. As protein crystals generally have large unit cells they result in diffraction spots that are separated by much less distance. It can be concluded that this diffraction pattern is not from a protein crystal but from a salt crystal. Further attempts to enhance the crystallisability of Yih1 are outlined in the next chapter.

Table 3.3 Crystallisation Screening Experiments

Protein	Concentration	Screen Name	Method	Temperature
Untagged Yih1	10 mg/ml	PACT Premier	SD-VD	21°C
		Crystal Screen I +II	SD-VD	21°C + 10°C
	5.2 mg/ml	Structure Screen	SD-VD	21°C
	20 mg/ml	Crystal Screen I +II	MB-Paraffin	21°C
	15 mg/mL	PACT Premier	MB-Al's oil	21°C
		Crystal Screen I +II	SD-VD	21°C
untagged Yih1 pool from Source Q	10.2 mg/mL	PACT Premier	SD-VD	21°C
		Crystal Screen I +II	SD-VD	21°C
His_6-Yih1	11.2 mg/mL	PACT Premier	SD-VD	21°C
		Crystal Screen I +II	SD-VD	21°C
Yih1-His_6	7.4 mg/mL	PACT Premier	SD-VD	21°C
		Crystal Screen I +II	SD-VD	21°C
His_6-$Yih1_{cys-}$	6.5 mg/mL	PACT Premier	SD-VD	21°C
		Crystal Screen I +II	SD-VD	21°C

SD-VD=Sitting Drop Vapour Diffusion, MB-paraffin= Microbatch with paraffin oil, MB- Al's oil= Microbatch with Al's oil

Given the lack of success in crystallisation trials of tagged and untagged Yih1, it appears that Yih1 may intrinsically lack the required features to form crystals; the most likely factor being conformational homogeneity.

Interestingly, the RWD domain family show examples of proteins displaying conformational heterogeneity. Both the RWD-containing proteins GIR2 from yeast, and RWDD1 from humans, are intrinsically unstructured proteins (IUP). IUP's contain very little if any ordered structure but remain soluble. Often an ordered fold is only obtained upon interaction with another molecule (Dyson and Wright, 2002). This makes IUP's very adaptable to the molecules they are able to interact with and they tend to display interactions with a large range of molecules due to their flexibility. Although published analysis of Yih1 by circular dichroism indicates that Yih1 forms an ordered structure, it also suggests that the linker region is disordered (Sattlegger *et al.*, 2011) and this is supported by FoldIndex prediction data (See Figure 1.6). Therefore the linker region may act as an intrinsically disordered domain (IDD). This may explain how Yih1 is potentially able to interact with such a wide variety of proteins. IDD's tend to be highly charged and display higher rates of evolution than ordered domains (Brown *et al.*, 2002) imparting new/altered functionality to the

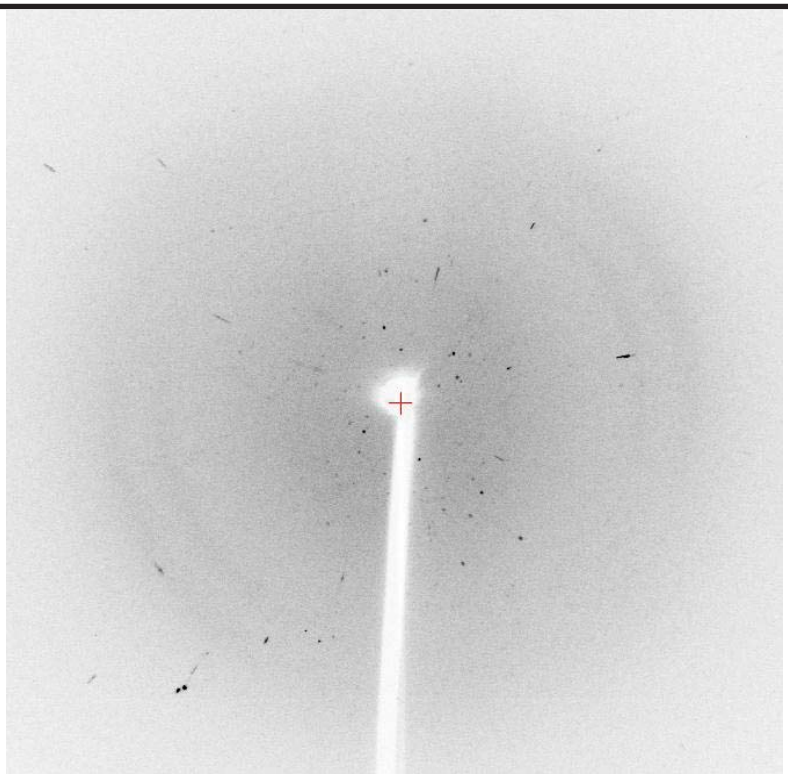

Figure 3.15 X-ray Diffraction Pattern of a Salt Crystal

A crystal that had grown in a PACT Premier Screen (Molecular Dimensions) was analysed by X-ray diffraction.

protein often without disrupting prior functionality. The linker region of Yih1 displays considerable species variation in both sequence and length although it has retained a high proportion of charged residues throughout evolution (Sattlegger *et al.*, 2011), supporting its proposed role as an IDD. Further to this, binding requirements for both Gcn1 and G-actin include the linker region of Yih1 (Sattlegger *et al.*, 2011) indicating that it is likely that the linker region is an IDD and as such, has evolved to allow Yih1 to carry out functions requiring interaction with a plethora of different proteins. If this is the case, the linker region of Yih1 may form different conformations dependent on the identity of the protein bound to it.

4. ATTEMPTS TO ENHANCE THE CRYSTALLISABILITY OF YIH1

4.1 Introduction

Attempts to limit the predicted conformational heterogeneity of Yih1 for crystallisation experiments are outlined below.

4.1.1 *In situ* Proteolysis

In situ proteolysis has been used successfully in many in crystallisation studies to crystallise proteins that either had previously been unable to form crystals, or to increase the resolution of the crystals formed (Dong *et al.*, 2007, Wernimont and Edwards, 2009). It appears to work on the basis that flexible regions of a protein, often joining domains, are more prone to proteolysis due to the increased accessibility of these regions. In an attempt to remove the flexible regions of Yih1, *in situ* proteolysis was used whereby protease was added directly to the crystallisation drop.

4.1.2 Expression of Yih1 Binding Partners

The assembly of protein-protein complexes often rely upon an “induced fit” whereby the assembly of the complex causes changes to the structure of a protein, such as stabilisation of flexible loops or occasionally even directing folding of an unstructured region into secondary structure elements (Dyson and Wright, 2002). To attempt to stabilize Yih1 for crystallographic analysis; expression and purification of the known Yih1-binding partners, Gcn1 and G-actin, was attempted in order to try and crystallise each with Yih1. In addition to the possible stabilisation of Yih1 and therefore the possibility of solving its structure, the structure determination of any complexes formed would also provide detailed information about the molecular interactions involved and therefore the functionality of the two molecules.

Gcn1 is a large protein of 296.7 kDa; and as such is too large to be expressed in an *E. coli* host in a soluble form. To solve this problem, a fragment of Gcn1 (residues 2052-2428) encompassing a region that had been shown to bind specifically to Yih1 by Sattlegger and co-workers (2004) was used.

To obtain monomeric actin for co-crystallisation studies, a construct expressing recombinant yeast actin in *E. coli* was used. Given the ability of actin to polymerise, purification conditions that would promote the depolymerisation of actin were used.

4.1.3 Surface Entropy Reduction of Yih1

The amino acids lysine, arginine, glutamine and glutamic acid consist of very flexible side-chains. Patches of a protein displaying a high proportion of these amino acids can be detrimental to crystallisation due to the increased conformational heterogeneity of these highly entropic regions that can impede the formation of an ordered crystalline lattice. As these amino acids are also highly charged they may also inhibit crystal formation due to electrostatic repulsion. Surface entropy reduction (SER) involves the substitution of these highly charged and flexible residues with the uncharged, constrained amino acid alanine (Derewenda, 2004), thus removing or reducing the entropic shield that may be preventing crystal contacts from forming. This is achieved by modification of the plasmid construct encoding the protein of interest by PCR-based site-directed mutagenesis.

4.1.4 Cloning of the Ancient Domain of Yih1

Yih1 is predicted to have a flexible linker region joining its two domains (Sattlegger *et al.*, 2011) that may possibly interfere with or prevent formation of an ordered crystal structure due to conformational heterogeneity. Removal of this region by expressing the two domains separately is a valid approach to attempt to limit conformational heterogeneity increasing the likelihood of forming well-ordered, diffraction-quality crystals for X-ray analysis.

Given the lack of known function for the Ancient domain of Yih1, the elucidation of the structure of this domain may lead to predictions about its function *in vivo*. To attempt to solve the structure of the Yih1 Ancient domain, a construct expressing the Ancient domain was required. This was achieved by cloning the Ancient domain cDNA into a modified pET32a expression vector with the aim to produce recombinant protein for structural studies.

4.2 Results and Discussion

4.2.1 *In situ* Proteolysis

Crystal screens were carried out as described in section 2.2.44. The screens set-up are outlined in Table 4.1.

Table 4.1 Crystallisation Screens of In situ Proteolysis

Protein	Concentration	Screen Name	Protease	Method	Temperature
Yih1	12 mg/mL	Crystal Screen I+II (Hampton Research)	Trypsin	SD-VD	21°C
			Chymotrypsin	SD-VD	21°C
		Structure I+II (Molecular Dimensions)	Trypsin	SD-VD	21°C + 4°C
			Chymotrypsin	SD-VD	21°C

Some conditions containing chymotrypsin appeared crystalline, these tended to include the buffer, sodium HEPES pH 7.5; the precipitant, 2-Methyl-2,4-pentanediol (MPD); and the salts, calcium chloride, sodium acetate or sodium citrate. These chemicals were used to optimise the conditions in 24 well plates (2.2.43). The drops appeared crystalline but no protein macrocrystals were formed in any of the conditions tested.

It is possible that the crystalline appearance of these drops was due to nucleation of very small chymotrypsin crystals. However, there was a very low amount of chymotrypsin present (24 ng compared to 24 µg Yih1) making this possibility less likely.

To visualise the likely fragments produced by proteolysis of Yih1, Yih1 was subjected to proteolysis *in vitro* and visualised by SDS-PAGE (2.2.45). Figure 4.1 shows that Yih1 is accessible to degradation by trypsin, chymotrypsin and papain. Trypsin appears to cleave Yih1 in many places, giving many fragments of different sizes in both dilutions used. Chymotrypsin appears to yield two large fragments of YIH1, indicating that it is likely to have cleaved a short N- or C-terminal fragment off. However, many other bands are present with chymotrypsin-treated Yih1. Papain is interesting as it degrades Yih1 to yield discrete bands when used at a higher

concentration. Therefore digestion of YIH1 by papain is more likely to result in the formation of crystals as more discrete fragments are produced. However no crystal screens were performed with this protease due to time constraints.

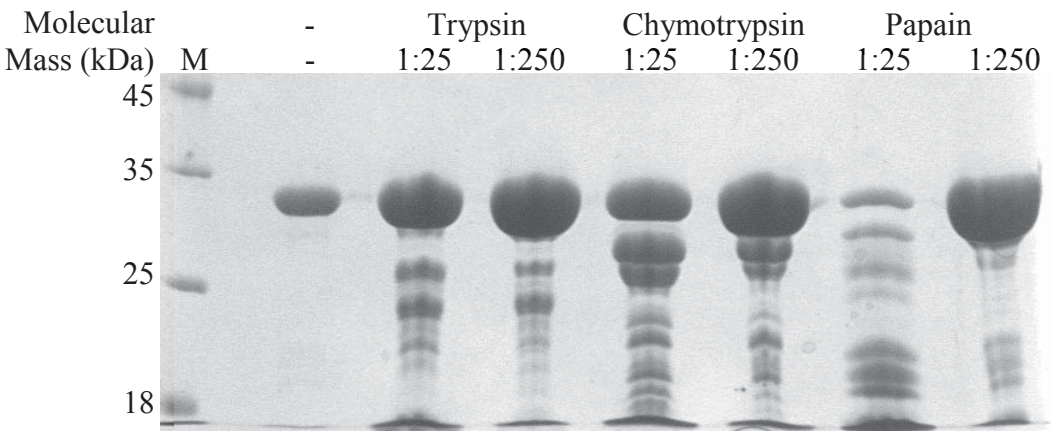

Figure 4.1 In vivo Proteolysis of Yih1

YIh1 was subject to proteolysis and analysed by 12.5% SDS-PAGE. YIH1 was treated with the indicated protease at the indicated Protease:Yih1 ratio (2.2.45). Lane M: Molecular Weight Marker.

In situ proteolysis of Yih1 did not yield crystals of Yih1. This may be due to the increased heterogeneity of the sample caused by the release of various sized fragments. A possible way to reduce this heterogeneity would be to perform in vitro proteolysis of Yih1, and concentrate in a 20,000 Da molecular weight cut-off concentrator to remove smaller fragments. Alternatively, proteolysed His_6-Yih1 or YIH1-His_6 could be purified by immobilised metal affinity chromatography to isolate only the N-terminal or C-terminal Yih1 fragment. This would be especially suited to papain-digested Yih1 as it may result in the ability to extract out the separate domains of YIH1 for use in crystallisation studies.

4.2.2 Expression of Yih1 Binding Partners

4.2.2.1 Gcn1 Fragment Expression and solubility

Although expression of the Gcn1 fragment ($Gcn1_{frag)}$ was successful as judged by a large band on SDS-PAGE (Lane 2, Figure 4.2), a large proportion of it appeared to be insoluble (Lane 4). This could have been due to the fragment boundaries not encompassing distinct domain(s) of Gcn1 which may prevent formation of a functional, soluble fold. Although the majority of $Gcn1_{frag}$ was insoluble, a small proportion of the protein present was soluble (Lane 3).

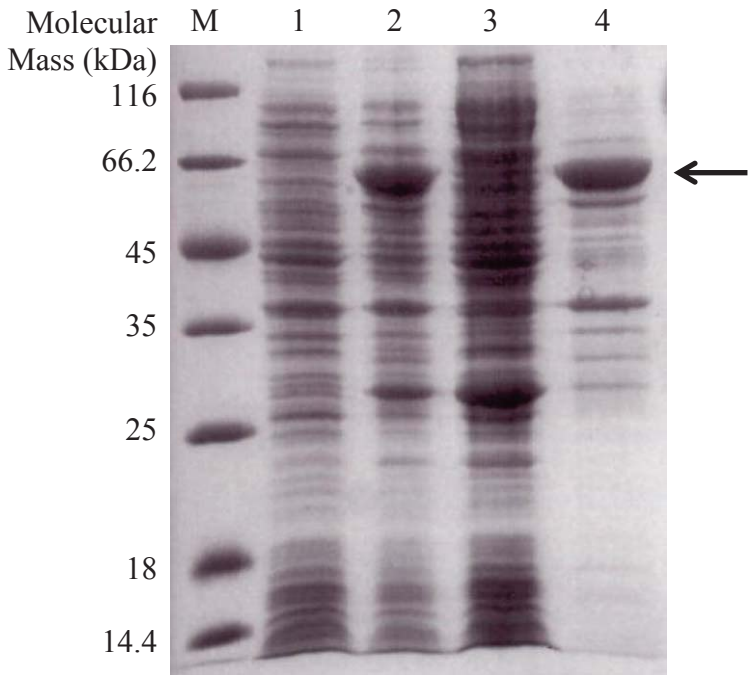

Figure 4.2 SDS-PAGE of Gcn1 Expression and Solubility Test

Recombinant $Gcn1_{frag}$ was expressed in *E. coli* and lysed by sonication as described in section 2.2.14. The resulting fractions were analysed by 12.5% SDS-PAGE. Lane M: Molecular weight marker; Lane 1: Whole cell lysate of uninduced cells; Lane 2: Whole cell lysate of cells induced with 0.1mM IPTG; Lane 3: Soluble fraction of induced cells; Lane 4: insoluble fraction of induced cells. The $Gcn1_{frag}$ band is indicated by an arrow.

4.2.2.2 $Gcn1_{frag}$ Purification By Glutathione Agarose

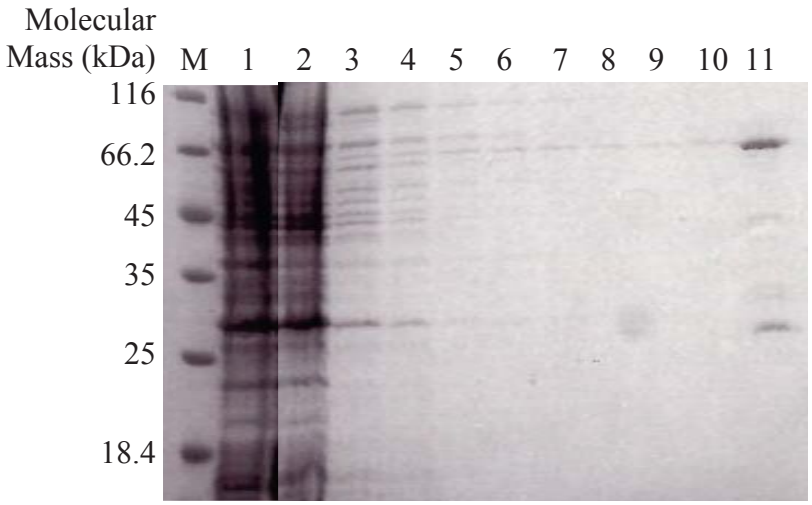

Figure 4.3 SDS-PAGE analysis of Glutathione-agarose Binding of $Gcn1_{frag}$.

A cell lysate containing Gcn1-frag was bound to glutathione agarose. Unbound and wash fractions were analysed by 12.5% SDS-PAGE. Lane M: Molecular Weight Marker; Lane 1: Unbound Fraction; Lanes 2-10: wash fractions; Lane 11: Protein bound to resin.

As $Gcn1_{frag}$ had been provided in a Glutathione-S Transferase (GST)-fused construct, glutathione-agarose was utilised for purification, exploiting the affinity that GST has for its substrate glutathione. As Figure 4.3 shows, GST-$Gcn1_{frag}$ (~60.1 kDa) had successfully bound to the glutathione-agarose (Lane 11) with most contaminants removed by the GEQ buffer wash steps.

After treatment with PreScission Protease overnight, $Gcn1_{frag}$ was expected to elute in the initial washes as it should be freed from its GST-tag and subsequently have no affinity for the glutathione-agarose. Analysis of the wash step fractions by SDS-PAGE (Figure 4.4, Lanes 1-3) showed no protein had been eluted under these conditions. Only upon the addition of free reduced glutathione was $Gcn1_{frag}$ released (Lanes 4-6). As the largest proportion of the protein eluted was ~60kDa, it appears that the cleavage was incomplete and this would explain the lack of protein eluting in the expected wash steps. Cleaved $Gcn1_{frag}$ is ~35 kDa. There does appear to be a band at that mobility in the elution fractions that doesn't appear to be present before treatment with the protease (Figure 4.3, Lane 11). If this band is indeed cleaved

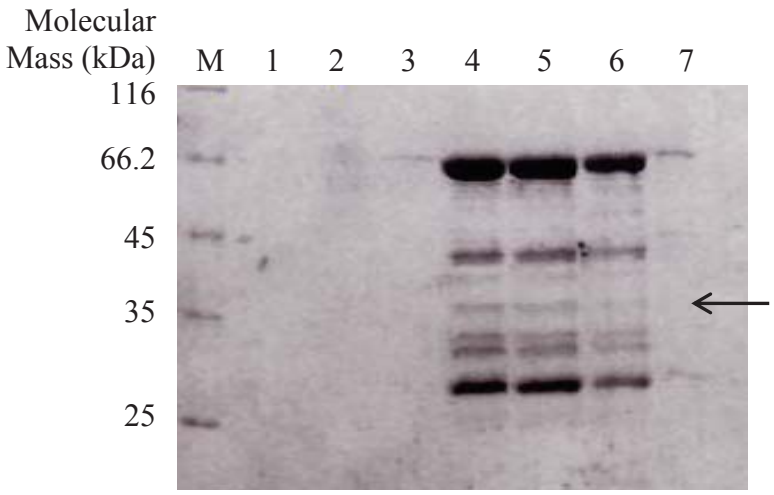

Figure 4.4 SDS-PAGE of $Gcn1_{frag}$ Elution from Glutathione Agarose

Protein was eluted from glutathione-agarose with buffer containing 25 mM reduced glutathione and subjected to 12.5% SDS-PAGE. Lane M: Molecular Weight Marker; Lanes 1-3: Wash fractions; Lanes 4-6: Glutathione elution fractions; Lane 7: Post-elution Glutathione agarose. Arrow indicates position of possible cleaved $GCN1_{frag}$ band.

$Gcn1_{frag}$, it seems odd that it would be eluted only upon the addition of glutathione. Since GST is known to aid in solubilizing protein, removal of the tag from $Gcn1_{frag}$ may result in it becoming insoluble and forming hydrophobic interactions with the bound proteins resulting in the glutathione-dependent elution we see. It is also possible that this may be due to a previously unknown glutathione-binding activity of Gcn1. As mentioned in Section 1.1.5, deletion of Yih1 results in increased levels of the antioxidant glutathione. If indeed Gcn1 does bind to glutathione, this may implicate Gcn1 and Yih1 in oxidation sensory or response pathways. This would also cast some doubt on pull-down experiments that have been published using GST-YIH1 and Gcn1 as any potential glutathione-binding activity of Gcn1 may provide aberrant results. Therefore it would be worth investigating further to exclude the possibility.

Due to the low yield of Gcn1 the preparation was abandoned. It is likely that the issues with solubility were due to the fragment boundaries chosen and optimisation of these boundaries would yield soluble protein in the large amounts required for crystallography trials.

4.2.2.3 Actin Expression and Solubility

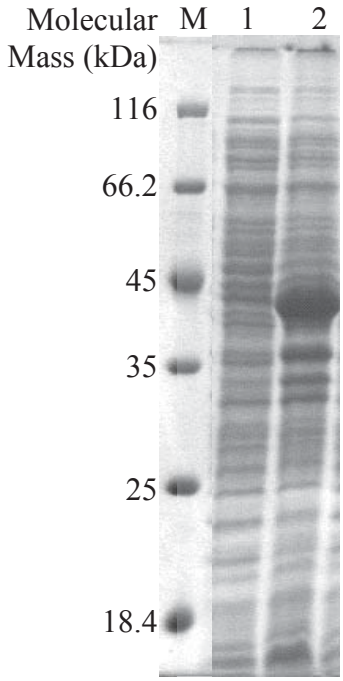

Figure 4.5 SDS PAGE of Actin Solubility

12.5% SDS PAGE of soluble and insoluble cellular fractions. Lane M: Molecular Weight Marker; Lane 1: soluble protein; Lane 2: Insoluble protein

Although Actin was highly expressed in the *E. coli* host cells, the protein was insoluble (Figure 4.5, Lane 2). As it was possible the insolubility was due to polymerisation, the sample was dialysed against depolymerisation buffer to try to remove any cations that would promote polymerisation. As there was no apparent difference in the sample post dialysis, it is improbable that polymerisation was responsible for the insolubility. It has been shown that actin recombinantly expressed in *E. coli* forms interactions with outer-membrane proteins upon lysis that result in insolubility (Kimball, 1999). To attempt to combat this, 0.2% w/v sarkosyl was included in the lysis buffer. Again, SDS-PAGE analysis showed actin to be insoluble; dialysis of the pellet against depolymerisation buffer was still not able to solubilize any actin. A possible way to combat this may be to perform lysis in a much larger volume, in the hope of reducing the rate of protein aggregation.

4.2.2.4 Actin and Yih1 Size Exclusion Chromatography

In an attempt to isolate an actin:Yih1 complex for crystallography, rabbit actin was incubated with an equimolar concentration of Yih1, then subjected to size exclusion chromatography to separate complexed from uncomplexed molecules. The chromatogram of the material formed during this incubation eluted as a single peak that eluted at a smaller elution volume than each of the single proteins (Figure 4.6). It would thus appear that a complex had formed. However, when SDS-PAGE is also brought into the analysis (Figure 4.7), it appears that this shifted peak contains no Yih1 and therefore is most likely to be polymerised actin.

The input samples and fractions of the size exclusion run were analysed by native PAGE in order to detect possible interaction between actin and Yih1 (Figure 4.8). Although the actin input sample (Figure 4.8, Lane 8) was expected to migrate through the native gel to a lesser degree than Yih1 due to its larger size and less acidic pI (5.44), the degree to which it was retarded and smearing of bands indicated multiple species of actin were present, with some protein unable to penetrate the higher percentage resolving gel indicating that actin was in a polymerised form and thus unavailable for interaction with Yih1. Attempts were made to depolymerise the commercial rabbit actin by dialysis against depolymerisation buffer, but these were unsuccessful.

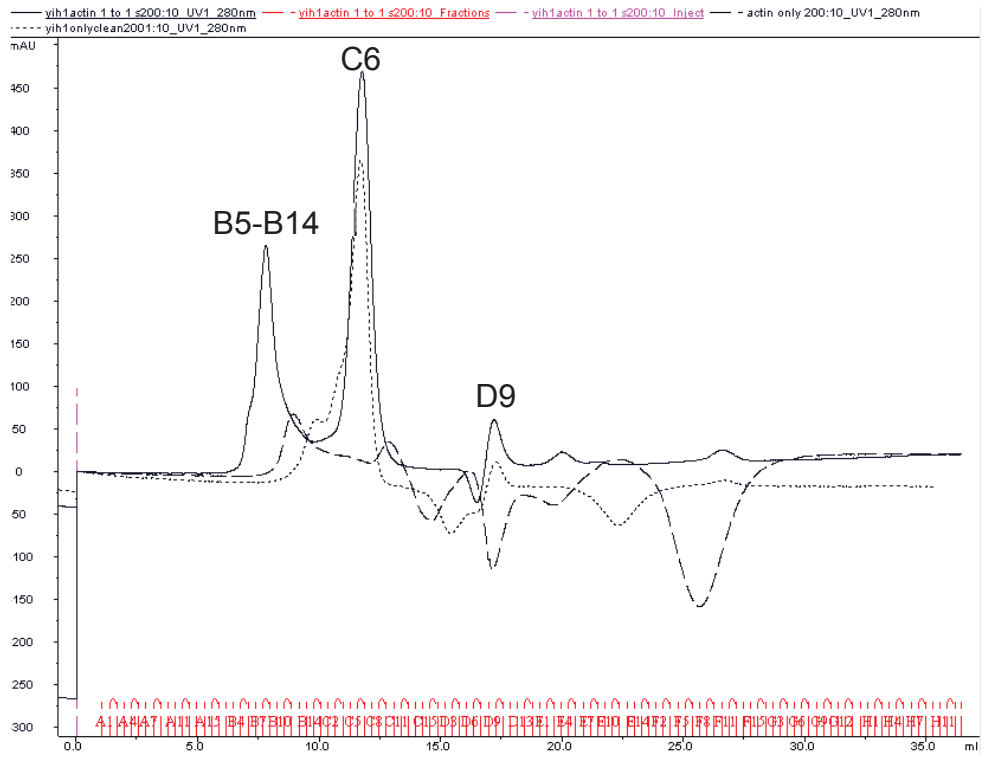

Figure 4.6 Chromatogram overlay of Yih1:actin SEC

Solid line: actin and Yih1; Dotted line: Yih1; Dashed line: actin.

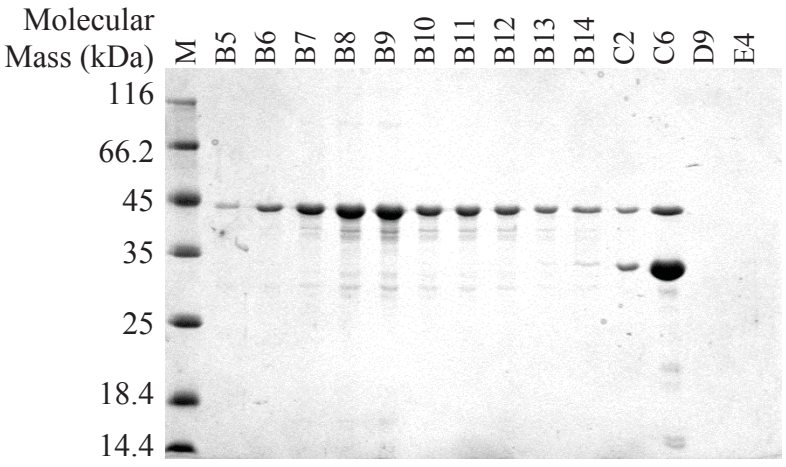

Figure 4.7 SDS PAGE of Yih1:Actin SEC

Lane M: Molecular Weight Marker; Lanes 1-14: Yih1:actin Size exclusion fractions from Figure 4.6.

Unexpectedly, Yih1 exhibited multiple species when subjected to native PAGE (Figure 4.8, Lane 1). This is further explored in Chapter 5.

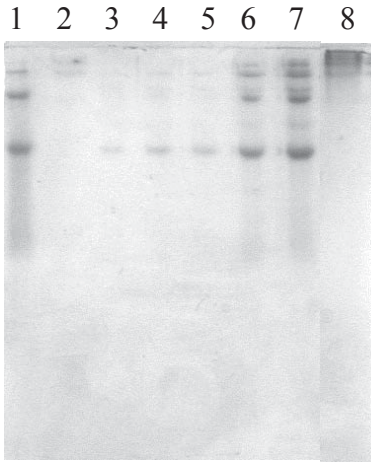

Figure 4.8 Native PAGE of Yih1:Actin SEC

Lane 1: Yih1 input; Lane 2: Fraction C11; Lanes 3-7 fractions C2-C6; Lane 8: Actin input

4.2.3 Surface Entropy Reduction of Yih1

4.2.3.1 Prediction of Sites for Surface Entropy Reduction

The amino acid sequence of Yih1 was submitted to the Surface Entropy Reduction Prediction Server at the Eisenberg Laboratory, UCLA (http://nihserver.mbi.ucla.edu/SER/). The mutations proposed by the server are outlined in Table 4.2. The SERp score is calculated using parameters such as calculated entropy, evolutionary conservation and secondary structure prediction. The higher the score, the more appropriate it is to mutate that residue or residue cluster. The scoring system gives preference to residue(s) that are not conserved or predicted to be within α-helical or β-sheet/strand structures and that are calculated to have high entropy. For example, in Yih1 there is a cluster of high entropy residues within the Ancient domain, DDGE. Although this cluster was predicted to have high entropy and be neither α-helical nor β-strand in structure, the server did not suggest this cluster to be mutated due to its high conservation. Since the residues chosen are charged, they are more likely to be on the surface of the protein as it is uncommon for residues in charged patches to be in the hydrophobic core of soluble proteins. Therefore it is unlikely that their mutation to alanine will result in a significant difference in the protein structure.

Complementary Primers were designed to introduce the respective mutations indicated in Table 4.2 (Appendix 8).

Table 4.2 Recommended Mutations for Surface Entropy Reduction

Current Sequence	Proposed Mutation	SERp Score
25-KQE-27	25-AAA-27	6.9
56-EE-57	56-AA-57	6.61
116-EEE-118	116-AAA-118	5.9

4.2.3.2 Site-Directed Mutagenesis of PCR Products

Site-Directed Mutagenesis was carried out (2.2.16) using the pES317-15b construct encoding untagged Yih1 (DNA template). An untagged construct was chosen over a His_6-tagged construct as it has been noted that His-tags show electron density in less than 10% of crystal structure annotated as being His-tagged constructs in the Protein Data Bank (Carson *et al.*, 2007). Lack of electron density indicates that the His-tag is disordered and flexible. As the purpose of this experiment was to reduce the surface entropy of Yih1, the use of tags that are possibly flexible would potentially negate the positive effects of SER.

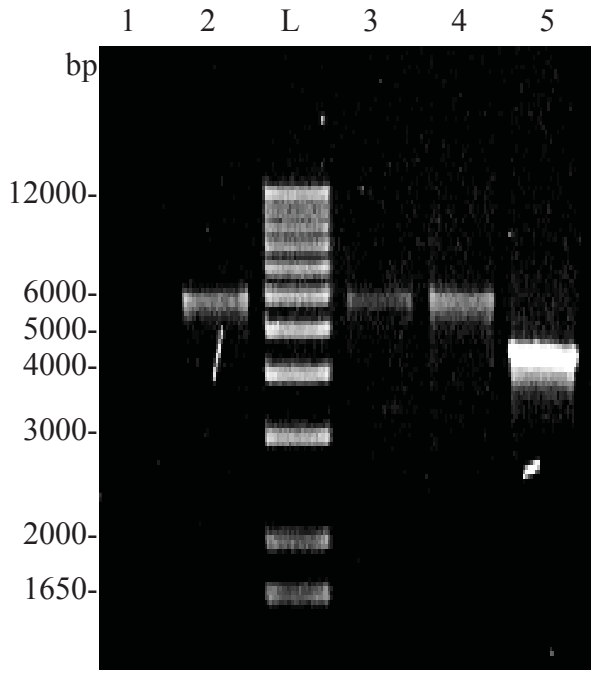

Figure 4.9 Agarose Gel of Site Directed Mutagenesis PCR product

DNA fragments were separated by 1% agarose gel electrophoresis as described in Materials and Methods (2.2.6).Lane 1: Reaction mix with no DNA template; Lane 2:Yih1 EE56AA reaction; Lane L: DNA ladder; Lane 3: Yih1 KQE26AAA; Lane 4: Yih1 EEE116AAA; Lane 5: DNA template (pES317-15b)

Analysis by ethidium bromide-stained agarose electrophoresis (Figure 4.9) shows there was only one visible band in each mutagenesis reaction at ~5.8 kbp, the mobility predicted for the linearized plasmid. As there is no band in the reaction mix containing no DNA template (Lane 1), it appears that the primers did not amplify any possible contaminants in the different components of the reaction indicating that the bands present in lanes 2, 4 and 5 are specifically amplified from the template plasmid.

4.2.3.3 Direct Sequencing of Modified Plasmids

After *Dpn*I treatment to remove template DNA and transformation, a number of colonies grew overnight. A selection of these colonies were picked from the LB-AB-agar and grown in sterile liquid LB-AB overnight. The plasmids were extracted (2.2.8) and sent for sequencing to confirm if the correct mutation(s) had been introduced. The sequences for residues at positions 56-57 and 116-118 were correct, whereas the sequence for residues 26-28 was that of the wild-type, indicating that the site-directed mutagenesis had not been successful. The Yih1 EE56AA and EEE116AAA mutants are referred to as Yih1-56 and Yih1-116 and their encoding plasmids, pNAT56 and pNAT116 respectively in this thesis

4.2.3.4 Expression Trials of Yih1 Surface Entropy Reduction Single Mutants

As SER involves the replacement of hydrophilic charged residues with neutral residues, it is possible to affect the solubility of a protein by performing SER. To confirm the expression and solubility of the SDM Yih1 variants, induced cells were lysed (2.2.14) and their soluble and insoluble fractions were analysed by SDS PAGE (Figure 4.10). As there is a dark band in both the whole cell extract and supernatant fractions at the expected molecular weight for both the mutants, it appears that the site-directed mutagenesis successfully produced SER mutants that were able to be overexpressed in a soluble form.

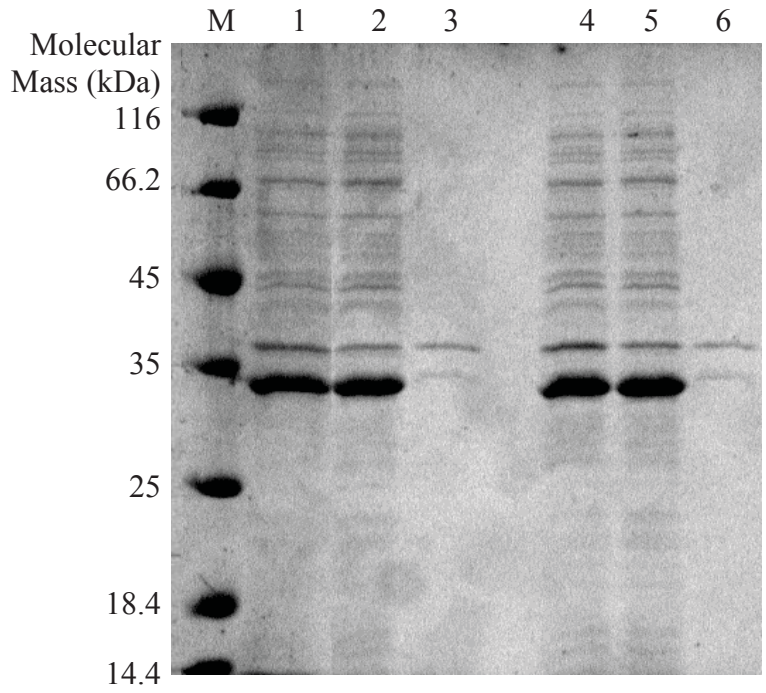

Figure 4.10 SDS PAGE of expression and solubility of SER Yih1 variants

12.5% SDS PAGE analysis of *E. coli* expressing Yih1 varients.

Lane M: Molecular Weight Marker; Lane 1: Yih1-56 whole cell extract; Lane 2: Yih1-56 soluble fraction; Lane 3: Yih1-56 insoluble fraction; Lane 4: Yih1-116 whole cell extract; Lane 5: Yih1-116 soluble fraction; Lane 6: Yih1-116 insoluble fraction.

4.2.3.5 Site-directed mutagenesis to produce EE56AA,EEE116AAA double mutant

Site-directed mutagenesis was performed as outlined in Section 2.2.16 using the plasmid encoding Yih1-116 (pNAT116) as the DNA template and primers directing the EE56AA mutation. The resulting plasmid was extracted and the sequence was confirmed as Yih1 EE56AA, EEE116AAA. An expression and solubility test confirmed that the expressed protein was soluble. This mutant is referred to as Yih1-56.116 and its encoding plasmid pNAT56.116 in this thesis.

4.2.3.6 Purification of Yih1 Surface Entropy Mutants

The Yih1-56, Yih1-166 and Yih1-56.116 mutants were recombinantly produced, harvested by centrifugation, lysed by mechanical disruption and purified by anion exchange and size exclusion chromatography as outlined in sections 2.2.20, 2.2.21, 2.2.22 and 2.2.24. The Yih1 mutants were eluted at a lower NaCl concentration in anion exchange compared to the wild-type protein. This was expected due to the replacement of negatively charged glutamic acid residues with the uncharged alanine. No other differences in the purifications were observed compared to that of the wild-type Yih1.

4.2.3.7 Circular Dichroism of Yih1 Surface Entropy Mutants

The residues mutated for surface entropy reduction are not conserved and due to their charge, likely reside on the exterior of the protein. Although these factors indicate that mutation of these residues is unlikely to result in structural changes, it does not ensure it. To assess the effect of the single SER mutations, the far-UV circular dichroism spectra of purified Yih1-56 and Yih1-116 was measured as described in Section 2.2.26. Figure 4.11 shows the measured spectra for each mutant. Comparison of the spectra to that of wild-type Yih1 shows that there are differences between each of the Yih1 variants. Although there appears to be significant differences in the 190nm-200nm range, this range can be sensitive to differences in the solution such as the concentration of inorganic ions or dissolved oxygen and therefore are often excluded from analysis (Wetlaufer, 1963). Yih1-56 shows very little difference to WT Yih1, indicating it is likely to have retained the same fold, whereas Yih1-116 is markedly different from wild-type. Given that residues 116-118 reside in the linker region, it is possible that replacement of the charged, flexible glutamic acid residues with the amino acid alanine may have resulted in the extension of a helix from the C-terminal end of the RWD domain. However, given the presence of proline (a known helix-breaking residue) surrounding these residues (115-**P**AAATE**P**-121) it is unlikely, and this is further supported by secondary structure prediction of Yih1-116 by Psipred (http://bioinf.cs.ucl.ac.uk/psipred/) that shows that 116-118AAA is predicted to be

unstructured. The CD spectra show that Yih1-56 and Yih1-116 were suitable for crystallisation experiments.

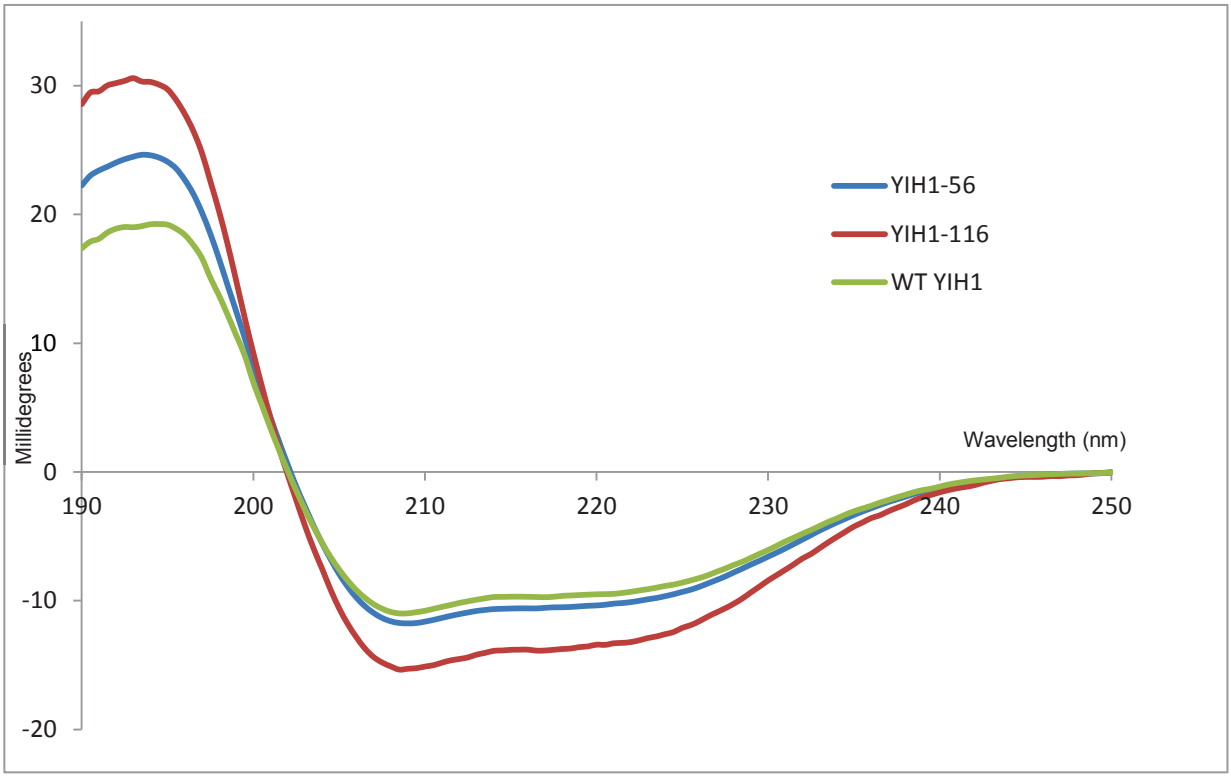

Figure 4.11 CD spectra of Yih1 Surface Entropy Mutants

4.2.3.8 Crystallisation of Yih1 Surface Entropy Mutants

Crystallisation trials of the Yih1 surface entropy reduced mutants are outlined in Table 4.3.

Table 4.3 Crystallisation Screens of Yih1 surface entropy mutants

Protein	Concentration	Screen Name	Supplier	Method	Temperature
Yih1-56	7.6 mg/mL	Crystal Screen I+II	Hampton Research	SD-VD	21°C
		PACT premier	Molecular Dimensions	SD-VD	21°C
Yih1-116	11.2 mg/mL	Crystal Screen I+II	Hampton Research	SD-VD	21°C + 4°C
		PACT premier	Molecular Dimensions	SD-VD	21°C
Yih1-56.116	6.5 mg/mL	Crystal Screen I+II	Hampton Research	SD-VD	21°C
		PACT premier	Molecular Dimensions	SD-VD	21°C

Only one condition produced crystals that appeared to be protein. Yih1-116 crystallised in a PACT premier screen in the conditions 0.2 M ammonium chloride, 0.1 M MES, pH 6.0, 20% PEG 6000 after one month (Figure 4.12). The crystals were very fragile, indicative of protein crystals. Due to their size and needle-like morphology, the crystals were not suitable for X-ray diffraction analysis. The conditions (pH, PEG 6000 concentration) were optimised in 24-well format (2.2.43) but did not yield any crystals. Additionally, a seed stock of the crystals was produced and used in a matrix-seeding experiment as described in section 2.2.47 using the matrix screen “Crystal screen I + II” (Hampton Research). Crystals that formed were found to be salt when analysed by X-ray diffraction.

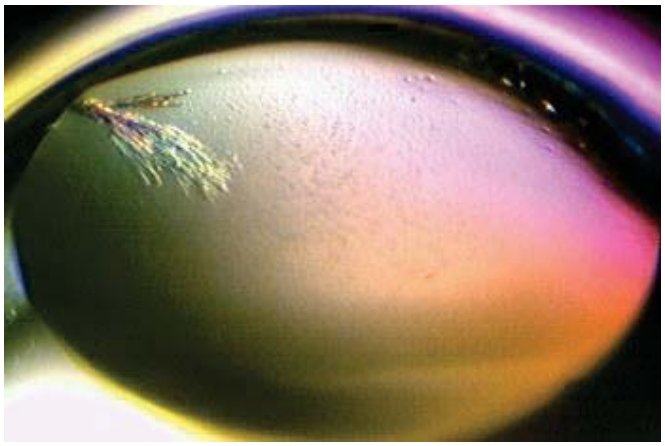

Figure 4.12 Crystal Grown of Yih1-116

Crystals grown after one month in a PACT premier screen (0.2M ammonium chloride, 0.1M MES, pH 6.0, 20% PEG 6000).

4.2.4 Cloning of the Ancient Domain of Yih1

4.2.4.1 PCR and Agarose Gel Electrophoretic Analysis

The Ancient domain was amplified from the pES317-15b construct encoding full-length Yih1 using primers specific to the borders of the domain with restriction site adaptors on their 5′ ends to assist with ligation into an expression vector. The

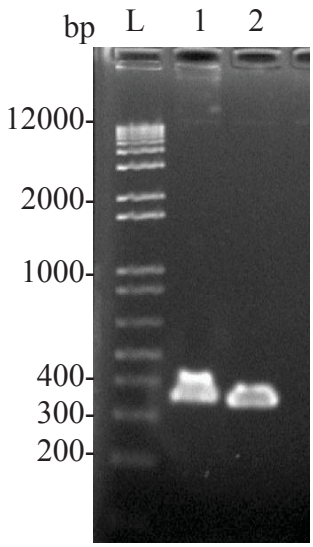

Figure 4.13 Agarose Gel of Ancient Domain PCR

PCR reactions were subjected to 1.5% Agarose Gel Electrophoresis (2.2.6). Lane 1: 1kB^{+} DNA Ladder; Lane 2: Ancient domain PCR; Lane 3: No DNA Template control.

reaction amplified the correctly sized product, yielding a fragment of approximately 380bp (Figure 4.13, Lane 1). As there was also a band of a similar mobility in the no DNA template control (Lane 2), the PCR product was sent for sequencing and the results confirmed that it was the correct sequence encoding the Ancient domain. The reason for the double-banded nature of the PCR-product in both lanes is unknown. As the Ancient domain is highly conserved, the primers may have amplified contaminating DNA from the *E. coli* host strain or another organism. It is also possible that the restriction site clamps placed on the 5′ end of one of the primers may have annealed to its cognate restriction site the multiple cloning site of the pES317-15b plasmid, amplifying a longer sequence. However, this is unlikely as the

3′ end of the primer requires an interaction with the template DNA to allow in the polymerase to extend it.

4.2.4.2 Agarose Gel Electrophoresis of Restriction Enzyme Digested Plasmid

The PCR product and modified pET32a plasmid (pET32a(*Bam*HI)) were cut with the restriction enzymes *Xho*I and *Bam*HI (2.2.18). To assess the success of the restriction enzyme digest, samples of the vector that had been cut with either *Xho*I, *Bam*HI or both were analysed by agarose gel electrophoresis along with an uncut control (Figure 4.14). As all three cut plasmid reactions contained a single band at the mobility expected for the linearized modified pET32a plasmid, it appears that the restriction digest was successful. It could not be ascertained by agarose gel electrophoresis if the insert restriction digests were successful as the difference in the mobility of the insert on an agarose gel would not be obvious due to the short fragments released. However, as the insert was treated in the same way as the vectors at the same time, it is most likely that it too was cut.

After ligation of the cut insert and plasmid, *Hind*III digestion was performed to remove

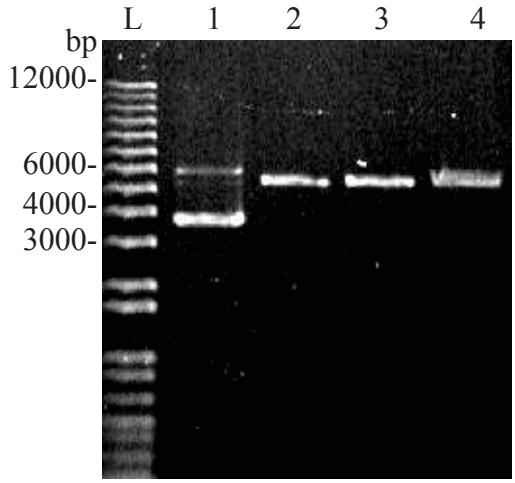

Figure 4.14 Agarose Gel of Digested Vector

pET32a-His was digested (2.2.18) and analysed by 0.5% agarose gel electrophoresis (2.2.6). Lane L: 1 kB+ DNA ladder; Lane 1: Uncut vector; Lane 2: *Xho*I cut vector; Lane 3: *Bam*HI cut vector; Lane 4: *Xho*I and *Bam*HI double cut vector.

background recircularisation of the plasmid lacking the insert. XL1-blue cells were transformed by heat-shock and yielded 33 colonies in contrast to the ~1000 colonies that grew when no *Hind*III digestion was performed.

Five colonies were selected to check that the correctly sized insert had been inserted into the plasmid by restriction digest with *Xho*I and *Bam*HI (2.2.18). When analysed by agarose gel electrophoresis (Figure 4.15), all five clones appeared to yield an insert of the correct size (~380 bp) while the resulting empty vector had the same mobility as the pET32a-His cut vector, good evidence the cloning of the Ancient domain into the pET32a-His vector had been successful.

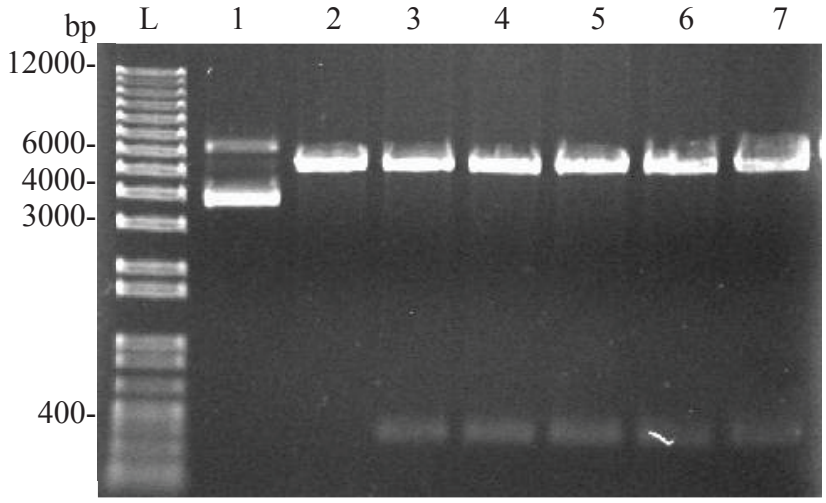

Figure 4.15 Agarose Gel of Digested Constructs to Confirm Ligation

Constructs were digested with *Xho*I and *Bam*HI (2.2.18) and subjected to 0.5% Agarose Gel Electrophoresis (2.2.6). Lane L: 1 kB^{+} DNA ladder; Lane 1: Uncut pET32a-His vector; Lane 2: Digested pET32a-His; Lane 3-7: Digested constructs 1-5.

To confirm the integrity of the sequence, clone 1 was sent for sequencing. The sequence was correct. This clone was named pNAT04-1

4.2.4.3 Ancient Domain Expression Trials

pNAT04-1 was transformed using heat shock (2.2.7.2) into *E. coli* BL21 (DE3) cells and protein expression was analysed by SDS-PAGE (Figure 4.16). There did not appear to be any overexpressed protein at the mobility expected for an N-terminal His-tagged Ancient domain (~14kDa) and this was further confirmed by the inability to enrich for the expected sized protein using immobilised metal affinity chromatography (data not shown) as described in Section 2.2.23. As the function of the Ancient domain is unknown, it is possible that overexpression of the domain by itself may be toxic to the cell. Although the Ancient domain of Yih1 has been successfully expressed in *S. cerevisiae* (Sattlegger *et al.,* 2011), there is no published account of expression of the Yih1 Ancient domain in *E. coli*. With this in mind, pNAT04-1 was transformed into OverExpress C41 (DE3) competent cells. C41 is a strain of E. *coli* derived from BL21 (DE3) that carries an uncharacterised mutation that prevents cell death associated with expression of many non-

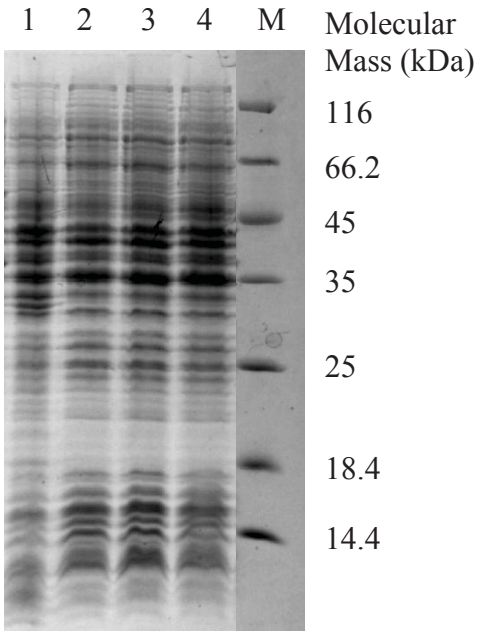

Figure 4.16 SDS PAGE of pNAT04-1 expression in BL21 E .coli

Cells were lysed in 2x SDS PAGE loading buffer and subjected to 15% SDS PAGE. Lane 1: Uninduced cells; Lane 2: Clone 1 induced with 0.1mM IPTG; Lane 3: Clone 2 induced with 0.1mM IPTG; Lane 4: Clone 3 induced with 0.1mM IPTG; Lane M: Molecular weight marker.

endogenous toxic proteins. Analysis of protein expression by SDS-PAGE (Figure 4.17) showed no overexpressed band at the molecular weight expected for the His-tagged Ancient domain. It may also be that the modified pET32a-(*Bam*HI) plasmid was defective, potentially carrying a mutation outside of the multiple cloning site that had its sequence confirmed that may have resulted in the lack of transcription of the Ancient domain cDNA.

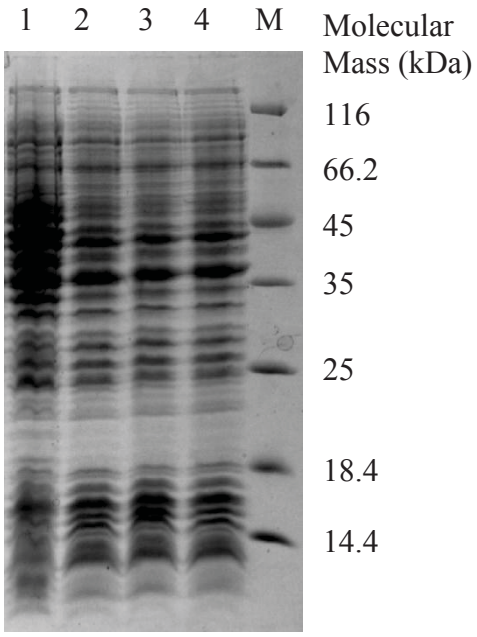

Figure 4.17 SDS PAGE of pNAT04-1 Expression in C41 E. coli

Cells were lysed in 2x SDS PAGE loading buffer, boiled and subjected to 15% SDS PAGE. Lane 1: Uninduced cells; Lane 2: Clone 1 induced with 0.1mM IPTG; Lane 3: Clone 2 induced with 0.1mM IPTG; Lane 4: Clone 3 induced with 0.1mM IPTG; Lane M: Molecular weight marker.

5. INVESTIGATION INTO THE HETEROGENEITY OF YIH1

5.1 Introduction

Heterogeneity of a protein population can be caused by a variety of reasons: multimerisation, modification, unfolding, conformational changes, interactions with another molecule (protein or otherwise) or degradation. As native gels separate protein based on both mass and charge, alternative methods were required to deduce the nature of the differences seen in the native gels shown in Figure 4.8. To do this, the protein was subjected to analytical anion exchange to look for charge differences in the protein population; the protein was crosslinked with glutaraldehyde to stabilize any interactions between Yih1, itself and other molecules; various methods were used to investigate the potential for the formation of a Yih1-nucleic acid complex. The effects of a selection of salts and small molecules on the observed heterogeneity of Yih1 in native gels were investigated.

5.2 Results and Discussion

5.2.1 Native Polyacrylamide Gel Electrophoresis of Yih1 Variants

Analysis of Yih1 by native PAGE in Figure 4.8 revealed the presence of multiple bands. To check whether this was due to protein denaturation at the high temperatures reached during electrophoresis at room temperature, Yih1 and its variants were subjected to Native PAGE at 4°C and 150V. The results confirmed that at this reduced temperature, all Yih1 variants tested resolved as multiple species (Figure 5.1). Furthermore the multiple bands seen in the native gel could not be attributed to the presence of contaminating proteins because of the absence of bands of similar intensities in SDS-PAGE (Figure 5.2). This was the case for all variants tested. These species generally consisted of a high mobility double-band, an average mobility smear and multiple bands of lower mobility, and were thought to be different oligomeric states of Yih1. As His-Yih1$_{cys-}$ also exhibited this phenomenon, the lower mobility species could not be attributed to the formation of disulfide bonds (The decrease in mobility exhibited by His$_6$-Yih1$_{cys-}$ (C67A,C99A) is due to a longer sequence between the His$_6$-tag and the protein resulting in an increased mass to charge ratio, retarding its mobility through the gel relative to the other Yih1 variants).

The thiol sidechain of cysteine is highly reactive and has been shown to undergo a variety of post-translational modifications both enzymatically and redox driven including glutathiolation, ADP-ribosylation and nitrosylation. It is possible that a cysteine modification may be the cause of the double band, most likely a redox based modification that is readily reversible which would account for inconsistencies between different experimental methods.

Due to their reduced negative charge, the surface entropy mutants of Yih1 (Figure 5.1, Lanes 2 and 3) sit higher on the gel than WT Yih1. Consistent with this, Yih1-116 displays a slightly retarded mobility compared to Yih1-56 due to the replacement of three glutamic acids with alanine whereas Yih1-56 has only two glutamic acid residues replaced with alanine. As expected, the His_6-tagged variants of Yih1 (Figure 5.1, Lanes 4 and 6) display lesser mobility than WT Yih1 due to the size difference that the tag confers. This is also shown by SDS-PAGE (Figure 5.2). However, they also appear to differ slightly in their mobility relative to one another in native gels. This may indicate there are differences in the folding between these two constructs which is consistent with their CD spectra (Figure 3.11). The differences could also be due to the packing of the His_6-tags. If this is the case, given the slight increase in mobility of Yih1-His_6, it may better pack the His_6-tag resulting in a more compact conformation and less exposed positive charge than His_6-Yih1. As the C-terminus of the Ancient domain is modelled to be in close proximity to the linker region which carries a high proportion of negatively charged residues, the His_6-tag may be forming electrostatic interactions with this region.

Interestingly Yih1-56 displays a larger proportion of the lower mobility bands that are likely to be multimers. Given the positions of these residues is within the triple turn of the RWD domain, this may implicate this motif, characteristic of RWD domains, in preventing or regulating multimerisation under different cellular conditions as required.

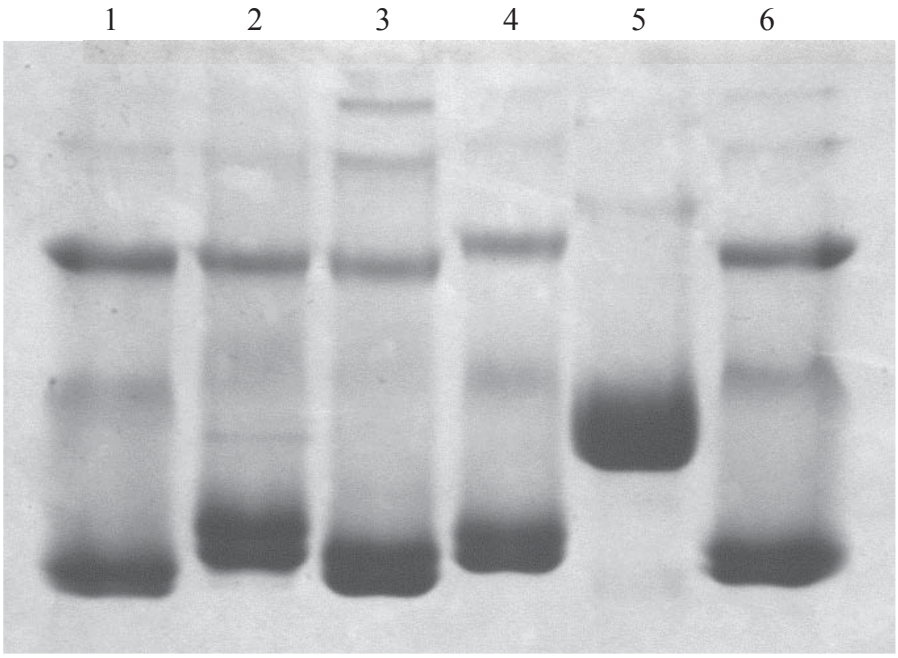

Figure 5.1 Native PAGE of Yih1 Variants

Lane 1: WT Yih1; Lane 2: Yih1-116 (EEE116-118AAA); Lane 3: Yih1-56 (EE56-57AA); Lane 4: His_6-Yih1 Lane 5: His_6-$Yih1_{cys-}$ (C67A, C99A); Lane 6: Yih1-His_6.

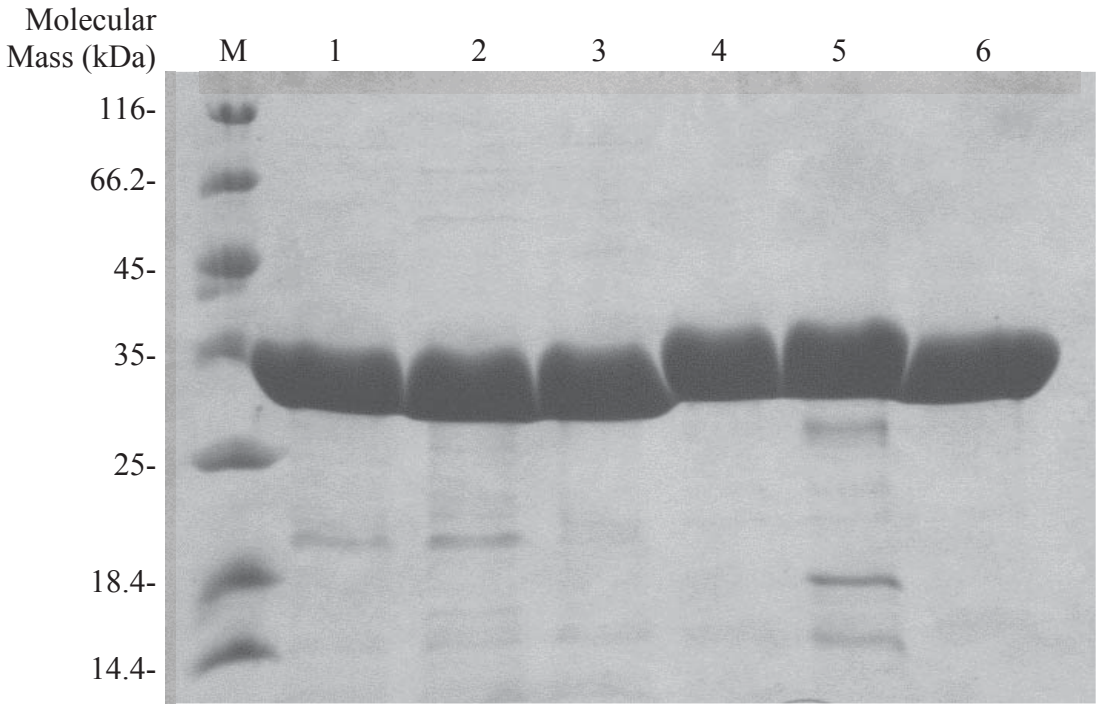

Figure 5.2 SDS-PAGE of Yih1 Variants

Lane M: Molecular Weight Marker; Lane 1: WT Yih1; Lane 2: Yih1-116; Lane 3: Yih1-56; Lane 4: His_6-Yih1 Lane 5: His_6-$Yih1_{cys-}$; Lane 6: Yih1-His_6.

5.2.2 Source Q Anion Exchange Chromatography

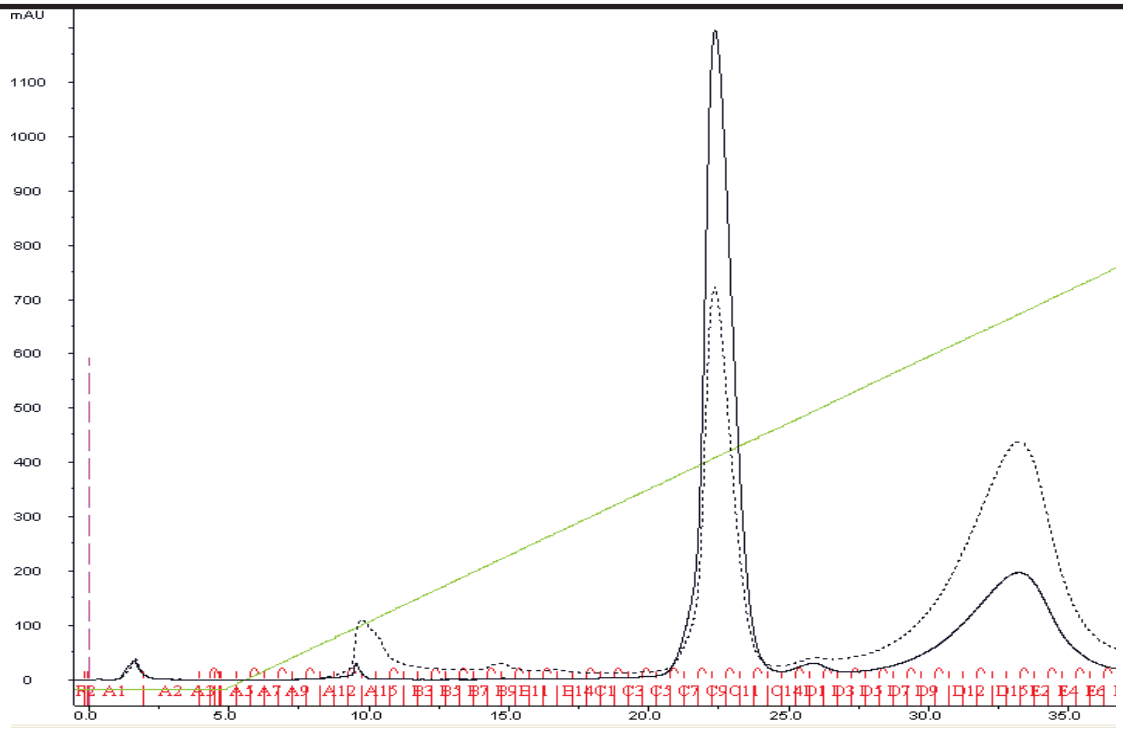

Figure 5.3 Analysis of Yih1 by Analytical Anion Exchange Chromatography

Yih1 was subjected to separation on a Source Q column and elution was performed by a NaCl gradient. Solid blue line: A_{280}; dotted blue line: A_{260}; green line: NaCl gradient.

Untagged wild-type Yih1 was analysed by Source Q anion exchange chromatography as described in section 2.2.33. Two main peaks were observed (Figure 5.3): one well resolved peak with a low A_{260}:A_{280} absorbance eluting at approximately 0.3 M NaCl; and a less well resolved peak eluting at approximately 0.45M NaCl with a higher A_{260}:A_{280} ratio. SDS-PAGE showed that the first peak contained Yih1 whereas the second peak had no detectable protein content when visulised by Coomassie blue staining. Analysis of the second peak by agarose gel electrophoresis followed by ethidium bromide staining revealed a smeared band of the same mobility as ~20-200 bp of dsDNA (Figure 5.4A). As the band could be visulised by ethidium bromide staining, it appeared that the peak contained nucleic acid, consistant with the high A_{260}:A_{280} ratio. If this is the case, it would appear that Yih1 had released nucleic acid that had been co-purified from the host *E. coli*. It is possible that Yih1 had started to unfold or undergo some unknown change to release this nucleic acid, possibly due to an increase in NaCl concentration disrupting ionic

interactions within the Yih1 molecule. It is also possible that the increase in NaCl concentration disrupted the ionic interactions between the DNA and Yih1. This has been shown to be the case for the lac repressor and other transcription factors (Hart *et al.*, 1999, Barkley *et al.*, 1981). Although Yih1 had been through a high concentration of NaCl in its preparative ion exchange step, the difference in pH (pH 5.8 in preparation, pH 8.0 in analytical) may have affected the state of ionisable

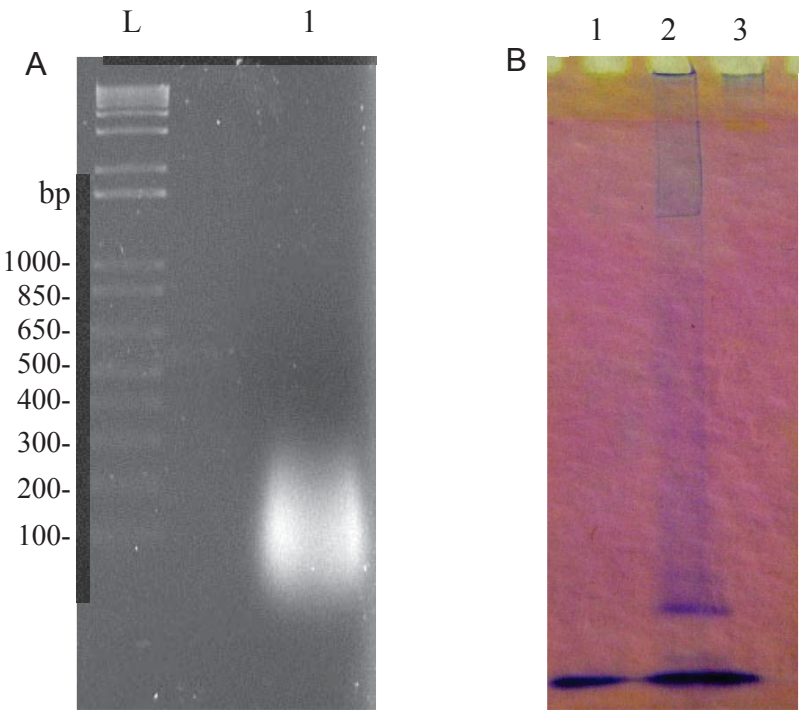

Figure 5.4 Gel Electrophoresis of Source Q A_{260} Peak

Fraction E1 from Yih1 source Q chromatography was subjected to: (A) Agarose gel electrophoresis and subsequent staining with ethidium bromide. Lane L: DNA 1kB+ ladder, Lane 1: 20 µL Fraction E1; (B) Native PAGE and subsequent staining with Stains-all. Lane 1:10 µL Fraction E1, Lane 2: RNA control (contains some higher molecular weight DNA plasmid), Lane 3: DNA plasmid control.

groups on Yih1, resulting in the release of the nucleic acid. The N-terminal amino group and the sidechains of histidine and cysteine change ionisation between those two pH's, although that does not exclude other sidechains from being affected at these pH values due to modulation of their pK_a values by the local environment of the residues (Isom *et al.*, 2011). The pooled fractions from the protein peak were re-

subjected to AEX multiple times using the same conditions; each time the putative nucleic acid peak eluted at a lower NaCl concentration at a lower intensity. This probably reflected the gradual removal of the nucleic acid from the protein during each passage through the column.

The putative nucleic acid sample was subsequently analysed by native PAGE, then stained with the dye Stains-all (Figure 5.4B). Stains-all is a cationic dye that stains protein and nucleic acid different colours dependent on the mode of binding (Sharma *et al.*, 1989). The sample appeared as a blue band at the dye front indicating that it is a very small molecule and/or carrying a large negative charge. The blue staining colour was similar to that of the RNA control sample, whereas a DNA sample run on the same gel stained a purple-blue colour. The lesser mobility species in the RNA control lane was contaminating DNA plasmid. This suggests that the sample is RNA that has been displaced from purified Yih1.

5.2.3 Glutaraldehyde Crosslinking

Glutaraldehyde is a crosslinking agent that is able to adopt two different conformations allowing the formation of a covalent linkage between reactive groups that are within 5-8 angstrom in distance from one another (Nagarajan *et al.*, 1996). To determine if Yih1 forms intermolecular interactions with itself, Yih1 was subjected to glutaraldehyde crosslinking and analysed by SDS-PAGE. Figure 5.5 shows Yih1 successfully crosslinked with prominent bands at ~30, ~60 and ~90 kDa most likely representing monomer, dimer and trimers present in the sample. Obviously these results may not be physiologically relevant as they may be due to non-specific interactions or aggregation events driven by the high (compared to *in vivo*) concentration of Yih1 (34 μM).

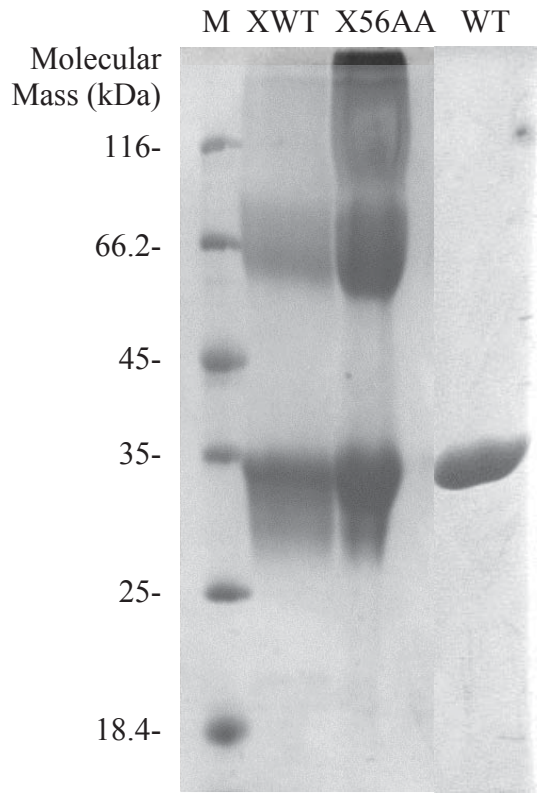

Figure 5.5 SDS PAGE of Glutaraldehyde Crosslinked Yih1

Yih1 was incubated with glutaraldehyde and subjected to SDS-PAGE. M: Molecular Weight Marker; XWT: Wild-type Yih1 treated with glutaraldehyde; X56AA; Yih1-56 treated with glutaraldehyde; WT: untreated wild-type Yih1

5.2.4 tRNA EMSA

A predicted function for Gcn1 is to load Gcn2 with uncharged tRNA (Marton *et al.*, 1993, Marton *et al.*, 1997). As Yih1 appears to bind to Gcn1 in a manner similar to Gcn2, it was thought that Yih1 may have tRNA binding activity. To test this hypothesis, *E. coli* tRNA was incubated with increasing amounts of Yih1, before being subjected to agarose electrophoretic analysis. As shown in Figure 5.6, there was no shift in either the Yih1 or the tRNA bands suggesting that no interaction had occurred under the conditions tested. It is possible that this may be a false negative result for the following reasons: very low rates of complex formation may not be able to be visualised because of the detection limits of ethidium bromide and Coomassie blue either of which do not have very high sensitivity; Yih1 cannot form an interaction

with the *E. coli* tRNA due to species variation; Yih1 is not able to form an interaction with tRNA without the presence of cellular machinery such as Gcn1 and other ribosomal constituents.

Although equal amounts of tRNA were added to the reaction mixtures, it appears that there are differences in the intensity of the tRNA band in the different gel lanes. This may just be due to inaccurate pipetting, or it may be that the tRNA was degrading over the timecourse due to the likely presence of RNase. As the reactions containing higher amounts of Yih1 appear to have higher intensity tRNA bands, Yih1 may have acted to protect the RNA from the action of RNase. Alternatively it may be that the conditions used in incubation and/or electrophoresis dissociated tRNA that Yih1 already had bound to it before incubation thus increasing the intensity of the band.

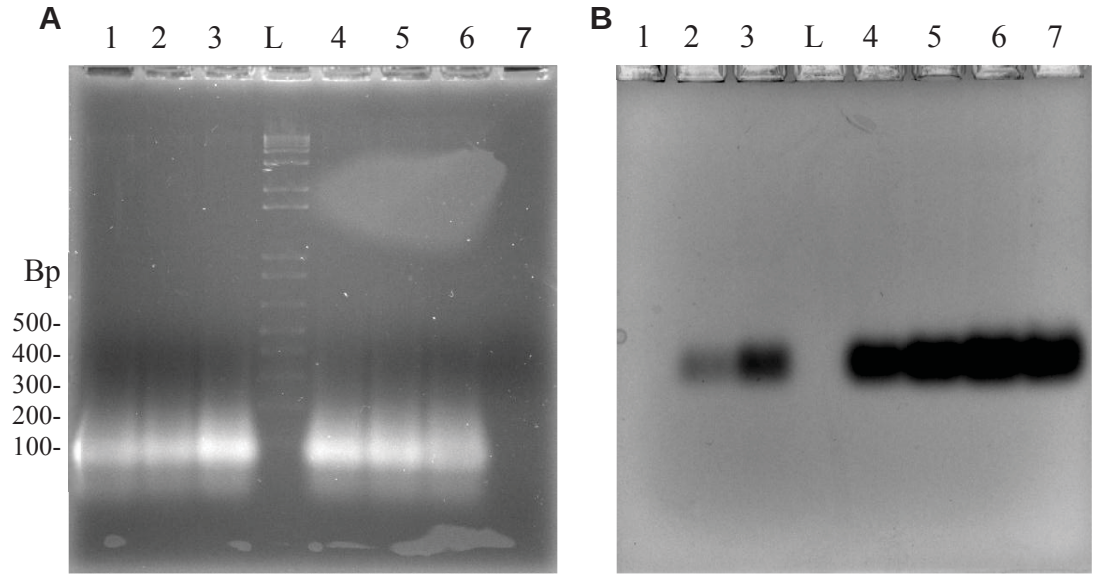

Figure 5.6 Electrophoretic Mobility Shift Assay of Yih1 and tRNA

Various concentrations of His_6-Yih1 was incubated with *E. coli* tRNA and subjected to 2% Agarose gel electrophoresis stained with (A) Ethidium Bromide and (B) Coomassie Blue. Lane 1: 1 mg/mL tRNA; Lane 2: 1 mg/mL tRNA + 0.25 mg/mL Yih1; Lane 3: 1 mg/mL tRNA + 0.5 mg/mL Yih1; Lane L: 1 kB+ DNA ladder; Lane 4: 1 mg/mL tRNA + 1 mg/mL Yih1; Lane 5: 1 mg/mL tRNA + 1.5 mg/mL Yih1; Lane 6: 1 mg/mL tRNA + 2 mg/mL Yih1; Lane 7: 2 mg/mL Yih1.

5.2.5 Production of Yeast Total RNA

In order to investigate if the binding did not occur because of the species differences in RNA, total RNA was isolated from yeast (2.2.36), and analysed by agarose gel electrophoresis to ascertain the successfulness of the extraction procedure (Figure 5.7). There appears to be a distinct ladder of ribosomal RNA indicating that the sample has not been substantially degraded (Lane 1). The smear seen is likely due to all the different species of RNA present as opposed to degradation. As treatment with RNase A results in an “empty lane” (Lane 2), it appears that there is very little contamination of the preparation with DNA, indicating that the DNase I treatment step of the protocol was successful.

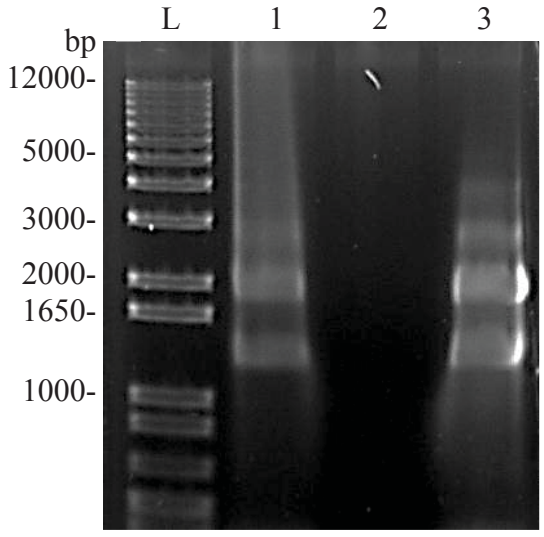

Figure 5.7 Agarose Gel Electrophoresis of Extracted RNA

1% Agarose gel electrophoresis stained with ethidum bromide. Lane L: 1 kB+ DNA Ladder; Lane 1: RNA isolated from yeast; Lane 2: RNA isolated from yeast treated with RNase A; RNA isolated from yeast treated with DNase I.

5.2.6 *In vitro* UV Crosslinking with Yeast Total RNA

Exposure of RNA-protein complexes to ultraviolet light forms covalent bonds between the RNA and protein preventing dissociation (Luo and Reed, 2003). It is a method commonly used to identify RNA binding proteins or the RNA that they are bound to. SDS PAGE of Yih1 and RNA subjected to UV crosslinking (2.2.37) showed a shift in the mobility of Yih1 (Figure 5.8A, Lane 3) which did not occur when Yih1 was exposed to UV in the absence of total RNA (Figure 5.8A, Lane 1). This suggests that Yih1 formed a complex with an RNA species present in the yeast total RNA extract. This shift wasn't reversed when treated with RNase A (Figure 5.8A, Lane 4), indicating that any bound RNA was protected from the action of RNase A, however no RNA is visible in this sample (Figure 5.8B, Lane 4). This may indicate that no RNA has bound to Yih1 or that the RNA bound is not concentrated enough to be visualised by ethidium bromide or is occluded from interaction with ethidium bromide

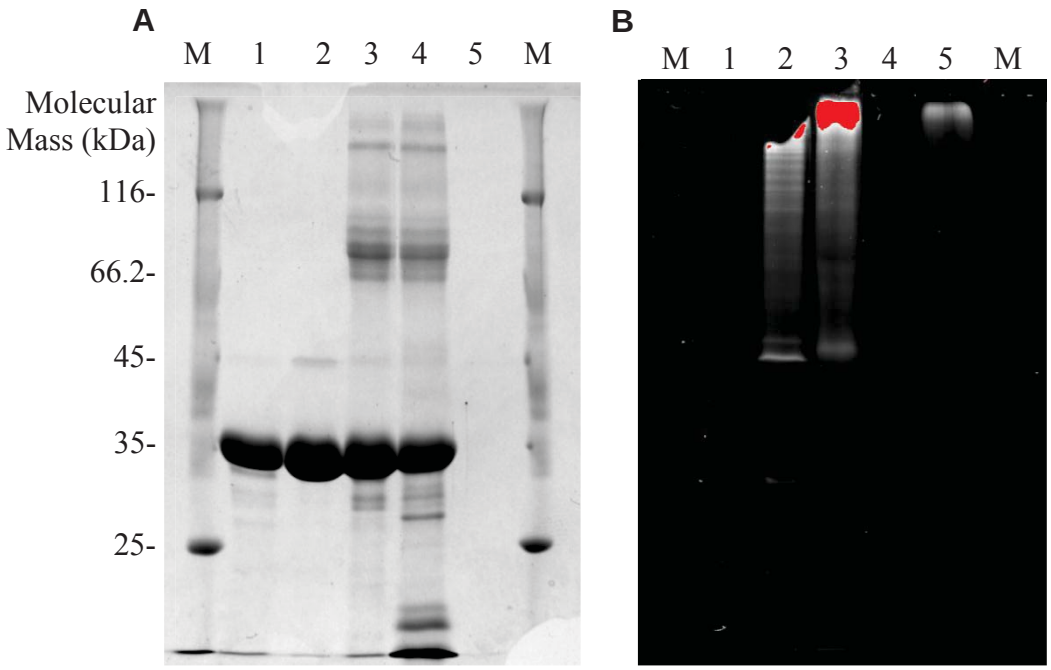

Figure 5.8 SDS PAGE analysis of UV Cross-linked Yih1 and Yeast Total RNA

10% SDS PAGE stained with Coomassie Blue **(A)** and Ethidium Bromide **(B)**. Lane M: Molecular Weight Marker; Lane 1: UV cross-linked Yih1; Lane 2: Yih1 and RNA not subjected to crosslinking; Lane 3: UV cross-linked Yih1 and RNA; Lane 4: UV cross-linked Yih1 and RNA treated with RNase A; Lane 5: UV cross-linked RNA.

by its interaction with Yih1. It is also possible that the shift in mobility was caused by trimerisation of Yih1 as the shifted band is at ~90kDa. A small molecule with similar chemical properties to RNA may have co-purified with the RNA and be capable of directing oligomerisation of Yih1 when activated by UV light. This would support the results obtained from glutaraldehyde cross-linking that suggests that Yih1 is able to form multimers. The additional higher mobility bands present in the RNase A-treated sample (Figure 5.8A, Lane 4) were likely due to protease contamination of the RNase I as they no longer occurred after the RNase I was boiled to denature any proteases present.

However, the experiment could not be reproduced using a number of different conditions. It is most likely that whatever had bound to this particular preparation of Yih1 was serendipitous, possibly a contaminant of that particular RNA purification.

5.2.7 Phenol/Chloroform Extraction of Yih1

To isolate any RNA bound to the purified Yih1, an acidic phenol/chloroform extraction was carried out on 4.5 mg of Yih1 in 200 µL as outlined in Section 2.2.38. The resulting extract was run on urea-PAGE (2.2.12.3) and silver-stained (2.2.12.6) to visualise protein and nucleic acid (Figure 5.9). The Yih1 sample and protein ladder both stained a dark brown, whereas the extracted sample stained a golden light brown, similar to the colour the DNA ladder stained suggesting that the sample is likely to be nucleic acid or similar and not protein contaminants that had been carried through the extraction.

It appears that the extracted sample is not one species as it was visualised as a large smear encompassing a wide range of molecular weights as judged against the DNA ladder. As the samples appear to narrow during the run, it is possible that there was some variation in salt concentration between the samples and the gel. This had likely influenced the mobility of the samples, preventing any conclusions from being drawn with confidence.

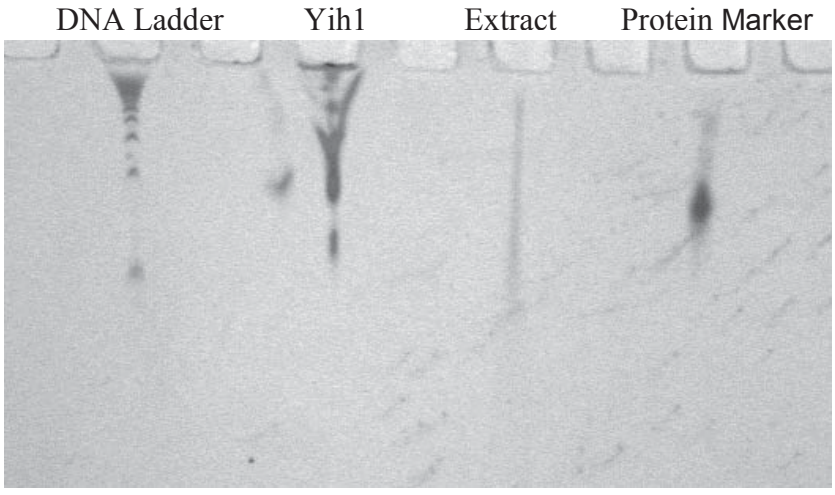

Figure 5.9 Urea-PAGE of Yih1 Phenol/Chloroform extraction

12% Urea PAGE stained with silver. DNA ladder: 1kb+ DNA ladder; Yih1: Yih1 sample before extraction; Extract: sample extracted from Yih1 by phenol/chloroform method; Protein Marker: Protein Molecular Weight Marker.

5.2.8 The Effects of Salt on the Heterogeneity of Yih1

To assess if the environmental ionic strength has any influence on the heterogeneity of Yih1, it was analysed by native PAGE in the presence of various salts (2.2.39). There appeared to be no differences in the proportions of each species when exposed to salt except for KCl (Figure 5.10). At higher concentrations of KCl, the lower band of the doublet decreased in intensity and there was an increase in the proportion of the higher bands proposed to be multimers. This may be due to KCl destabilising interactions within the Yih1 molecule or between Yih1 and another molecule; or it may be due to KCl driving the formation of multimers due to the increased ionic strength of the solvent. Sakurai and co-workers (2001) have reported that in the case of β-lactoglobulin, the addition of salt stabilizes the dimeric form of the protein, this is also the case for dimerization of the bacteriophage λ cI repressor (Koblan, 1991). It is possible that the multimeric form of Yih1 is stabilised under higher concentrations of KCl, driving changes in the proportions of the different protein species. Whether or not this is relevant for Yih1 in the cellular environment is unknown, but it may hint towards regulation of Yih1 by changes in intracellular salt concentrations.

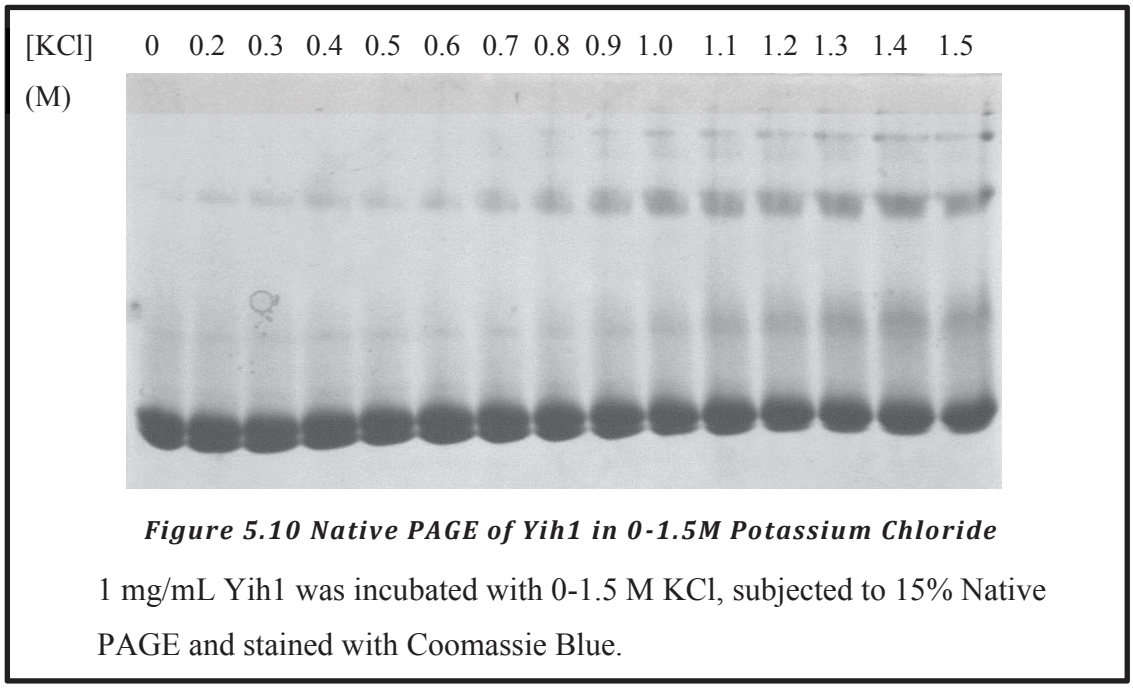

Figure 5.10 Native PAGE of Yih1 in 0-1.5M Potassium Chloride

1 mg/mL Yih1 was incubated with 0-1.5 M KCl, subjected to 15% Native PAGE and stained with Coomassie Blue.

5.2.9 The effects of Small Molecules on the Heterogeneity of Yih1

In light of literature evidence possibly implicating Yih1/IMPACT in NAD^+/H pathways (outlined in Chapter 6), small molecules related to these pathways were investigated in regard to their ability to modulate the proportions of the different Yih1 species seen by native PAGE (2.2.40). The molecules tested were $NADP^+$, NAD^+, NADH and tryptophan. None of the molecules at the concentrations tested (0mM-3mM) modified the ratio of Yih1 species as observed by native PAGE (Data not shown). Given these results, it does not appear that the apparent Yih1 multimerisation is affected directly by these molecules at the concentrations tested. However, this does not exclude the possibility that Yih1 interacts with these or any other biomolecules, or that such molecules indirectly influence the *in vivo* multimerisation of Yih1.

5.3 Conclusion

One preparation of Yih1 appeared to have co-purified with a nucleic acid species that is most likely RNA. Yih1 also appears to interact with itself to form multimers and these may be modulated by salt concentration, the presence of RNA or contaminants that had co-purified with RNA. Subsequent preparations of Yih1 showed no evidence of RNA in the preparation despite rigorous investigation. Reluctantly it was concluded that the particular preparation in question was contaminated with DNA. At that time the DNase being used for the preparations was very old. Subsequent preparations used fresh DNase and the second peak in source Q anion exchange was never observed.

6. GENERAL DISCUSSION AND CONCLUSIONS

6.1 Crystallisation

There are many reasons as to why a particular protein will not crystallise. In the case of Yih1 it is likely a combination of a few reasons, all of which are related to heterogeneity. As seen on native gels, Yih1 displays heterogeneity. Regardless of what causes this heterogeneity, a protein is unlikely to crystallise if the solution it is in contains a mixture of species due to the attempted incorporation of these 'odd' molecules deforming what should be a homogeneous ordered array of molecules. An additional problem for Yih1 is its apparent bilobate structure; two distinct domains joined by a flexible linker region which has been confirmed by NMR (A. Goroncy, Personal Communication). This inherent flexibility in the Yih1 molecule results in additional conformational heterogeneity and this is likely the reason for the lack of nucleation observed in crystallisation trials. Regardless of heterogeneity, a protein will not crystallise if it lacks symmetrical crystal contacts; that is, if a protein molecule is unable to interact with an identical molecule *via* surface-exposed residues to form a regular lattice; nucleation will never occur.

Yih1 is not a good candidate for X-ray crystallography. Determination of the structure of Yih1 by alternative methods is more likely to yield results that can enhance our knowledge of Yih1 and provide leads as to its function *in vivo*.

6.2 Multimerisation

Although no conclusive evidence has been found regarding the odd behaviour that Yih1 exhibits on native gels, it appears that Yih1 form multimers. This has been shown by glutaraldehyde crosslinking, multiple bands on native gel that can be modulated by salt concentration and possibly by the formation of what appears to be a trimeric species upon UV irradiation in the presence of RNA. Multimerisation has also been investigated due to results obtained by Sattlegger and co-workers (2011) showing that Yih1 fragments that are unable to form an interaction with actin in a yeast strain lacking endogenous Yih1, are able to form an interaction when endogenous Yih1 is present. Despite all the evidence pointing towards Yih1 forming multimers, there is also evidence to the contrary such as the presence of only one

peak on size exclusion chromatography that is not altered by the addition of the chaotropic salt KI (Sattlegger *et al.*, 2011). These results indicate that multimerisation of Yih1 is likely to be dependent on the cellular environment.

6.3 Glutathione

The only demonstrated link between the IMPACT family and glutathione is that Yih1 knockout strains have increased levels of glutathione (Suzuki *et al.*, 2011), but the reasons for this have yet to be investigated. The levels of IMPACT protein in different cell types is inversely correlated with the basal levels of eIF2α phosphorylation (Pereira *et al.*, 2005) which itself has been linked to cellular antioxidant status (Tan *et al.*, 2001). Mimicking increased levels of eIF2α-P results in increased glutathione production (Tan *et al.*, 2001). This was shown to occur due to an increase in the levels of ATF4 which transcriptionally increases expression levels of xCT, the functional subunit of the cysteine/glutamate antiporter system X_c^- that is expressed the brain (Lewerenz and Maher, 2009). System X_c^- is of interest as it acts to import cysteine; the limiting factor for synthesis of glutathione (Lewerenz *et al.*, 2011) and it also acts to control extracellular glutamate levels (Baker *et al.*, 2002).

With these results in mind, it is not farfetched to suggest that IMPACT may play a role in regulating and/or responding to changes in cellular oxidation. It is logical that prevention of eIF2α phosphorylation by IMPACT would lead to changes in amino acid transporter expression. In the case of X_c^-, is not just an amino acid transporter for protein synthesis but also for maintenance of the cells redox state. Further work is required to test this hypothesis as this may help to explain the functionality of IMPACT.

6.4 $NAD(P)^+/H$

Further to the role proposed for IMPACT in sensing/regulation of the redox state of the cell *via* glutathione, evidence seems to suggest that IMPACT may also be involved in NAD(P)+/H regulation. As mentioned in Section 1.1.8, IMPACT has been shown to protect cells from IDO-induced cell-death (Habibi *et al.*, 2010). IDO catalyses the first step in the *de novo* NAD^+/H biosynthetic pathway, the conversion of tryptophan to form N-formylkynurenine which is subsequently converted to

kynurenine. Kynurenine is a toxic compound that has been shown at high concentrations to non-enzymatically covalently modify proteins (Garner *et al.*, 2000). Of interest is the ability of kynurenine to form adducts with glutathione. It appears that increased concentrations of glutathione can act to protect proteins from kynurenine-modification by sequestration of kynurenine (Garner *et al.*, 2000). This may be a potential link between IMPACT, IDO, Glutathione and NAD^+/H.

As IMPACT mRNA and protein levels are both increased when fibroblasts are grown in tryptophan-free media (Habibi *et al.*, 2010), it appears that the *impact* gene is regulated by tryptophan levels. This may implicate IMPACT in a role assisting the cell to respond to tryptophan starvation. As the level of IMPACT protein rise during IDO-induced Trp-starvation, Gcn2 would become inactivated. The activity of IDO is often induced by IFN-γ (Aune and Pogue, 1989), causing a reduction in tryptophan levels to act as a protective mechanism to inhibit viral replication. Activation of Gcn2 would not be advantageous to the cell under these circumstances. (Habibi *et al.*, 2010). It is therefore possible that the high expression of IMPACT in IDO-expressing cells is a result of the low tryptophan concentration maintained by the activity of IDO, and that the role of IMPACT is to respond to low levels of tryptophan in a manner that Gcn2 is unable to as mammalian cells lack the molecular machinery to synthesize tryptophan *de novo*.

Yih1 has been shown to interact with Urh1 (Uetz *et al.*, 2000), a protein involved in the NAD^+/H salvage pathway that catalyses the conversion of nicotinamide riboside to nicotinamide (Belenky *et al.*, 2009). It is possible that Yih1 plays a role in cross-talk between the *de novo* and salvage pathways of NAD^+/H synthesis, possibly regulated by levels of tryptophan. As amino acid biosynthetic pathways utilise NAD(P)+/H, it would be advantageous to ensure that there are sufficient levels of NAD^+/H in the cell before investing energy in upregulating enzymes of the amino acid biosynthetic pathways.

However, it cannot be emphasised enough that the relationship between IMPACT, glutathione and NAD^+/H is mostly speculation based on extrapolation of research that does not directly address the role of IMPACT. These ideas form the basis of a

hypothesis that requires further testing. Further experiments that would test this hypothesis are outlined in section 7.3.

7. FUTURE DIRECTIONS

7.1 Yih1 Structure, Multimerisation and Binding Partners

As mentioned earlier, attempts are currently underway to solve the structure of Yih1 by NMR. Yih1 is a good candidate for NMR studies as its molecular weight is within the comfortable range for current NMR technology. An NMR structure of Yih1 would not only provide a 3D structure of this highly conserved protein which may assist in determining its function, but it would also provide additional dynamic data that may shed some light on the apparent conformational heterogeneity of Yih1 observed in this study.

Crosslinking combined with mass spectrometry is a method that would provide evidence about the intramolecular interactions of Yih1 possibly leading to a structural model of Yih1 or validation of the model already proposed by Sattlegger and co-workers (2011). The use of novel heterotrifunctional, cleavable crosslinkers have made this method much easier in the past few years allowing: specificity of reactive groups undergoing crosslinking; the use of affinity tags such as biotin to retrieve crosslinked peptides; and the presence of MS/MS cleavable bonds to allow easier identification of cross-linked residues. This method may also be applied to mapping intermolecular interactions between Yih1 and its binding partners.

Small Angle X-ray Scattering (SAXS) is a method where protein in solution is subjected to X-ray scattering and the intensity of the X-ray scattering provides information about the protein's shape and size allowing the creation of very low resolution models that fit the SAXS data. Given the inability of Yih1 to crystallise, the utilisation of this method would deduce the conformation of the two domains relative to one another. This would allow the available models of each domain of Yih1 (Sattlegger *et al.*, 2011) to be fit to the SAXS data to provide a pseudo-higher resolution model. SAXS could also be used to monitor changes in multimerisation as a function of concentration, allowing measurement of the dissociation constant (K_D) of Yih1 oligomers. This could also be done with Yih1 complexed to actin or a fragment of Gcn1 to reveal the mode of binding and measure dissociation constants

of the respective complexes. This would provide a template to fit higher resolution structures of the Yih1 domains and actin, although no structure for Gcn1 is available.

Another method that could be used to measure the dissociation constants of Yih1 from itself, actin, or Gcn1 is analytical ultracentrifugation. This would also provide more accurate measurement of the proportions of Yih1 species that vary in size.

Crosslinking and immunoprecipitation (CLIP) is a method that utilises UV crosslinking *in vivo* followed by immunoprecipitation of the target protein to identify RNA that interacts with the protein of interest (Jensen and Darnell, 2008). To identify any cross-linked RNA component, RNA is purified, ligated to adaptors, reverse-transcribed, amplified and sequenced. Identification of any RNA bound to Yih1 could help in the understanding of the role Yih1 plays *in vivo*.

7.2 The role of Yih1 in Glutathione Production

In order to exclude the possibility of an interaction between Gcn1 and glutathione, $Gcn1_{frag}$ without a fused GST tag could be incubated with glutathione-agarose. If Gcn1 interacts with the matrix, it would be good evidence that Gcn1 contains glutathione-binding activity. Additionally, radiolabelled glutathione could be mixed with Gcn1 and run on a native gel. Any radiation co-migrating with Gcn1 indicates an interaction with glutathione is occurring.

7.3 The potential role of Yih1/IMPACT in NAD+ pathways

Analysis of the Yih1 RWD and Ancient domain models by PocketFinder (http://www.modelling.leeds.ac.uk/pocketfinder/) indicates that it may contain ligand binding pockets. Given the proposed role of Yih1/IMPACT in sensing or regulating NAD^+ biosynthetic pathways, it is possible that Yih1/IMPACT may form an interaction with one of the molecules involved in this pathway such as tryptophan, kynurenine, $NAD(P)^+/H$ or ATP. To investigate this, radiolabelled molecules could be incubated with Yih1 and analysed by native PAGE. Alternatively, analysis by surface plasmon resonance may allow quantitative identification of any interactions occurring.

Investigating the relative concentrations of compounds involved in the kynurenine pathway in Yih1 knockout yeast compared to wild type under different growth

conditions may provide evidence for or against the involvement of Yih1 in these pathways. This could be achieved using known HPLC-ESI-MS/MS-based methods to quantify the various compounds in a wild-type and Yih1/IMPACT knockout strains (Dollmann *et al.*, 1997).

Together, these experiments that I am proposing will shed new light on both the structure and function of the highly conserved IMPACT family of proteins that appear to play a regulatory role in a variety of important and interesting cellular processes including the regulation of protein synthesis.

REFERENCES

Acker, M. G. & Lorsch, J. R. 2008. Mechanism of ribosomal subunit joining during eukaryotic translation initiation. *Biochemical Society Transactions,* 36**,** 653-657.

Aune, T. M. & Pogue, S. L. 1989. Inhibition of tumor cell growth by interferon-γ is mediated by two distinct mechanisms dependent upon oxygen tension: Induction of tryptophan degradation and depletion of intracellular nicotinamide adenine dinucleotide. *Journal of Clinical Investigation,* 84**,** 863-875.

Baker, D. A., Xi, Z. X., Shen, H., Swanson, C. J. & Kalivas, P. W. 2002. The origin and neuronal function of in vivo nonsynaptic glutamate. *Journal of Neuroscience,* 22**,** 9134-9141.

Barkley, M. D., Lewis, P. A. & Sullivan, G. E. 1981. Ion effects on the lac repressor-operator equilibrium. *Biochemistry,* 20**,** 3842-3851.

Belenky, P., Christensen, K. C., Gazzaniga, F., Pletnev, A. A. & Brenner, C. 2009. Nicotinamide riboside and nicotinic acid riboside salvage in fungi and mammals quantitative basis for urh1 and purine nucleoside phosphorylase function in nad+ metabolism. *Journal of Biological Chemistry,* 284**,** 158-164.

Bittencourt, S., Pereira, C. M., Avedissian, M., Delamano, A., Mello, L. E. & Castilho, B. A. 2008. Distribution of the protein IMPACT, an inhibitor of GCN2, in the mouse, rat, and marmoset brain. *Journal of Comparative Neurology,* 507**,** 1811-1830.

Brown, C. J., Takayama, S., Campen, A. M., Vise, P., Marshall, T. W., Oldfield, C. J., Williams, C. J. & Keith Dunker, A. 2002. Evolutionary Rate Heterogeneity in Proteins with Long Disordered Regions. *Journal of Molecular Evolution,* 55**,** 104-110.

Brown, E. J., Albers, M. W., Bum Shin, T., ichikawa, K., Keith, C. T., Lane, W. S. & Schreiber, S. L. 1994. A mammalian protein targeted by G1-arresting rapamycin-receptor complex. *Nature,* 369**,** 756-758.

Carson, M., Johnson, D. H., McDonald, H., Brouillette, C. & DeLucas, L. J. 2007. His-tag impact on structure. *Acta Crystallographica Section D,* 63**,** 295-301.

Cherkasova, V. A. & Hinnebusch, A. G. 2003. Translational control by TOR and TAP42 through dephosphorylation of eIF2 alpha kinase GCN2. *Genes & Development,* 17**,** 859-872.

Costa-Mattioli, M., Gobert, D., Harding, H., Herdy, B., Azzi, M., Bruno, M., Bidinosti, M., Ben Mamou, C., Marcinkiewicz, E., Yoshida, M., Imataka, H., Cuello, A. C., Seidah, N., Sossin, W., Lacaille, J. C., Ron, D., Nader, K. & Sonenberg, N. 2005. Translational control of hippocampal synaptic plasticity and memory by the eIF2[alpha] kinase GCN2. *Nature,* 436**,** 1166-1173.

Costa-Mattioli, M., Gobert, D., Stern, E., Gamache, K., Colina, R., Cuello, C., Sossin, W., Kaufman, R., Pelletier, J., Rosenblum, K., Krnjević, K., Lacaille, J. C., Nader, K. & Sonenberg, N. 2007. eIF2α Phosphorylation Bidirectionally Regulates the Switch from Short- to Long-Term Synaptic Plasticity and Memory. *Cell,* 129**,** 195-206.

Deng, J., Harding, H. P., Raught, B., Gingras, A. C., Berlanga, J. J., Scheuner, D., Kaufman, R. J., Ron, D. & Sonenberg, N. 2002. Activation of GCN2 in UV-irradiated cells inhibits translation. *Current Biology,* 12**,** 1279-1286.

Derewenda, Z. S. 2004. Rational protein crystallization by mutational surface engineering. *Structure,* 12**,** 529-535.

Dever, T. E., Feng, L., Wek, R. C., Cigan, A. M., Donahue, T. F. & Hinnebusch, A. G. 1992. Phosphorylation of initiation factor 2α by protein kinase GCN2 mediates gene-specific translational control of GCN4 in yeast. *Cell,* 68**,** 585-596.

Di Como, C. J. & Arndt, K. T. 1996. Nutrients, via the Tor proteins, stimulate the association of Tap42 with type 2A phosphatases. *Genes and Development,* 10**,** 1904-1916.

Dollmann, B., Richling, E., Herderich, M., Kohler, H., Schwab, A., Schmitt, A. & Schreier, P. 1997. High-performance liquid chromatography-electrospray ionization tandem mass spectrometry (HPLC/ESI/MS/MS) for quantification of l-kynurenine and indole-3-acetic acid in grape must by isotope dilution assay. *Vitis,* 36**,** 97-101.

Dong, A., Xu, X., Edwards, A. M., Chang, C., Chruszcz, M., Cuff, M., Cymborowski, M., Di Leo, R., Egorova, O., Evdokimova, E., Filippova, E., Gu, J., Guthrie, J., Ignatchenko, A., Joachimiak, A., Klostermann, N., Kim, Y., Korniyenko, Y., Minor, W., Que, Q., Savchenko, A., Skarina, T., Tan, K., Yakunin, A., Yee, A., Yim, V., Zhang, R., Zheng, H., Akutsu, M., Arrowsmith, C., Avvakumov, G. V., Bochkarev, A., Dahlgren, L. G., Dhe-Paganon, S., Dimov, S., Dombrovski, L., Finerty, P., Flodin, S., Flores, A., Gräslund, S., Hammerström, M., Herman, M. D., Hong, B. S., Hui, R., Johansson, I., Liu, Y., Nilsson, M., Nedyalkova, L., Nordlund, P., Nyman, T., Min, J., Ouyang, H., Park, H. W., Qi, C., Rabeh, W., Shen, L., Shen, Y., Sukumard, D., Tempel, W., Tong, Y., Tresagues, L., Vedadi, M., Walker, J. R.,

Weigelt, J., Welin, M., Wu, H., Xiao, T., Zeng, H. & Zhu, H. 2007. In situ proteolysis for protein crystallization and structure determination. *Nature Methods,* 4**,** 1019-1021.

Dong, J. S., Qiu, H. F., Garcia-Barrio, M., Anderson, J. & Hinnebusch, A. G. 2000. Uncharged tRNA activates GCN2 by displacing the protein kinase moiety from a bipartite tRNA-Binding domain. *Molecular Cell,* 6**,** 269-279.

Dyson, H. J. & Wright, P. E. 2002. Coupling of folding and binding for unstructured proteins. *Current Opinion in Structural Biology,* 12**,** 54-60.

Garcia-Barrio, M., Dong, J. S., Ufano, S. & Hinnebusch, A. G. 2000. Association of GCN1-GCN20 regulatory complex with the N-terminus of elF2 alpha kinase GCN2 is required for GCN2 activation. *Embo Journal,* 19**,** 1887-1899.

Garner, B., Shaw, D., Lindner, R., Carver, J. & Truscott, R. 2000. Nonoxidative modification of lens crystallins by kynurenine: a novel post-translational protein modification with possible relevance to ageing and cataract. *Biochim Biophys Acta.,* 1476**,** 265-278.

Goossens, A., Dever, T. E., Pascual-Ahuir, A. & Serrano, R. 2001. The Protein Kinase Gcn2p Mediates Sodium Toxicity in Yeast. *Journal of Biological Chemistry,* 276**,** 30753-30760.

Habibi, D., Jalili, R. B., Forouzandeh, F., Ong, C. J. & Ghahary, A. 2010. High expression of IMPACT protein promotes resistance to indoleamine 2,3-dioxygenase-induced cell death. *Journal of Cellular Physiology,* 225**,** 196-205.

Hagiwara, Y., Hirai, M., Nishiyama, K., Kanazawa, I., Ueda, T., Sakaki, Y. & Ito, T. 1997. Screening for imprinted genes by allelic message display: Identification of a paternally expressed gene Impact on mouse chromosome 18. *Proceedings of the National Academy of Sciences of the United States of America,* 94**,** 9249-9254.

Hart, D. J., Speight, R. E., Cooper, M. A., Sutherland, J. D. & Blackburn, J. M. 1999. The salt dependence of DNA recognition by NF-κB p50: A detailed kinetic analysis of the effects on affinity and specificity. *Nucleic Acids Research,* 27**,** 1063-1069.

Hinnebusch, A. G. 1984. Evidence for translational regulation of the activator of general amino acid control in yeast. *Proceedings of the National Academy of Sciences of the United States of America,* 81**,** 6442-6446.

Hinnebusch, A. G. 1988. Mechanisms of gene regulation in the general control of amino acid biosynthesis in Saccharomyces cerevisiae. *Microbiological Reviews,* 52**,** 248-273.

Hope, I. A. & Struhl, K. 1985. GCN4 protein, synthesized in vitro, binds HIS3 regulatory sequences: Implications for general control of amino acid biosynthetic genes in yeast. *Cell,* 43**,** 177-183.

Isom, D. G., Castañeda, C. A., Cannon, B. R. & García-Moreno E., B. 2011. Large shifts in pKa values of lysine residues buried inside a protein. *Proceedings of the National Academy of Sciences,* 108**,** 5260-5265.

Jalili, R. B., Forouzandeh, F., Moeenrezakhanlou, A., Rayat, G. R., Rajotte, R. V., Uludag, H. & Ghahary, A. 2009. Mouse pancreatic islets are resistant to indoleamine 2,3 dioxygenase-induced general control nonderepressible-2 kinase stress pathway and maintain normal viability and function. *American Journal of Pathology,* 174**,** 196-205.

Jensen, K. B. & Darnell, R. B. 2008. CLIP: Crosslinking and immunoprecipitation of in vivo RNA targets of RNA-binding proteins.

Kimball, S. R. 1999. Eukaryotic initiation factor eIF2. *International Journal of Biochemistry and Cell Biology,* 31**,** 25-29.

Koblan, K. S. 1991. Energetics of Subunit Dimerization in Bacteriophage λ cI Repressor: Linkage to Protons, Temperature, and KCl. *Biochemistry®,* 30**,** 7817-7821.

Krogan, N. J., Cagney, G., Yu, H., Zhong, G., Guo, X., Ignatchenko, A., Li, J., Pu, S., Datta, N., Tikuisis, A. P., Punna, T., Peregrín-Alvarez, J. M., Shales, M., Zhang, X., Davey, M., Robinson, M. D., Paccanaro, A., Bray, J. E., Sheung, A., Beattie, B., Richards, D. P., Canadien, V., Lalev, A., Mena, F., Wong, P., Starostine, A., Canete, M. M., Vlasblom, J., Wu, S., Orsi, C., Collins, S. R., Chandran, S., Haw, R., Rilstone, J. J., Gandi, K., Thompson, N. J., Musso, G., St Onge, P., Ghanny, S., Lam, M. H. Y., Butland, G., Altaf-Ul, A. M., Kanaya, S., Shilatifard, A., O'Shea, E., Weissman, J. S., Ingles, C. J., Hughes, T. R., Parkinson, J., Gerstein, M., Wodak, S. J., Emili, A. & Greenblatt, J. F. 2006. Global landscape of protein complexes in the yeast Saccharomyces cerevisiae. *Nature,* 440**,** 637-643.

Kubota, H., Obata, T., Ota, K., Sasaki, T. & Ito, T. 2003. Rapamycin-induced translational derepression of GCN4 mRNA involves a novel mechanism for activation of the eIF2 alpha kinase GCN2. *Journal of Biological Chemistry,* 278**,** 20457-20460.

Kubota, H., Sakaki, Y. & Ito, T. 2000. GI domain-mediated association of the eukaryotic initiation factor 2α kinase GCN2 with its activator GCN1 is required for general amino acid control in budding yeast. *Journal of Biological Chemistry,* 275**,** 20243-20246.

Laemmli, U. K. 1970. Cleavage of structural proteins during the assembly of the head of bacteriophage T4. *Nature,* 227**,** 680-685.

Lewerenz, J. & Maher, P. 2009. Basal Levels of eIF2α Phosphorylation Determine Cellular Antioxidant Status by Regulating ATF4 and xCT Expression. *Journal of Biological Chemistry,* 284**,** 1106-1115.

Lewerenz, J., Maher, P. & Methner, A. 2011. Regulation of xCT expression and system X^{-c} function in neuronal cells. *Amino Acids***,** 1-9.

Luo, M. J. & Reed, R. 2003. Identification of RNA binding proteins by UV cross-linking. *Current protocols in molecular biology / edited by Frederick M. Ausubel ... [et al.],* Chapter 27.

Marton, M. J., Crouch, D. & Hinnebusch, A. G. 1993. GCN1, a translational activator of GCN4 in Saccharomyces cerevisiae, is required for phosphorylation of eukaryotic translation initiation factor 2 by protein kinase GCN2. *Molecular and Cellular Biology,* 13**,** 3541-3556.

Marton, M. J., deAldana, C. R. V., Qiu, H. F., Chakraburtty, K. & Hinnebusch, A. G. 1997. Evidence that GCN1 and GCN20, translational regulators of GCN4, function on elongating ribosomes in activation of eIF2 alpha kinase GCN2. *Molecular and Cellular Biology,* 17**,** 4474-4489.

Mehler, A. H. & Knox, W. E. 1950. The Conversion of Tryptophan to Kynurenine in Liver. *Journal of Biological Chemistry,* 187**,** 431-438.

Mueller, P. P. & Hinnebusch, A. G. 1986. Multiple upstream AUG codons mediate translational control of GCN4. *Cell,* 45**,** 201-207.

Nagarajan, V., Pattabhi, V. & Sundaram, P. V. 1996. Distance Mapping as a Tool in Protein Modification. *Annals of the New York Academy of Sciences,* 799**,** 413-417.

Nomura, W., Maeta, K., Kita, K., Izawa, S. & Inoue, Y. 2010. Methylglyoxal activates Gcn2 to phosphorylate eIF2α independently of the TOR pathway in Saccharomyces cerevisiae. *Applied Microbiology and Biotechnology,* 86**,** 1887-1894.

Okamura, K., Hagiwara-Takeuchi, Y., Li, T., Vu, T. H., Hirai, M., Hattori, M., Sakaki, Y., Hoffman, A. R. & Ito, T. 2000. Comparative genome analysis of the mouse imprinted gene Impact and its nonimprinted human homolog IMPACT: Toward the structural basis for species-specific imprinting. *Genome Research,* 10**,** 1878-1889.

Okamura, K., Sakaki, Y. & Ito, T. 2005. Comparative genomics approach toward critical determinants for the imprinting of an evolutionarily conserved gene Impact. *Biochemical and Biophysical Research Communications,* 329**,** 824-830.

Okamura, K., Yamada, Y., Sakaki, Y. & Ito, T. 2004. An evolutionary scenario for genomic imprinting of Impact lying between nonimprinted neighbors. *DNA Research,* 11**,** 381-390.

Pavitt, G. D., Ramaiah, K. V. A., Kimball, S. R. & Hinnebusch, A. G. 1998. eIF2 independently binds two distinct eIF2b subcomplexes that catalyze and regulate guanine-nucleotide exchange. *Genes and Development,* 12**,** 514-526.

Peng, J., Schwartz, D., Elias, J. E., Thoreen, C. C., Cheng, D., Marsischky, G., Roelofs, J., Finley, D. & Gygi, S. P. 2003. A proteomics approach to understanding protein ubiquitination. *Nature Biotechnology,* 21**,** 921-926.

Pereira, C. M., Sattlegger, E., Jiang, H. Y., Longo, B. M., Jaqueta, C. B., Hinnebusch, A. G., Wek, R. C., Mello, L. & Castilho, B. A. 2005. IMPACT, a protein preferentially expressed in the mouse brain, binds GCN1 and inhibits GCN2 activation. *Journal of Biological Chemistry,* 280**,** 28316-28323.

Pestova, T. V., Kolupaeva, V. G., Lomakin, I. B., Pilipenko, E. V., Shatsky, I. N., Agol, V. I. & Hellen, C. U. T. 2001. Molecular mechanisms of translation initiation in eukaryotes. *Proceedings of the National Academy of Sciences of the United States of America,* 98**,** 7029-7036.

Pfefferkorn, E. R. 1984. Interferon gamma blocks the growth of Toxoplasma gondii in human fibroblasts by inducing the host cells to degrade tryptophan. *Proceedings of the National Academy of Sciences,* 81**,** 908-912.

Qiu, H., Dong, J., Hu, C., Francklyn, C. S. & Hinnebusch, A. G. 2001. The tRNA-binding moiety in GCN2 contains a dimerization domain that interacts with the kinase domain and is required for tRNA binding and kinase activation. *Embo Journal,* 20**,** 1425-1438.

Qiu, H., Garcia-Barrio, M. T. & Hinnebusch, A. G. 1998. Dimerization by translation initiation factor 2 kinase GCN2 is mediated by interactions in the C-terminal ribosome-binding region and the protein kinase domain. *Molecular and Cellular Biology,* 18**,** 2697-2711.

Qiu, H. F., Hu, C. H., Dong, J. S. & Hinnebusch, A. G. 2002. Mutations that bypass tRNA binding activate the intrinsically defective kinase domain in GCN2. *Genes & Development,* 16**,** 1271-1280.

Ramirez, M., Wek, R. C. & Hinnebusch, A. G. 1991. Ribosome association of GCN2 protein kinase, a translational activator of the GCN4 gene of Saccharomyces cerevisiae. *Molecular and Cellular Biology,* 11**,** 3027-3036.

Rolfes, R. J. & Hinnebusch, A. G. 1993. Translation of the yeast transcriptional activator GCN4 is stimulated by purine limitation: Implications for activation of the protein kinase GCN2. *Molecular and Cellular Biology,* 13**,** 5099-5111.

Romano, P. R., Garcia-Barrio, M. T., Zhang, X., Wang, Q., Taylor, D. R., Zhang, F., Herring, C., Mathews, M. B., Qin, J. & Hinnebusch, A. G. 1998. Autophosphorylation in the activation loop is required for full kinase activity in vivo of human and yeast eukaryotic initiation factor 2α kinases PKR and GCN2. *Molecular and Cellular Biology,* 18**,** 2282-2297.

Sakurai, K., Oobatake, M. & Goto, Y. 2001. Salt-dependent monomer-dimer equilibrium of bovine β-lactoglobulin at pH 3. *Protein Science,* 10**,** 2325-2335.

Sattlegger, E., Barbosa, J. A. R. G., Moraes, M. C. S., Martins, R. M., Hinnebusch, A. G. & Castilho, B. A. 2011. Gcn1 and actin binding to Yih1: Implications for activation of the eIF2 kinase GCN2. *Journal of Biological Chemistry,* 286**,** 10341-10355.

Sattlegger, E. & Hinnebusch, A. G. 2000. Separate domains in GCN1 for binding protein kinase GCN2 and ribosomes are required for GCN2 activation in amino acid-starved cells. *Embo Journal,* 19**,** 6622-6633.

Sattlegger, E., Swanson, M. J., Ashcraft, E. A., Jennings, J. L., Fekete, R. A., Link, A. J. & Hinnebusch, A. G. 2004. YIH1 is an actin-binding protein that inhibits protein kinase GCN2 and impairs general amino acid control when overexpressed. *Journal of Biological Chemistry,* 279**,** 29952-29962.

Sharma, Y., Mohan Rao, C., Chenchal Rao, S., Gopala Krishna, A., Somasundaram, T. & Balasubramanian, D. 1989. Binding site conformation dictates the color of the dye Stains-all. A study of the binding of this dye to the eye lens proteins crystallins. *Journal of Biological Chemistry,* 264**,** 20923-20927.

Starita, L. M., Lo, R. S., Eng, J. K., von Haller, P. D. & Fields, S. 2012. Sites of ubiquitin attachment in Saccharomyces cerevisiae. *Proteomics,* 12**,** 236-240.

Suzuki, T., Yokoyama, A., Tsuji, T., Ikeshima, E., Nakashima, K., Ikushima, S., Kobayashi, C. & Yoshida, S. 2011. Identification and characterization of genes involved in glutathione production in yeast. *Journal of Bioscience and Bioengineering,* 112**,** 107-113.

Tan, S., Somia, N., Maher, P. & Schubert, D. 2001. Regulation of antioxidant metabolism by translation initiation factor 2α. *Journal of Cell Biology,* 152**,** 997-1006.

Triana-Alonso, F. J., Chakraburtty, K. & Nierhaus, K. H. 1995. The Elongation Factor 3 Unique in Higher Fungi and Essential for Protein Biosynthesis Is an E Site Factor. *Journal of Biological Chemistry,* 270**,** 20473-20478.

Uetz, P., Glot, L., Cagney, G., Mansfield, T. A., Judson, R. S., Knight, J. R., Lockshon, D., Narayan, V., Srinivasan, M., Pochart, P., Qureshi-Emlli, A., Li, Y., Godwin, B., Conover, D., Kalbfleisch, T., Vijayadamodar, G., Yang, M., Johnston, M., Fields, S. & Rothberg, J. M. 2000. A comprehensive analysis of protein-protein interactions in Saccharomyces cerevisiae. *Nature,* 403**,** 623-627.

Vazquez de Aldana, C. R., Marton, M. J. & Hinnebusch, A. G. 1995. GCN20, a novel ATP binding cassette protein, and GCN1 reside in a complex that mediates activation of the elF-2α kinase GCN2 in amino acid-starved cells. *Embo Journal,* 14**,** 3184-3199.

Walton, G. M. & Gill, G. N. 1975. Nucleotide regulation of a eukaryotic protein synthesis initiation complex. *Biochimica et Biophysica Acta,* 390**,** 231-245.

Wang, L., Liu, Y. & Wu, S. 2010. The roles of nitric oxide synthase and eIF2alpha kinases in regulation of cell cycle upon UVB-irradiation. *Cell cycle (Georgetown, Tex.),* 9**,** 38-42.

Webb, B. L. J. & Proud, C. G. 1997. Eukaryotic initiation factor 2B (eIF2B). *International Journal of Biochemistry and Cell Biology,* 29**,** 1127-1131.

Wek, R. C., Jackson, B. M. & Hinnebusch, A. G. 1989. Juxtaposition of domains homologous to protein kinase and histidyl-tRNA synthetases in GCN2 protein suggests a mechanism for coupling GCN4 expression to amino acid availability. *Proceedings of the National Academy of Sciences of the United States of America,* 86**,** 4579-4583.

Wek, S., Zhu, S. & Wek, R. 1995. The histidyl-tRNA synthetase-related sequence in the eIF-2 alpha protein kinase GCN2 interacts with tRNA and is required for activation in response to starvation for different amino acids. *Mol. Cell. Biol.,* 15**,** 4497-4506.

Wernimont, A. & Edwards, A. 2009. In Situ proteolysis to generate crystals for structure determination: An update. *PLoS ONE,* 4.

Wetlaufer, D. B. 1963. Ultraviolet spectra Of Proteins and Amino Acids. *In:* C.B. ANFINSEN, K. B. M. L. A. & JOHN, T. E. (eds.) *Advances in Protein Chemistry.* Academic Press.

Yamada, Y., Hagiwara, Y., Shiokawa, K., Sakaki, Y. & Ito, T. 1999. Spatiotemporal, allelic, and enforced expression of Ximpact, the Xenopus homolog of mouse imprinted gene Impact. *Biochemical and Biophysical Research Communications,* 256**,** 162-169.

Yang, R. J., Wek, S. A. & Wek, R. C. 2000. Glucose limitation induces GCN4 translation by activation of gcn2 protein kinase. *Molecular and Cellular Biology,* 20**,** 2706-2717.

Zhu, S. & Wek, R. C. 1998. Ribosome-binding domain of eukaryotic initiation factor-2 kinase GCN2 facilitates translation control. *Journal of Biological Chemistry,* 273**,** 1808-1814.

APPENDIX

Appendix 1: Chemicals Used in this Thesis

Chemical name	Formula/ Abbreviation	Supplier	Location
3-(N-morpholino) propanesulfonic acid	MOPS	Fisher Scientific	New Jersey, USA
Acetic Acid	CH_3COOH	RCI Labscan	Bangkok, Thailand
Acetonitrile		Fisher Scientific	New Jersey, USA
40% Acrylamide/Bis 29.1:0.9		Merck	Darmstadt, Germany
Agar	-	Bacto	NSW, Australia
Agarose		Sigma	Auckland, NZ
Ammonium persulfate	APS	Sigma	Auckland, NZ
Ammonium Sulfate	$(NH_4)_2SO_4$	Ajax UNIVAR;	VIC, Australia
β-mecaptoethanol	BME	Sigma	Auckland, NZ
Boric Acid	H_3BO_3	Scharlau	Sentmenat, Spain
Bromophenol Blue		USB	Ohio, USA
Calcium Chloride dihydrate	$CaCl_2.2H_2O$	Ajax UNIVAR	VIC, Australia
Chloroform		SDS	Peypin, France
Coomassie Brilliant Blue R-250	Coomassie	Sigma	Auckland, NZ
Diethylpyrocarbonate	DEPC	Sigma	Auckland, NZ
Dithiothreitol	DTT	Goldbio	St Louis, USA
Ethanol	EtOH	Ajax	
Ethidium Bromide	EtBr	USB	Ohio, USA
Ethylenediaminetetraacetic acid	EDTA	Sigma	Auckland, NZ
Formaldehyde		Merck	Darmstadt, Germany
Formamide		Merck	Darmstadt, Germany
Glucose	Glu	Sigma	Auckland, NZ
Glutaraldehyde	$CH_2(CH_2CHO)_2$	Sigma	Auckland, NZ
Glycerol		Fisher Scientific	New Jersey, USA
Hydrochloric acid	HCl	Merck	Darmstadt, Germany

Isoleucine	Ile	Sigma	Auckland, NZ
Isopropanol		Scharlau	Sentmenat, Spain
Isopropyl-β-D-thio-galactoside	IPTG	Goldbio	St Louis, USA
Leucine	Leu	Sigma	Auckland, NZ
Lithium chloride	$LiCl_2$	Sigma	Auckland, NZ
Luria Broth powder	LB	Invitrogen	Scotland
Manganese Chloride tetrahydrate	$MnCl_2.4H_2O$	May & Baker Ltd	England
Methanol	MeOH	Ajax	
NAD^+	-	Sigma	Auckland, NZ
NADH	-	Sigma	Auckland, NZ
$NADP^+$	-	Sigma	Auckland, NZ
Phenol		BDH	Poole, England
Potassium Acetate	CH_3CO_2K	Merck	Darmstadt, Germany
Potassium chloride	KCl	Ajax UNIVAR	VIC, Australia
Reduced Glutathione	GSH	Sigma	Auckland, NZ
Rubidium chloride	RbCl	Sigma	Auckland, NZ
Silver Nitrate	$AgNO_3$	Merck	Darmstadt, Germany
Sodium Acetate		Ajax UNIVAR	VIC, Australia
Sodium Adenosine-5'-triphosphate	Na_2ATP	Sigma	Auckland, NZ
Sodium Carbonate	$NaCO_3$	Sigma	Auckland, NZ
Sodium Cholride	NaCl	Ajax UNIVAR	VIC, Australia
Sodium dodecyl sulfate	SDS	Gibco BRL	Cergy Pontoise, France
Sodium Hydroxide	NaOH	Ajax UNIVAR	VIC, Australia
Sodium Thiosulfate	$Na_2S_2O_3.5H_2O$	BDH	Poole, England
Stains All	-	Sigma	Auckland, NZ
Tetramethylethylenediamine	TEMED	Sigma	Auckland, NZ
Trifluoroacetic acid	TFA	Apollo Scientific	Manchester, England
Tris		Pure Science	Porirua, NZ
Tris(2-carboxyethyl) phosphine	TCEP	Soltec Ventures	Beverly, USA
Triton X-100		BDH	Poole, England
Tryptophan	Trp	Sigma	Auckland, NZ

Urea		May & Baker Ltd	England
Valine	Val	Sigma	Auckland, NZ
Yeast Nitrogen Base	YNB	Formedium	Hunstanton, England

Appendix 2: DNA ladder and Protein Molecular Weight Marker

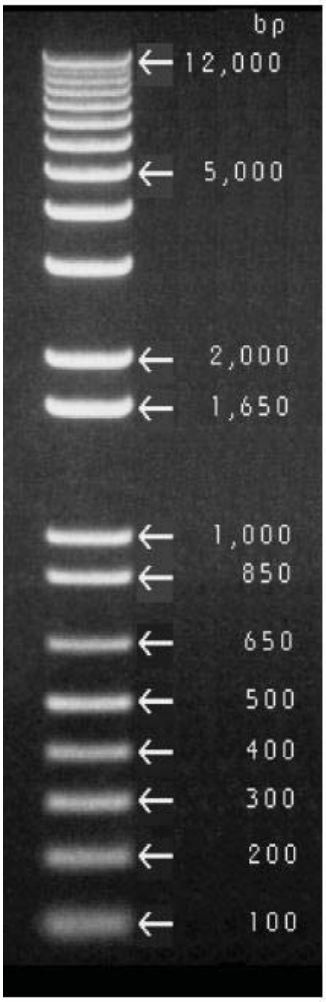

1 Kb Plus DNA Ladder
0.7 µg/lane
0.9% agarose gel

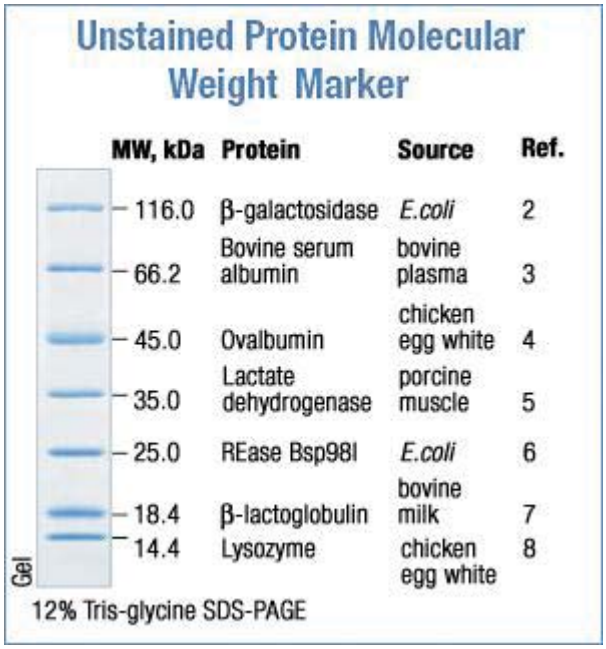

Appendix 3: Nucleotide and Amino Acid sequence of Yih1

```
atggatgacgatcacgaacagttggtcgaagaactggaggccgtcgaggccatctatccg
 M  D  D  D  H  E  Q  L  V  E  E  L  E  A  V  E  A  I  Y  P
gatcttctctccaagaagcaggaagacggaagcatcatcgttgtgaaagtgccgcagcat
 D  L  L  S  K  K  Q  E  D  G  S  I  I  V  V  K  V  P  Q  H
gaatacatgacactgcagatctccttcccgacacactacccctccgaggaggctcctaat
 E  Y  M  T  L  Q  I  S  F  P  T  H  Y  P  S  E  E  A  P  N
gtcatcgaagttggtgtctgcacttctttggctaagcgcgatctctacgataccaagtac
 V  I  E  V  G  V  C  T  S  L  A  K  R  D  L  Y  D  T  K  Y
cttcagcatttgttccaggaagtgatggactctgttttccaccgcggatctgtctgtcta
 L  Q  H  L  F  Q  E  V  M  D  S  V  F  H  R  G  S  V  C  L
tttgacttcctcacagaactcgacggtgtcttgtacgttgaaccagaggaggagacagaa
 F  D  F  L  T  E  L  D  G  V  L  Y  V  E  P  E  E  E  T  E
ccggtccagcagagtgacattcccacagacccccttcgagggctggaccgcgtcggacccc
 P  V  Q  Q  S  D  I  P  T  D  P  F  E  G  W  T  A  S  D  P
attactgatagaggctcgactttcatggcctttgcagcacatgttacctccgaggaacaa
 I  T  D  R  G  S  T  F  M  A  F  A  A  H  V  T  S  E  E  Q
gcgtttgccatgctagacctactgaagaccgactccaagatgcgtaaggcaaaccatgtc
 A  F  A  M  L  D  L  L  K  T  D  S  K  M  R  K  A  N  H  V
atgagtgcatggcgaatcaagcaggatggctctgcggcaacatatcaagattccgatgat
 M  S  A  W  R  I  K  Q  D  G  S  A  A  T  Y  Q  D  S  D  D
gacggtgaaacggccgccggctccagaatgctgcacctcatcaccatcatggatgtgtgg
 D  G  E  T  A  A  G  S  R  M  L  H  L  I  T  I  M  D  V  W
aacgtcatcgttgtggtggcccgttggttcggcggtgcccacataggtcccgaccggttt
 N  V  I  V  V  V  A  R  W  F  G  G  A  H  I  G  P  D  R  F
aaacacatcaattctacggcaagagaagctgttgtcagggccggcttcgactcgtaa
 K  H  I  N  S  T  A  R  E  A  V  V  R  A  G  F  D  S  -
```

Appendix 4: Plasmid Map of pET28a (Novagen)

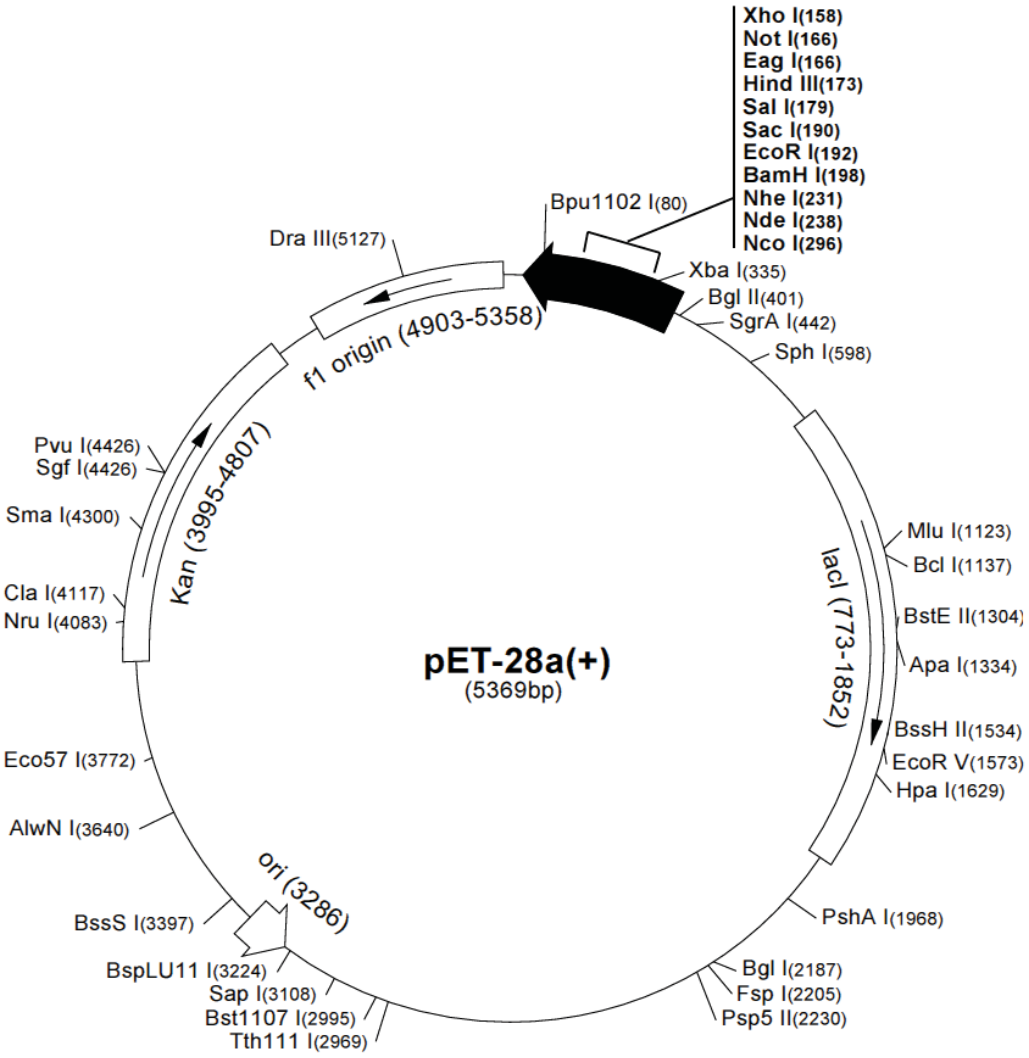

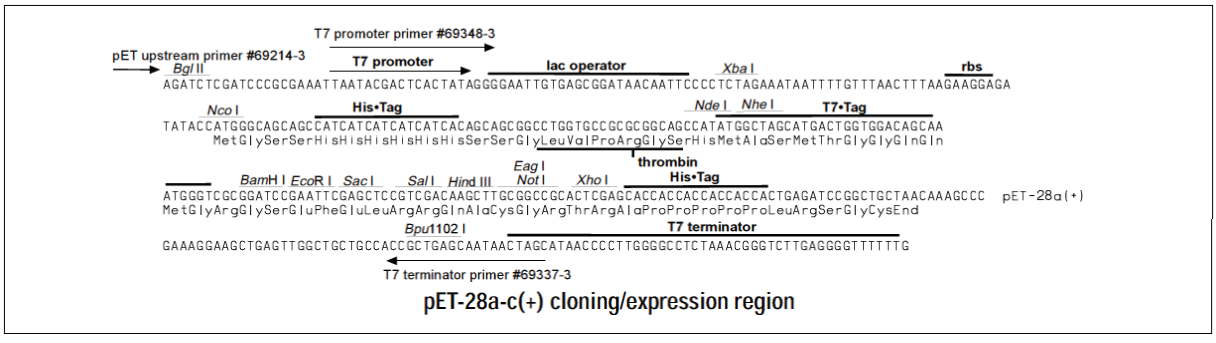

pET-28a-c(+) cloning/expression region

Appendix 5: pGEX-6P-3 vector (GE Healthcare)

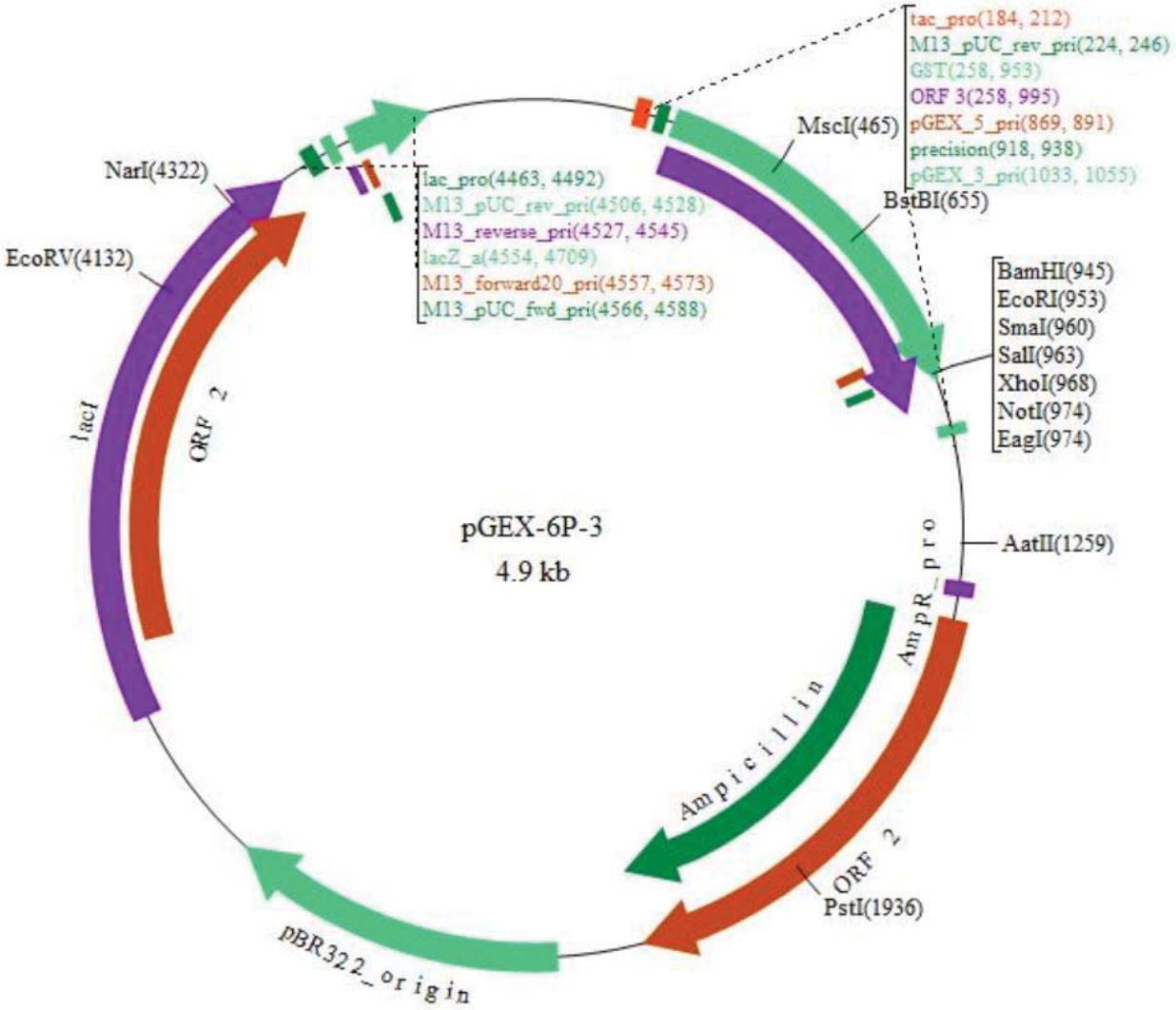

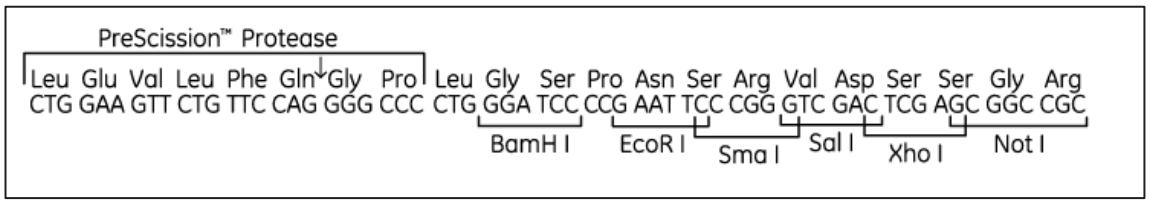

Appendix 6: Plasmid map of pETDUET-1 (Novagen)

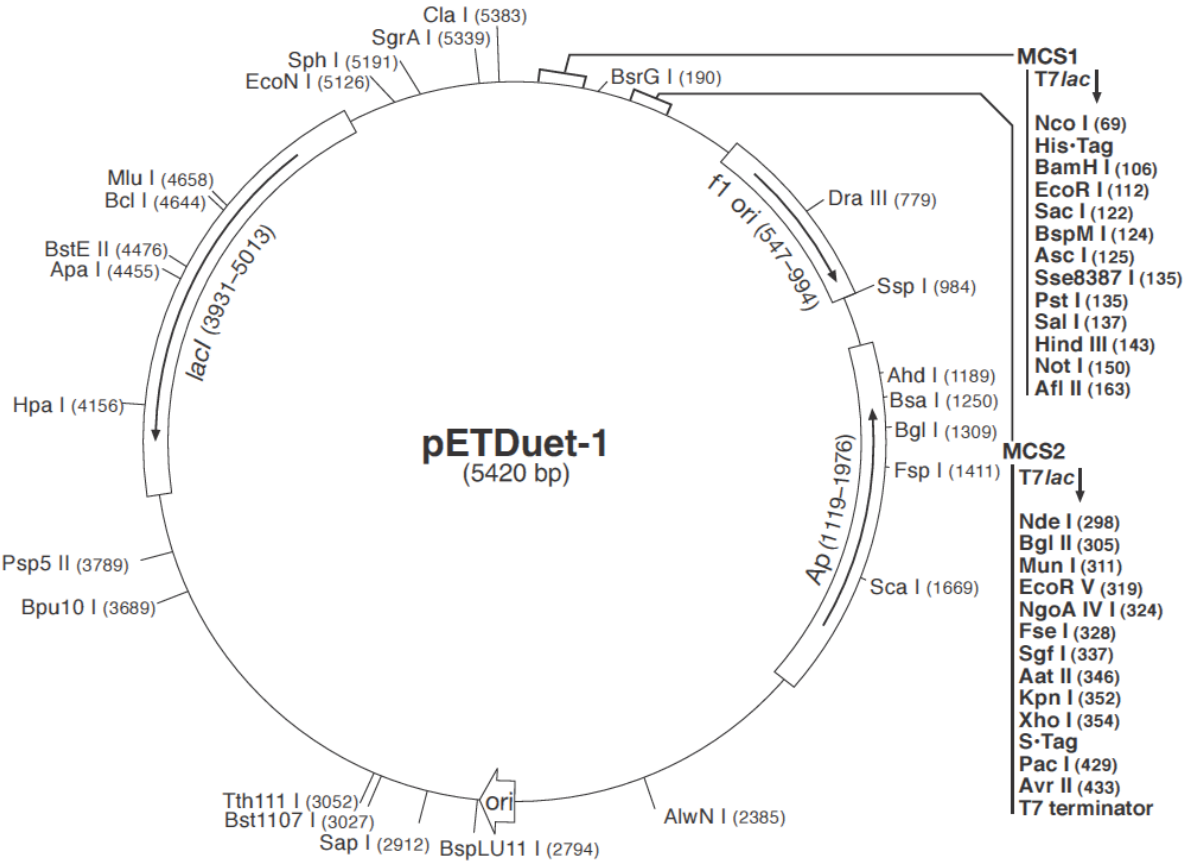

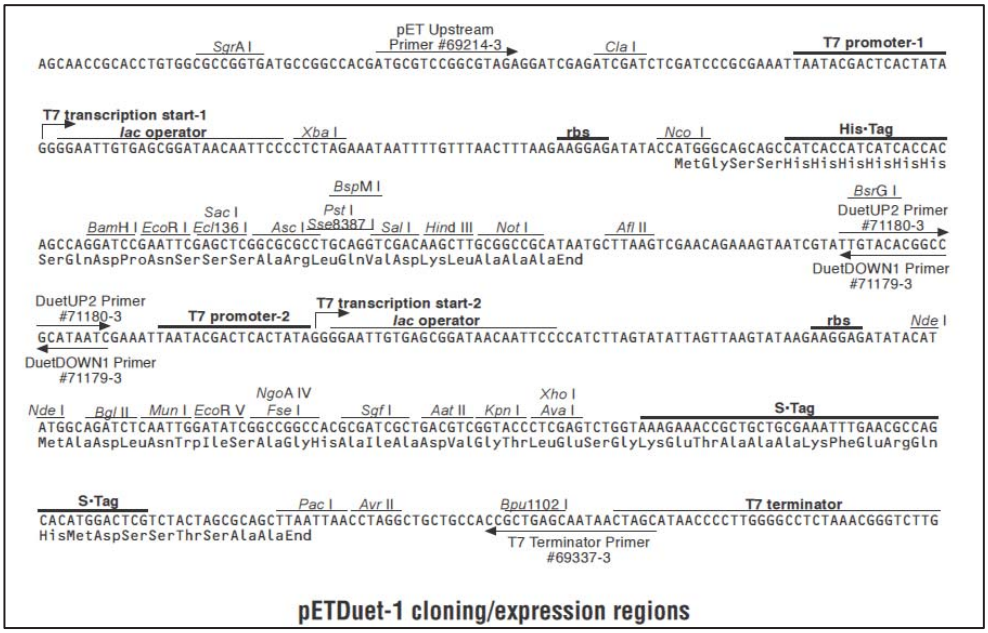

pETDuet-1 cloning/expression regions

Appendix 7: Plasmid Map of pET32a-(BamHI)

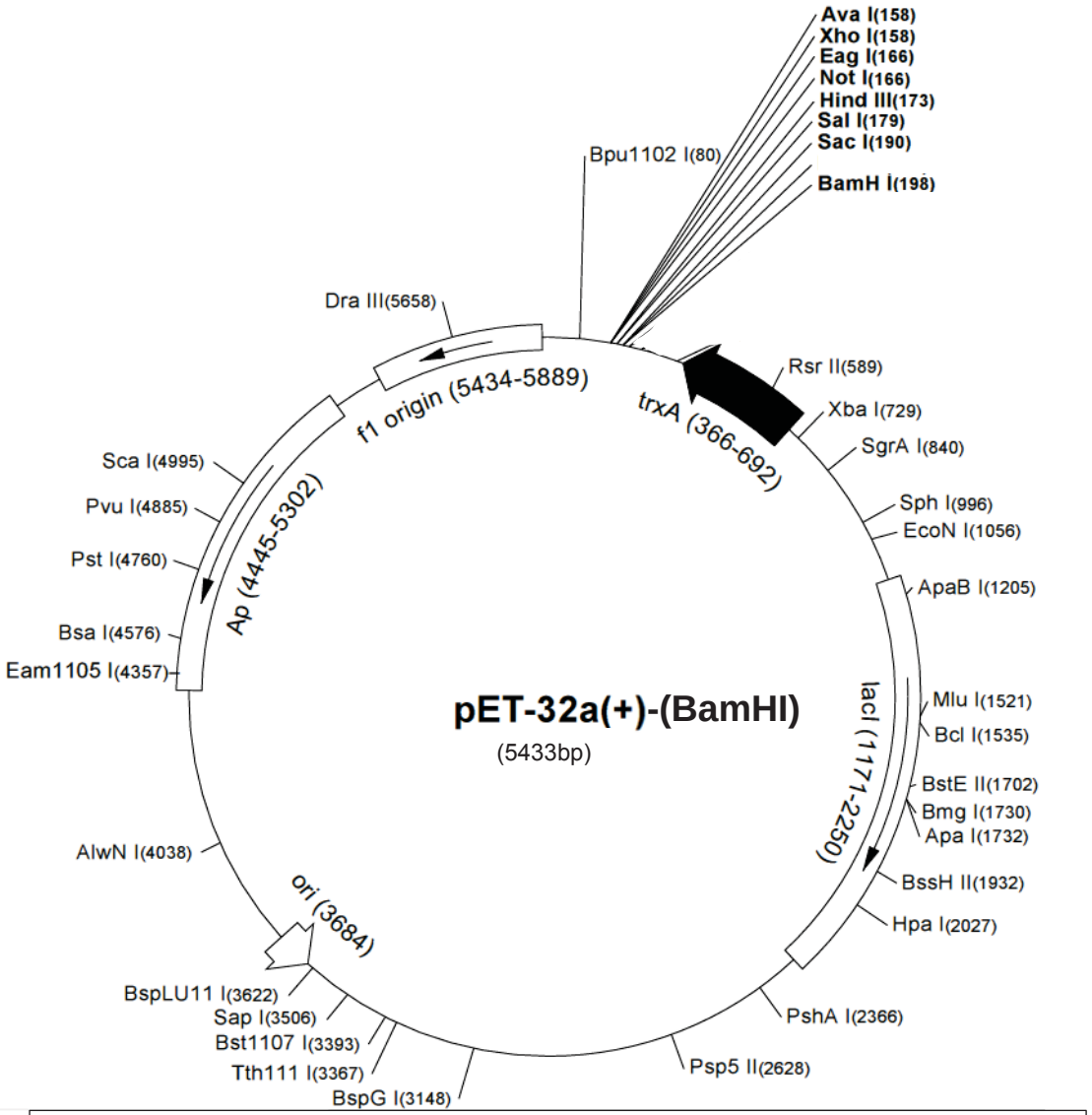

Appendix 8: Primer Sequences

Primer Name	Sequence (5'→ 3')
KQE26AAA Forward	GGATCTTCTCTCCAAGGCGGCGGCAGACGGAAGCATCATCGT
KQE26AAA Reverse	ACGATGATGCTTCCGTCTGCCGCCGCCTTGGAGAGAAGATCC
EE56AA Forward	CTACCCCTCCGCGGCGGCTCCTAATGTCATCGAAGTTGG
EE56AA Reverse	CCAACTTCGATGACATTAGGAGCCGCCGCGGAGGGGTAG
EEE116AAA Forward	CGTTGAACCAGCGGCGGCGACAGAACCGGTCCAGCAGAGTGA
EEE116AAA Reverse	TCACTCTGCTGGACCGGTTCTGTCGCCGCCGCTGGTTCAACG
His_6-Ancient Forward	AAGGATCCGCATCAGACCCCATTACTG
His_6-Ancient Reverse	CCGCTCGAGTTACCTGACAACAGCTTCTCTTG
Lac_oper_F sequencing	GAATTGTGAGCGGATAAC
T7_term_R Sequencing	TGCTAGTTATTGCTCAGCGGT

Appendix 9A: PACT Premier Conditions (Molecular Dimensions)

Well	Concentration Units Chemical, pH
A1	25.000 w/v polyethylene glycol 1500; 10.000 v/v succinate-phosphate-glycine, pH=4.0;
A2	25.000 w/v polyethylene glycol 1500; 10.000 v/v succinate-phosphate-glycine, pH=5.0;
A3	25.000 w/v polyethylene glycol 1500; 10.000 v/v succinate-phosphate-glycine, pH=6.0;
A4	25.000 w/v polyethylene glycol 1500; 10.000 v/v succinate-phosphate-glycine, pH=7.0;
A5	25.000 w/v polyethylene glycol 1500; 10.000 v/v succinate-phosphate-glycine, pH=8.0;
A6	25.000 w/v polyethylene glycol 1500; 10.000 v/v succinate-phosphate-glycine, pH=9.0;
A7	20.000 w/v polyethylene glycol 6000; 0.100 M sodium acetate, pH=5.0; 0.200 M sodium chloride;
A8	20.000 w/v polyethylene glycol 6000; 0.100 M sodium acetate, pH=5.0; 0.200 M ammonium chloride;
A9	20.000 w/v polyethylene glycol 6000; 0.100 M sodium acetate, pH=5.0; 0.200 M lithium chloride;
A10	20.000 w/v polyethylene glycol 6000; 0.100 M sodium acetate, pH=5.0; 0.200 M magnesium chloride;
A11	20.000 w/v polyethylene glycol 6000; 0.100 M sodium acetate, pH=5.0; 0.200 M calcium chloride;
A12	20.000 w/v polyethylene glycol 6000; 0.100 M sodium acetate, pH=5.0; 0.010 M zinc chloride;
B1	25.000 w/v polyethylene glycol 1500; 10.000 v/v malonate-imidazole-borate, pH=4.0;
B2	25.000 w/v polyethylene glycol 1500; 10.000 v/v malonate-imidazole-borate, pH=5.0;
B3	25.000 w/v polyethylene glycol 1500; 10.000 v/v malonate-imidazole-borate, pH=6.0;
B4	25.000 w/v polyethylene glycol 1500; 10.000 v/v malonate-imidazole-borate, pH=7.0;
B5	25.000 w/v polyethylene glycol 1500; 10.000 v/v malonate-imidazole-borate, pH=8.0;
B6	25.000 w/v polyethylene glycol 1500; 10.000 v/v malonate-imidazole-borate, pH=9.0;
B7	20.000 w/v polyethylene glycol 6000; 0.100 M MES, pH=6.0; 0.200 M sodium chloride;
B8	20.000 w/v polyethylene glycol 6000; 0.100 M MES, pH=6.0; 0.200 M ammonium chloride;
B9	20.000 w/v polyethylene glycol 6000; 0.100 M MES, pH=6.0; 0.200 M lithium chloride;
B10	20.000 w/v polyethylene glycol 6000; 0.100 M MES, pH=6.0; 0.200 M magnesium chloride;
B11	20.000 w/v polyethylene glycol 6000; 0.100 M MES, pH=6.0; 0.200 M calcium chloride;
B12	20.000 w/v polyethylene glycol 6000; 0.100 M MES, pH=6.0; 0.010 M zinc chloride;
C1	25.000 w/v polyethylene glycol 1500; 10.000 v/v propionate-cacodylate-bis tris propane, pH=4.0;
C2	25.000 w/v polyethylene glycol 1500; 10.000 v/v propionate-cacodylate-bis tris propane, pH=5.0;
C3	25.000 w/v polyethylene glycol 1500; 10.000 v/v propionate-cacodylate-bis tris propane, pH=6.0;
C4	25.000 w/v polyethylene glycol 1500; 10.000 v/v propionate-cacodylate-bis tris propane, pH=7.0;
C5	25.000 w/v polyethylene glycol 1500; 10.000 v/v propionate-cacodylate-bis tris propane, pH=8.0;
C6	25.000 w/v polyethylene glycol 1500; 10.000 v/v propionate-cacodylate-bis tris propane, pH=9.0;
C7	20.000 w/v polyethylene glycol 6000; 0.100 M HEPES, pH=7.0; 0.200 M sodium chloride;
C8	20.000 w/v polyethylene glycol 6000; 0.100 M HEPES, pH=7.0; 0.200 M ammonium chloride;
C9	20.000 w/v polyethylene glycol 6000; 0.100 M HEPES, pH=7.0; 0.200 M lithium chloride;
C10	20.000 w/v polyethylene glycol 6000; 0.100 M HEPES, pH=7.0; 0.200 M magnesium chloride;
C11	20.000 w/v polyethylene glycol 6000; 0.100 M HEPES, pH=7.0; 0.200 M calcium chloride;
C12	20.000 w/v polyethylene glycol 6000; 0.100 M HEPES, pH=7.0; 0.010 M zinc chloride;
D1	25.000 w/v polyethylene glycol 1500; 10.000 v/v malate-MES-tris, pH=4.0;
D2	25.000 w/v polyethylene glycol 1500; 10.000 v/v malate-MES-tris, pH=5.0;
D3	25.000 w/v polyethylene glycol 1500; 10.000 v/v malate-MES-tris, pH=6.0;
D4	25.000 w/v polyethylene glycol 1500; 10.000 v/v malate-MES-tris, pH=7.0;
D5	25.000 w/v polyethylene glycol 1500; 10.000 v/v malate-MES-tris, pH=8.0;
D6	25.000 w/v polyethylene glycol 1500; 10.000 v/v malate-MES-tris, pH=9.0;
D7	20.000 w/v polyethylene glycol 6000; 0.100 M tris, pH=8.0; 0.200 M sodium chloride;
D8	20.000 w/v polyethylene glycol 6000; 0.100 M tris, pH=8.0; 0.200 M ammonium chloride;
D9	20.000 w/v polyethylene glycol 6000; 0.100 M tris, pH=8.0; 0.200 M lithium chloride;
D10	20.000 w/v polyethylene glycol 6000; 0.100 M tris, pH=8.0; 0.200 M magnesium chloride;
D11	20.000 w/v polyethylene glycol 6000; 0.100 M tris, pH=8.0; 0.200 M calcium chloride;
D12	20.000 w/v polyethylene glycol 6000; 0.100 M tris, pH=8.0; 0.010 M zinc chloride;
E1	20.000 w/v polyethylene glycol 3350; 0.200 M sodium fluoride;

E2	20.000 w/v polyethylene glycol 3350; 0.200 M sodium bromide;
E3	20.000 w/v polyethylene glycol 3350; 0.200 M sodium iodide;
E4	20.000 w/v polyethylene glycol 3350; 0.200 M potassium thiocyanate;
E5	20.000 w/v polyethylene glycol 3350; 0.200 M sodium nitrate;
E6	20.000 w/v polyethylene glycol 3350; 0.200 M sodium formate;
E7	20.000 w/v polyethylene glycol 3350; 0.200 M sodium acetate;
E8	20.000 w/v polyethylene glycol 3350; 0.200 M sodium sulfate;
E9	20.000 w/v polyethylene glycol 3350; 0.200 M potassium sodium tartrate;
E10	20.000 w/v polyethylene glycol 3350; 0.020 M Na2H/KH2 phosphate;
E11	20.000 w/v polyethylene glycol 3350; 0.200 M tri-sodium citrate;
E12	20.000 w/v polyethylene glycol 3350; 0.200 M sodium malonate;
F1	20.000 w/v polyethylene glycol 3350; 0.100 M bis-tris propane, pH=6.5; 0.200 M sodium fluoride;
F2	20.000 w/v polyethylene glycol 3350; 0.100 M bis-tris propane, pH=6.5; 0.200 M sodium bromide;
F3	20.000 w/v polyethylene glycol 3350; 0.100 M bis-tris propane, pH=6.5; 0.200 M sodium iodide;
F4	20.000 w/v polyethylene glycol 3350; 0.100 M bis-tris propane, pH=6.5; 0.200 M potassium thiocyanate;
F5	20.000 w/v polyethylene glycol 3350; 0.100 M bis-tris propane, pH=6.5; 0.200 M sodium nitrate;
F6	20.000 w/v polyethylene glycol 3350; 0.100 M bis-tris propane, pH=6.5; 0.200 M sodium formate;
F7	20.000 w/v polyethylene glycol 3350; 0.100 M bis-tris propane, pH=6.5; 0.200 M sodium acetate;
F8	20.000 w/v polyethylene glycol 3350; 0.100 M bis-tris propane, pH=6.5; 0.200 M sodium sulfate;
F9	20.000 w/v polyethylene glycol 3350; 0.100 M bis-tris propane, pH=6.5; 0.200 M potassium sodium tartrate;
F10	20.000 w/v polyethylene glycol 3350; 0.020 M Na2H/KH2 phosphate; 0.100 M bis-tris propane, pH=6.5;
F11	20.000 w/v polyethylene glycol 3350; 0.100 M bis-tris propane, pH=6.5; 0.200 M tri-sodium citrate;
F12	20.000 w/v polyethylene glycol 3350; 0.200 M sodium malonate; 0.100 M bis-tris propane, pH=6.5;
G1	20.000 w/v polyethylene glycol 3350; 0.100 M bis-tris propane, pH=7.5; 0.200 M sodium fluoride;
G2	20.000 w/v polyethylene glycol 3350; 0.100 M bis-tris propane, pH=7.5; 0.200 M sodium bromide;
G3	20.000 w/v polyethylene glycol 3350; 0.100 M bis-tris propane, pH=7.5; 0.200 M sodium iodide;
G4	20.000 w/v polyethylene glycol 3350; 0.100 M bis-tris propane, pH=7.5; 0.200 M potassium thiocyanate;
G5	20.000 w/v polyethylene glycol 3350; 0.100 M bis-tris propane, pH=7.5; 0.200 M sodium nitrate;
G6	20.000 w/v polyethylene glycol 3350; 0.100 M bis-tris propane, pH=7.5; 0.200 M sodium formate;
G7	20.000 w/v polyethylene glycol 3350; 0.200 M sodium acetate; 0.100 M bis-tris propane, pH=7.5;
G8	20.000 w/v polyethylene glycol 3350; 0.100 M bis-tris propane, pH=7.5; 0.200 M sodium sulfate;
G9	20.000 w/v polyethylene glycol 3350; 0.100 M bis-tris propane, pH=7.5; 0.200 M potassium sodium tartrate;
G10	20.000 w/v polyethylene glycol 3350; 0.020 M Na2H/KH2 phosphate; 0.100 M bis-tris propane, pH=7.5;
G11	20.000 w/v polyethylene glycol 3350; 0.100 M bis-tris propane, pH=7.5; 0.200 M tri-sodium citrate;
G12	20.000 w/v polyethylene glycol 3350; 0.200 M sodium malonate; 0.100 M bis-tris propane, pH=7.5;
H1	20.000 w/v polyethylene glycol 3350; 0.100 M bis-tris propane, pH=8.5; 0.200 M sodium fluoride;
H2	20.000 w/v polyethylene glycol 3350; 0.100 M bis-tris propane, pH=8.5; 0.200 M sodium bromide;
H3	20.000 w/v polyethylene glycol 3350; 0.100 M bis-tris propane, pH=8.5; 0.200 M sodium iodide;
H4	20.000 w/v polyethylene glycol 3350; 0.100 M bis-tris propane, pH=8.5; 0.200 M potassium thiocyanate;
H5	20.000 w/v polyethylene glycol 3350; 0.100 M bis-tris propane, pH=8.5; 0.200 M sodium nitrate;
H6	20.000 w/v polyethylene glycol 3350; 0.100 M bis-tris propane, pH=8.5; 0.200 M sodium formate;
H7	20.000 w/v polyethylene glycol 3350; 0.200 M sodium acetate; 0.100 M bis-tris propane, pH=8.5;
H8	20.000 w/v polyethylene glycol 3350; 0.100 M bis-tris propane, pH=8.5; 0.200 M sodium sulfate;
H9	20.000 w/v polyethylene glycol 3350; 0.100 M bis-tris propane, pH=8.5; 0.200 M potassium sodium tartrate;
H10	20.000 w/v polyethylene glycol 3350; 0.100 M bis-tris propane, pH=8.5; 0.020 M Na2H/KH2 phosphate;
H11	20.000 w/v polyethylene glycol 3350; 0.100 M bis-tris propane, pH=8.5; 0.200 M tri-sodium citrate;

Appendix 9B: Crystal Screen I and II Conditions (Hampton Research)

Well	Concentration Units Chemical, pH
A1	30.000 v/v 2-methyl-2,4-pentanediol; 0.100 M sodium acetate, pH=4.6; 0.020 M calcium chloride;
A2	0.400 M potassium sodium tartrate;
A3	0.400 M ammonium dihydrogen phosphate;
A4	2.000 M ammonium sulfate; 0.100 M tris chloride, pH=8.5;
A5	30.000 v/v 2-methyl-2,4-pentanediol; 0.100 M sodium HEPES, pH=7.5; 0.200 M tri-sodium citrate;
A6	30.000 w/v polyethylene glycol 4000; 0.100 M tris chloride, pH=8.5; 0.200 M magnesium chloride;
A7	0.100 M sodium cacodylate, pH=6.5; 1.400 M sodium acetate;
A8	30.000 v/v 2-propanol; 0.100 M sodium cacodylate, pH=6.5; 0.200 M tri-sodium citrate;
A9	30.000 w/v polyethylene glycol 4000; 0.100 M tri-sodium citrate - citric acid, pH=5.6; 0.200 M ammonium acetate;
A10	30.000 w/v polyethylene glycol 4000; 0.100 M sodium acetate, pH=4.6; 0.200 M ammonium acetate;
A11	1.000 M ammonium dihydrogen phosphate; 0.100 M tri-sodium citrate - citric acid, pH=5.6;
A12	30.000 v/v 2-propanol; 0.100 M sodium HEPES, pH=7.5; 0.200 M magnesium chloride;
B1	30.000 v/v polyethylene glycol 400; 0.100 M tris chloride, pH=8.5; 0.200 M tri-sodium citrate;
B2	28.000 v/v polyethylene glycol 400; 0.100 M sodium HEPES, pH=7.5; 0.200 M calcium chloride;
B3	30.000 w/v polyethylene glycol 8000; 0.100 M sodium cacodylate, pH=6.5; 0.200 M ammonium sulfate;
B4	1.500 M lithium sulfate; 0.100 M sodium HEPES, pH=7.5;
B5	30.000 w/v polyethylene glycol 4000; 0.100 M tris chloride, pH=8.5; 0.200 M lithium sulfate;
B6	20.000 w/v polyethylene glycol 8000; 0.100 M sodium cacodylate, pH=6.5; 0.200 M magnesium acetate;
B7	30.000 v/v 2-propanol; 0.100 M tris chloride, pH=8.5; 0.200 M ammonium acetate;
B8	25.000 w/v polyethylene glycol 4000; 0.100 M sodium acetate, pH=4.6; 0.200 M ammonium sulfate;
B9	30.000 v/v 2-methyl-2,4-pentanediol; 0.100 M sodium cacodylate, pH=6.5; 0.200 M magnesium acetate;
B10	30.000 w/v polyethylene glycol 4000; 0.200 M sodium acetate; 0.100 M tris chloride, pH=8.5;
B11	30.000 v/v polyethylene glycol 400; 0.100 M sodium HEPES, pH=7.5; 0.200 M magnesium chloride;
B12	20.000 v/v 2-propanol; 0.100 M sodium acetate, pH=4.6; 0.200 M calcium chloride;
C1	0.100 M imidazole, pH=6.5; 1.000 M sodium acetate;
C2	30.000 v/v 2-methyl-2,4-pentanediol; 0.100 M tri-sodium citrate - citric acid, pH=5.6; 0.200 M ammonium acetate;
C3	20.000 v/v 2-propanol; 0.100 M sodium HEPES, pH=7.5; 0.200 M tri-sodium citrate;
C4	30.000 w/v polyethylene glycol 8000; 0.200 M sodium acetate; 0.100 M sodium cacodylate, pH=6.5;
C5	0.800 M potassium sodium tartrate; 0.100 M sodium HEPES, pH=7.5;
C6	30.000 w/v polyethylene glycol 8000; 0.200 M ammonium sulfate;
C7	30.000 w/v polyethylene glycol 4000; 0.200 M ammonium sulfate;
C8	2.000 M ammonium sulfate;
C9	4.000 M sodium formate;
C10	2.000 M sodium formate; 0.100 M sodium acetate, pH=4.6;
C11	0.800 M potassium dihydrogen phosphate; 0.100 M sodium HEPES, pH=7.5; 0.800 M sodium dihydrogen phosphate;
C12	8.000 w/v polyethylene glycol 8000; 0.100 M tris chloride, pH=8.5;
D1	8.000 w/v polyethylene glycol 4000; 0.100 M sodium acetate, pH=4.6;
D2	1.400 M tri-sodium citrate; 0.100 M sodium HEPES, pH=7.5;
D3	2.000 M ammonium sulfate; 0.100 M sodium HEPES, pH=7.5; 2.000 v/v polyethylene glycol 400;
D4	20.000 w/v polyethylene glycol 4000; 0.100 M tri-sodium citrate - citric acid, pH=5.6; 20.000 v/v 2-propanol;
D5	20.000 w/v polyethylene glycol 4000; 0.100 M sodium HEPES, pH=7.5; 10.000 v/v 2-propanol;
D6	20.000 w/v polyethylene glycol 8000; 0.050 M potassium dihydrogen phosphate;
D7	30.000 w/v polyethylene glycol 1500;
D8	0.200 M magnesium formate;
D9	18.000 w/v polyethylene glycol 8000; 0.100 M sodium cacodylate, pH=6.5; 0.200 M zinc acetate;
D10	18.000 w/v polyethylene glycol 8000; 0.100 M sodium cacodylate, pH=6.5; 0.200 M calcium acetate;
D11	2.000 M ammonium sulfate; 0.100 M sodium acetate, pH=4.6;
D12	2.000 M ammonium dihydrogen phosphate; 0.100 M tris chloride, pH=8.5;
E1	10.000 w/v polyethylene glycol 6000; 2.000 M sodium chloride;

E2	0.500 M sodium chloride; 0.010 M CTAB; 0.010 M magnesium chloride;
E3	25.000 v/v ethylene glycol;
E4	35.000 v/v dioxane;
E5	2.000 M ammonium sulfate; 5.000 v/v 2-propanol;
E6	1.000 M imidazole, pH=7.0;
E7	10.000 w/v polyethylene glycol 1000; 10.000 w/v polyethylene glycol 8000;
E8	10.000 v/v ethanol; 1.500 M sodium chloride;
E9	2.000 M sodium chloride; 0.100 M sodium acetate, pH=4.6;
E10	30.000 v/v 2-methyl-2,4-pentanediol; 0.100 M sodium acetate, pH=4.6; 0.200 M sodium chloride;
E11	1.000 M 1,6-hexanediol; 0.100 M sodium acetate, pH=4.6; 0.010 M cobalt chloride;
E12	30.000 v/v polyethylene glycol 400; 0.100 M sodium acetate, pH=4.6; 0.100 M cadmium chloride;
F1	30.000 w/v polyethylene glycol monomethyl ether 2000; 0.100 M sodium acetate, pH=4.6; 0.200 M ammonium sulfate;
F2	2.000 M ammonium sulfate; 0.100 M tri-sodium citrate - citric acid, pH=5.6; 0.200 M potassium sodium tartrate;
F3	1.000 M lithium sulfate; 0.100 M tri-sodium citrate - citric acid, pH=5.6; 0.500 M ammonium sulfate;
F4	2.000 w/v ethylene imine polymer; 0.100 M tri-sodium citrate - citric acid, pH=5.6; 0.500 M sodium chloride;
F5	35.000 v/v tert-butanol; 0.100 M tri-sodium citrate - citric acid, pH=5.6;
F6	10.000 v/v jeffamine M-600; 0.100 M tri-sodium citrate - citric acid, pH=5.6; 0.010 M ferric chloride;
F7	2.500 M 1,6-hexanediol; 0.100 M tri-sodium citrate - citric acid, pH=5.6;
F8	1.600 M magnesium sulfate; 0.100 M MES, pH=6.5;
F9	2.000 M sodium chloride; 0.100 M sodium dihydrogen phosphate; 0.100 M MES, pH=6.5; 0.100 M potassium dihydrogen
F10	12.000 w/v polyethylene glycol 20000; 0.100 M MES, pH=6.5;
F11	1.600 M ammonium sulfate; 0.100 M MES, pH=6.5; 10.000 v/v dioxane;
F12	30.000 v/v jeffamine M-600; 0.100 M MES, pH=6.5; 0.050 M cesium chloride;
G1	1.800 M ammonium sulfate; 0.100 M MES, pH=6.5; 0.010 M cobalt chloride;
G2	30.000 w/v polyethylene glycol monomethyl ether 5000; 0.100 M MES, pH=6.5; 0.200 M ammonium sulfate;
G3	25.000 v/v polyethylene glycol monomethyl ether 550; 0.100 M MES, pH=6.5; 0.010 M zinc sulfate;
G4	1.600 M tri-sodium citrate - citric acid, pH=6.5;
G5	30.000 v/v 2-methyl-2,4-pentanediol; 0.100 M HEPES, pH=7.5; 0.500 M ammonium sulfate;
G6	10.000 w/v polyethylene glycol 6000; 0.100 M HEPES, pH=7.5; 5.000 v/v 2-methyl-2,4-pentanediol;
G7	20.000 v/v jeffamine M-600; 0.100 M HEPES, pH=7.5;
G8	1.600 M ammonium sulfate; 0.100 M HEPES, pH=7.5; 0.100 M sodium chloride;
G9	2.000 M ammonium formate; 0.100 M HEPES, pH=7.5;
G10	0.050 M cadmium sulfate; 1.000 M sodium acetate; 0.100 M HEPES, pH=7.5;
G11	70.000 v/v 2-methyl-2,4-pentanediol; 0.100 M HEPES, pH=7.5;
G12	4.300 M sodium chloride; 0.100 M HEPES, pH=7.5;
H1	10.000 w/v polyethylene glycol 8000; 0.100 M HEPES, pH=7.5; 8.000 v/v ethylene glycol;
H2	20.000 w/v polyethylene glycol 10000; 0.100 M HEPES, pH=7.5;
H3	3.400 M 1,6-hexanediol; 0.100 M tris chloride, pH=8.5; 0.200 M magnesium chloride;
H4	25.000 v/v tert-butanol; 0.100 M tris chloride, pH=8.5;
H5	1.000 M lithium sulfate; 0.100 M tris chloride, pH=8.5; 0.010 M nickel (II) chloride;
H6	12.000 v/v glycerol; 0.100 M tris chloride, pH=8.5; 1.500 M ammonium sulfate;
H7	50.000 v/v 2-methyl-2,4-pentanediol; 0.100 M tris chloride, pH=8.5; 0.200 M ammonium dihydrogen phosphate;
H8	20.000 v/v ethanol; 0.100 M tris chloride, pH=8.5;
H9	20.000 w/v polyethylene glycol monomethyl ether 2000; 0.100 M tris chloride, pH=8.5; 0.010 M nickel (II) chloride;
H10	20.000 v/v polyethylene glycol monomethyl ether 550; 0.100 M bicine, pH=9.0; 0.100 M sodium chloride;
H11	2.000 M magnesium chloride; 0.100 M bicine, pH=9.0;

Appendix 9C: Structure Screen I and II (Molecular Dimensions)

Well	Concentration Units Chemical, pH
A1	30.000 v/v 2-methyl-2,4-pentanediol; 0.100 M sodium acetate, pH=4.6; 0.020 M calcium chloride;
A2	30.000 w/v polyethylene glycol 4000; 0.100 M sodium acetate, pH=4.6; 0.200 M ammonium acetate;
A3	25.000 w/v polyethylene glycol 4000; 0.100 M sodium acetate, pH=4.6; 0.200 M ammonium sulfate;
A4	2.000 M sodium formate; 0.100 M sodium acetate, pH=4.6;
A5	2.000 M ammonium sulfate; 0.100 M sodium acetate, pH=4.6;
A6	8.000 w/v polyethylene glycol 4000; 0.100 M sodium acetate, pH=4.6;
A7	30.000 w/v polyethylene glycol 4000; 0.100 M tri-sodium citrate - citric acid, pH=5.6; 0.200 M ammonium acetate;
A8	30.000 v/v 2-methyl-2,4-pentanediol; 0.100 M tri-sodium citrate - citric acid, pH=5.6; 0.200 M ammonium acetate;
A9	20.000 w/v polyethylene glycol 4000; 0.100 M tri-sodium citrate - citric acid, pH=5.6; 20.000 v/v 2-propanol;
A10	1.000 M ammonium dihydrogen phosphate; 0.100 M tri-sodium citrate - citric acid, pH=5.6;
A11	20.000 v/v 2-propanol; 0.100 M sodium acetate, pH=4.6; 0.200 M calcium chloride;
A12	0.100 M sodium cacodylate, pH=6.5; 1.400 M sodium acetate;
B1	30.000 v/v 2-propanol; 0.100 M sodium cacodylate, pH=6.5; 0.200 M tri-sodium citrate;
B2	30.000 w/v polyethylene glycol 8000; 0.100 M sodium cacodylate, pH=6.5; 0.200 M ammonium sulfate;
B3	20.000 w/v polyethylene glycol 8000; 0.100 M sodium cacodylate, pH=6.5; 0.200 M magnesium acetate;
B4	30.000 v/v 2-methyl-2,4-pentanediol; 0.100 M sodium cacodylate, pH=6.5; 0.200 M magnesium acetate;
B5	0.100 M imidazole, pH=6.5; 1.000 M sodium acetate;
B6	30.000 w/v polyethylene glycol 8000; 0.100 M sodium cacodylate, pH=6.5; 0.200 M sodium acetate;
B7	18.000 w/v polyethylene glycol 8000; 0.100 M sodium cacodylate, pH=6.5; 0.200 M zinc acetate;
B8	18.000 w/v polyethylene glycol 8000; 0.100 M sodium cacodylate, pH=6.5; 0.200 M calcium acetate;
B9	30.000 v/v 2-methyl-2,4-pentanediol; 0.100 M sodium HEPES, pH=7.5; 0.200 M tri-sodium citrate;
B10	30.000 v/v 2-propanol; 0.100 M sodium HEPES, pH=7.5; 0.200 M magnesium chloride;
B11	28.000 v/v polyethylene glycol 400; 0.100 M sodium HEPES, pH=7.5; 0.200 M calcium chloride;
B12	30.000 v/v polyethylene glycol 400; 0.100 M sodium HEPES, pH=7.5; 0.200 M magnesium chloride;
C1	20.000 v/v 2-propanol; 0.100 M sodium HEPES, pH=7.5; 0.200 M tri-sodium citrate;
C2	0.800 M potassium sodium tartrate; 0.100 M sodium HEPES, pH=7.5;
C3	1.500 M lithium sulfate; 0.100 M sodium HEPES, pH=7.5;
C4	0.800 M potassium dihydrogen phosphate; 0.100 M sodium HEPES, pH=7.5; 0.800 M sodium dihydrogen phosphate;
C5	1.400 M tri-sodium citrate; 0.100 M sodium HEPES, pH=7.5;
C6	2.000 M ammonium sulfate; 0.100 M sodium HEPES, pH=7.5; 2.000 v/v polyethylene glycol 400;
C7	20.000 w/v polyethylene glycol 4000; 0.100 M sodium HEPES, pH=7.5; 10.000 v/v 2-propanol;
C8	2.000 M ammonium sulfate; 0.100 M tris chloride, pH=8.5;
C9	30.000 w/v polyethylene glycol 4000; 0.100 M tris chloride, pH=8.5; 0.200 M magnesium chloride;
C10	30.000 v/v polyethylene glycol 400; 0.100 M tris chloride, pH=8.5; 0.200 M tri-sodium citrate;
C11	30.000 w/v polyethylene glycol 4000; 0.100 M tris chloride, pH=8.5; 0.200 M lithium sulfate;
C12	30.000 v/v 2-propanol; 0.100 M tris chloride, pH=8.5; 0.200 M ammonium acetate;
D1	30.000 w/v polyethylene glycol 4000; 0.200 M sodium acetate; 0.100 M tris chloride, pH=8.5;
D2	8.000 w/v polyethylene glycol 8000; 0.100 M tris chloride, pH=8.5;
D3	2.000 M ammonium dihydrogen phosphate; 0.100 M tris chloride, pH=8.5;
D4	0.400 M potassium sodium tartrate;
D5	0.400 M ammonium dihydrogen phosphate;
D6	30.000 w/v polyethylene glycol 8000; 0.200 M ammonium sulfate;
D7	30.000 w/v polyethylene glycol 4000; 0.200 M ammonium sulfate;
D8	2.000 M ammonium sulfate;
D9	4.000 M sodium formate;
D10	20.000 w/v polyethylene glycol 8000; 0.050 M potassium dihydrogen phosphate;
D11	30.000 w/v polyethylene glycol 1500;
D12	0.200 M magnesium formate;
E1	30.000 v/v polyethylene glycol monomethyl ether 550; 0.100 M bicine, pH=9.0; 0.100 M sodium chloride;

E2	2.000 M magnesium chloride; 0.100 M bicine, pH=9.0;
E3	10.000 w/v polyethylene glycol 20000; 0.100 M bicine, pH=9.0; 2.000 v/v dioxane;
E4	3.400 M 1,6-hexanediol; 0.100 M tris, pH=8.5; 0.200 M magnesium chloride;
E5	25.000 v/v tert-butanol; 0.100 M tris, pH=8.5;
E6	1.000 M lithium sulfate; 0.100 M tris, pH=8.5; 0.010 M nickel (II) chloride;
E7	12.000 v/v glycerol; 0.100 M tris, pH=8.5; 1.500 M ammonium sulfate;
E8	50.000 v/v 2-methyl-2,4-pentanediol; 0.100 M tris, pH=8.5; 0.200 M ammonium dihydrogen phosphate;
E9	20.000 v/v ethanol; 0.100 M tris, pH=8.5;
E10	20.000 w/v polyethylene glycol monomethyl ether 2000; 0.100 M tris, pH=8.5; 0.010 M nickel (II) chloride;
E11	30.000 v/v 2-methyl-2,4-pentanediol; 0.100 M HEPES, pH=7.5; 0.500 M ammonium sulfate;
E12	10.000 w/v polyethylene glycol 6000; 0.100 M HEPES, pH=7.5; 5.000 v/v 2-methyl-2,4-pentanediol;
F1	20.000 v/v jeffamine M-600; 0.100 M HEPES, pH=7.5;
F2	1.600 M ammonium sulfate; 0.100 M HEPES, pH=7.5; 0.100 M sodium chloride;
F3	2.000 M ammonium formate; 0.100 M HEPES, pH=7.5;
F4	0.050 M cadmium sulfate; 0.100 M HEPES, pH=7.5; 1.000 M sodium acetate;
F5	70.000 v/v 2-methyl-2,4-pentanediol; 0.100 M HEPES, pH=7.5;
F6	4.300 M sodium chloride; 0.100 M HEPES, pH=7.5;
F7	10.000 w/v polyethylene glycol 8000; 0.100 M HEPES, pH=7.5; 8.000 v/v ethylene glycol;
F8	1.600 M magnesium sulfate; 0.100 M MES, pH=6.5;
F9	2.000 M sodium chloride; 0.100 M sodium dihydrogen phosphate; 0.100 M MES, pH=6.5; 0.100 M potassium dihydrogen
F10	12.000 w/v polyethylene glycol 20000; 0.100 M MES, pH=6.5;
F11	1.600 M ammonium sulfate; 0.100 M MES, pH=6.5; 10.000 v/v dioxane;
F12	30.000 v/v jeffamine M-600; 0.100 M MES, pH=6.5; 0.050 M cesium chloride;
G1	1.800 M ammonium sulfate; 0.100 M MES, pH=6.5; 0.010 M cobalt chloride;
G2	30.000 w/v polyethylene glycol monomethyl ether 5000; 0.100 M MES, pH=6.5; 0.200 M ammonium sulfate;
G3	25.000 v/v polyethylene glycol monomethyl ether 550; 0.100 M MES, pH=6.5; 0.010 M zinc sulfate;
G4	20.000 w/v polyethylene glycol 10000; 0.100 M HEPES, pH=7.5;
G5	2.000 M ammonium sulfate; 0.100 M tri-sodium citrate - citric acid, pH=5.6; 0.200 M potassium sodium tartrate;
G6	1.000 M lithium sulfate; 0.100 M tri-sodium citrate - citric acid, pH=5.6; 0.500 M ammonium sulfate;
G7	4.000 w/v ethylene imine polymer; 0.100 M tri-sodium citrate - citric acid, pH=5.6; 0.500 M sodium chloride;
G8	35.000 v/v tert-butanol; 0.100 M tri-sodium citrate - citric acid, pH=5.6;
G9	10.000 v/v jeffamine M-600; 0.100 M tri-sodium citrate - citric acid, pH=5.6; 0.010 M ferric chloride;
G10	2.500 M 1,6-hexanediol; 0.100 M tri-sodium citrate - citric acid, pH=5.6; 0.010 M manganese (II) chloride;
G11	2.000 M sodium chloride; 0.100 M sodium acetate, pH=4.6;
G12	30.000 v/v 2-methyl-2,4-pentanediol; 0.100 M sodium acetate, pH=4.6; 0.200 M sodium chloride;
H1	1.000 M 1,6-hexanediol; 0.100 M sodium acetate, pH=4.6; 0.010 M cobalt chloride;
H2	30.000 v/v polyethylene glycol 400; 0.100 M sodium acetate, pH=4.6; 0.100 M cadmium chloride;
H3	30.000 w/v polyethylene glycol monomethyl ether 2000; 0.100 M sodium acetate, pH=4.6; 0.200 M ammonium sulfate;
H4	10.000 w/v polyethylene glycol 6000; 2.000 M sodium chloride;
H5	0.500 M sodium chloride; 0.010 M CTAB; 0.100 M magnesium chloride;
H6	25.000 v/v ethylene glycol;
H7	35.000 v/v dioxane;
H8	2.000 M ammonium sulfate; 5.000 v/v 2-propanol;
H9	1.000 M imidazole, pH=7.0;
H10	10.000 w/v polyethylene glycol 1000; 10.000 w/v polyethylene glycol 8000;
H11	10.000 v/v ethanol; 1.500 M sodium chloride;